Bioplume : a MEMS-based picoliter droplet dispenser with electrospotting means for patterning surfaces at the micro- and the nanometer scales

Thierry Leichle

Année: 2006

THESE

Préparée au
Laboratoire d'Analyse et d'Architecture des Systèmes du CNRS

En vue de l'obtention du
Doctorat de l'Université Toulouse III - Paul Sabatier

Spécialité
Matériaux, Technologie et Composants de l'Electronique

Par
Thierry Leïchlé

Bioplume: A MEMS-based Picoliter Droplet Dispenser with Electrospotting Means for Patterning Surfaces at the Micro- and the Nanometer Scales

Soutenue le 5 décembre 2006, devant le jury:

Président:	Robert PLANA
Directeurs de thèse:	Christian BERGAUD Liviu NICU
Rapporteurs:	Anja BOISEN Rosaria FERRIGNO
Examinateur:	Juergen BRUGGER
Invité:	Pascal MAILLEY

Une seule certitude suffit à celui qui cherche.

Albert Camus

Je n'offre pas ici une lecture d'amusement.
Indépendamment du sérieux du sujet, il demeure dans la façon dont il est traité,
un air de désordre que je n'ai pas eu la force de corriger.

Victor Riqueti, marquis de Mirabeau

Acknowledgments

Je tiens tout d'abord à remercier mes directeurs de thèse: Christian qui m'a initialement offert ce merveilleux projet, et Liviu avec qui j'ai partagé cette formidable aventure scientifique et qui compte maintenant parmi mes amis. Je remercie également les membres de mon jury de thèse pour leurs nombreux commentaires constructifs et pour le temps précieux qu'ils m'ont accordé.

Je veux exprimer ma gratitude envers tous les membres du laboratoire et de ses services, qui font du LAAS un cadre de travail idéal et épanouissant. Je pense en particulier aux personnels des services II et TEAM sans qui rien de concret n'aurait été enfanté.

Merci à tous les acteurs et collaborateurs de ce projet: Fabrice, JB et Daisuke au LAAS, Christiane à l'AIME, Thierry, Pascal et Emeline au CEA, Miguel, Pascal et Andrea au JRC, Maryna au Tyndall National Institute, et Nathalie à la Plateforme. Je pense aussi aux partenaires du projet européen NaPa, et spécialement à tous les membres du MEMS-based nanopatterning subproject, avec qui j'ai vécu une expérience européenne inoubliable car enrichissante tant sur le plan scientifique que sur le plan humain.

Je veux aussi remercier toutes les personnes du laboratoire avec qui j'ai passé les bons moments de détente nécessaires à une vie équilibrée de chercheur: tous les cadres et étudiants de notre très cher groupe Nanobiosystèmes; ainsi que mes camarades de bureau et mes amis du café et du privé: Laeti, Paul, Cédric, Laurent, Mat, Chris, Mathieu, Habib… Que ceux que je n'ai pas cités m'en excusent…

Enfin mes plus chaleureux remerciements s'adressent à ma famille, mes parents et mes frères qui m'ont soutenu pendant toutes ces années d'études et qui ont sûrement attendu longtemps ce moment…

Thank you, Ann, for your patience, your support and your love.

The partial financial supports of the EC-funded project NaPa (Contract no. NMP4-CT-2003-500120) and the Nano2Life European Network of Excellence (Contract no. NMP4-CT-2003-500057) are gratefully acknowledged.

Table of Contents

Prospective outlook

Introduction

Surface patterning consists in creating physical or chemical patterns on a substrate enabling differences in topographies, functionalities and surface properties. The process of drawing features exhibiting micrometer and nanometer scale resolutions is of great importance in modern science and technology. The invention of the solid-state transistor and the integration and the miniaturization of complex functions were possible thanks to an understanding and a control of the fundamental phenomena related to quantum physics and material science but also thanks to the development of reliable patterning tools for device manufacturing. This revolution that has already been effective in electronics, electro-optics and information technology (leading to powerful PCs, cell phones, or home electronics) is now starting to involve other scientific fields targeting all new applications. Because a multidisciplinary approach of science supported by technological breakthroughs is a key to study and understand life, new curing abilities will emerge (when technology helps us to live better) and new devices, more efficient and environmental friendly, will be designed and fabricated (when nature inspires technological advances). However, coupling biology and man-made systems raises two main technical issues: one is related to the chemical composition of the materials involved in both types of systems (organic versus mostly inorganic); the other one is the small size of the biological building blocks and entities (cells, DNA strands, or molecules) compared to the scale of the surrounding human world. In this context, surface patterning is foreseen to play a major role for the fabrication of hybrid devices and, as a result, will encounter numerous challenges. Size, resolution, uniformity, and alignment of the fabricated patterns are the main issues that are aggravated by the downsizing process. The cost of the techniques is not to be neglected and the writing speed and total covered area are important parameters when one thinks about industrial production. Giving the fact that all these issues can not be all addressed by a single tool, different techniques are now available.

The first surface patterning tool, the classical UV lithography process, has been initially developed to fabricate complex integrated circuit chips. However, because of its complexity and high cost, it is now not necessarily the most appropriate tool for the fabrication of simple novel devices such as, for instance, lab-on-chips or microlenses. Thus, lately, numerous techniques have emerged to propose solutions suited to specific applications. Generally there are two ways of patterning surfaces: by adding or by removing materials. In both ways, features can either be directly written or replicated from existing masters. Among the direct patterning techniques, some rely on the local delivery of liquids. Usually, liquids contain active species (i.e. biological molecules, nanoparticles, etching chemicals, and so on) consisting directly in the pattern feature, or

being part of an intermediate fabrication step. The currently existing tools address the millimeter and micrometer scales (pins, ink-jet printers) to the nanometer scale (dip-pen). However, creating patterns with 1 μm to 10 μm resolution is difficult because: i) it is time consuming using dip-pen and ii) other tools are too large, not precise enough or simply not mature at all.

In this thesis we present a patterning tool that allows the creation of micrometer scale features by changing the physical and biochemical properties of surfaces from the local liquid delivery of reactants. This tool, so-called bioplume, consists of an array of 12 microfabricated silicon cantilevers directly inspired from the well-known fountain pen. Thus, each cantilever incorporates a channel and a reservoir in its tip to allow liquid delivery and storage, respectively. Droplets of liquid are formed onto the deposition surface by a direct contact of the cantilever tip and the surface. By adjusting the wetting properties of the tip and the surface, as well as the contact time, deposited drops exhibit diameters ranging from several micrometers to a hundred micrometers, corresponding to picoliter volumes. Displacement of the cantilever array is achieved by mounting the silicon chip onto a four-degree-of-freedom automated spotter. To enable a control of the contact force and time during deposition, force sensors are incorporated into the array by means of piezoresistances integrated into the silicon cantilevers. The array includes 10 depositing pens, allowing the parallelization of the deposition process. The homogeneity of the array of printed droplets is guaranteed by using the force sensors to control the trim of the array regarding the depositing surface. The cantilever array, the PC-controlled spotting system and the electronics dedicated to the piezoresistance measurements form a closed-loop system that enables the automatic displacement of the array and the overall control of the deposition parameters. By using a specific external loading chip, different liquids can be loaded onto the cantilevers, enabling the parallel deposition of several entities in a single deposition run. Besides, a gold electrode is incorporated in the channel to allow using electrowetting and electrochemistry. The former is used to actively load the cantilever or to control the drop size during delivery, while the latter is used to drive electrochemical reactions in the deposited picoliter droplets. This tool has been used to print different types of solutions containing DNA or nanoparticles, and materials (i.e. polymers and metals) onto various substrates. The control of the printed features (resolution, thickness, and composition), the versatility of the printed materials and the added electro-assisted features prove that this tool has a real potential for research work and industrial applications.

The first chapter of this thesis provides a brief introduction to surface patterning. After presenting specific applications related to different technological fields, the main tools are reviewed with a particular focus on the liquid-based patterning techniques. In the second chapter, the bioplume system is introduced. Design considerations focusing on the mechanical and electrical properties of the piezoresistive cantilevers are given. The fabrication process, relying on conventional microfabrication techniques that allow the realization of low-cost and disposable devices, is then detailed. The electronics and the automated spotter are briefly discussed as well as the closed-loop implementation. This chapter ends with the testing of the fabricated chips within the system to prove its functionality. The last chapter finally presents two interesting deposition features relying on the use of nanoparticles and electrochemical reactions, respectively. Firstly, the bioplume tool is used to directly pattern particles suspended in liquid media. The formation of perfect crystals located in the deposited drop is successfully achieved by tuning the surface wettability, the particle concentration and the solvent evaporation rate. Secondly, by means of an electrode incorporated into the cantilever channel,

electrochemistry is carried out inside the drop during deposition. The in-situ local electrodeposition of copper and the electropolymerization of polypyrrole are studied and presented to prove the spotter potential in this configuration. A final conclusion presenting the highlights of this work is provided at the end of this manuscript.

This work has been conducted within the European project NaPa (Emerging Nanopatterning Methods) of the Sixth Framework Programme (Priority 3 - NMP). The objective of NaPa is to provide a set of new methods to enable the transfer from nanoscience to nanoengineering. In particular, it proposes a solution to two general problems: i) the fast and efficient fabrication of nanodevices and ii) the low-cost replication of nanodevices enabling them to be generally available on the market. Thematically, the project embraces and pushes forward the state-of-the-art developments in the physical and engineering sciences with the object-driven mission to provide European industrial and academic researchers with a library of novel nanopatterning processes needed to underpin radical innovations and further scientific developments in nanotechnology. The NaPa consortium integrates well over 80% of the viable existing European know-how in the new patterning methods into a single integrated project. The project complements the deep UV technology by providing low-cost scalable processes and tools to cover the needs of nanopatterning from CMOS back-end processes through photonics to biotechnology. To achieve this, research in three technology strands are currently being carried out: nanoimprint lithography, soft lithography & self-assembly, and MEMS-based nanopatterning. Our contribution to this project belongs to this last category and aims at developing and bringing to a maturity level the microcantilever-based liquid dispensing tool originally proposed by our research group.

Chapter I

Surface Patterning at the Micrometer and the Nanometer Scales

The aim of this chapter is to give an overview of surface patterning at the micrometer and the nanometer scales with a particular focus on the tools that rely on liquid delivery.

After introducing general notions on surface patterning, such as basic definitions and advantages of reducing the feature size, some specific applications that can benefit from the breakthrough and the maturity of the patterning technologies are explored. The important parameters used as characterization elements and the issues inherent to the quality control of the printed patterns are discussed. These characteristics and challenges are:

- Minimum resolution and feature size
- Uniformity and reproducibility of the replicated patterns
- Combination of different feature sizes
- Quality and functionality of the deposited materials
- Range and combination of materials
- Substrate state and pattern alignment

With these elements in mind, the different classes of techniques are briefly listed and described. These categories include the direct writing, the self-assembly and the replication of patterns. Details are given concerning the ink-based tools that use an external liquid source to create patterns or to locally functionalize surfaces by add-on processes or etching techniques.

The choice of focusing this chapter on tools is deliberately made because new devices and ideas are believed to emerge from technological breakthroughs even though technology is application driven. Indeed, the conventional microfabrication tools (for instance masks and aligners for photolithography, or reactive ion etching (RIE) equipment) that have initially been developed for the microelectronics industry later on rendered possible the invention of microelectromechanical systems (MEMSs). The emergence of MEMSs has successfully provided new systems, such as accelerometers used in the automotive industry or ink-jet heads for printers, targeting applications that could not have been envisioned without mature fabrication tools.

1. Introduction

1.1. Definitions - Notions on surface patterning

Surface patterning is a process resulting in printed features on a substrate. The patterns consist of differences in layer topography, differences in surface properties, or most often a combination of both structural and functional modifications.

Topography, defined as the variations in thickness of a layer, can be tuned by adding material or by partially or fully removing the layer. This type of surface structuration can either be used as a step in a fabrication process (the patterned layer serves as a mask for subsequent etch or deposition processes), as a mechanical constituent of a device, or as a direct way to change the final physical properties (usually mechanical or optical) of the area onto which the building-block features are replicated and arranged periodically.

Surface functionalization results in a local alteration of the physical, chemical or biological properties of a surface. The modification of the surface state is usually achieved by working with magnetic or dielectric materials, polymers, chemical monolayers or biomolecules. Each patterned entity exhibits a specific property and the parallelization of the patterns can lead to additional functionalities.

Hence, desired surface properties can be obtained by playing with the shape of the basic feature, the repetition drawing and the type of patterned materials. Being able to combine different physical and biochemical functions on different areas of a same surface is a key to the fabrication of complex devices, for example sensor arrays with high sensitivity and selectivity.

1.2. Benefits related to the size reduction

1.2.1. Toward smaller and more integrated devices

The first advantage inherent to the feature downsizing one can think of is the ability to create smaller devices, thus reaching higher integrations and performances in terms of computation capability and information capacity [1].

This has been the driving force of the microelectronics industry since the fabrication of the first working silicon transistor in 1954. Technical advances in the photolithographic area, one of the key steps of the semiconductor device fabrication, has been one of the major causes of integrated circuit linewidth reduction, from about 5 µm in the late 1960s to 65 nm nowadays. The reduction of the principal active components along with the optimization of material properties and design processes have led to the fabrication of highly powerful and fast integrated circuits (ICs). The intuitive law, expressed by Gordon Moore in 1965 [2], stating that the transistor density of semiconductor chips would double roughly every 18 months has been pretty accurate until now because the patterning methods have been constantly improved, from the classical optical lithography to the deep UV lithography. These technological breakthroughs have required huge investments, but at the same time, have enabled to decrease the overall cost of IC chips. Thus, due to the downsizing of the transistor critical size, leading to the increase of chip densities and number of computing functions, electronic equipment being faster, more powerful and complex is accessible for the consumers at a lower cost.

These obvious benefits that serve the microelectronics industry are to have a similar importance for biochip and biosensor development [3]. Biochips typically consist of a passive substrate (e.g. silicon or glass) onto which is printed a dense, two-dimensional grid of droplets that contain biological active compounds referred to as sensor molecules. These biochips are used to screen unknown target molecules (DNA or proteins) that specifically bind to their mirror affinity sensor molecules, providing the identity of the unknown molecules. Biochip is the major tool of the rapidly growing biotechnology industry, which encompasses a very diverse range of research efforts including genomics, proteomics, and pharmaceuticals, among other activities. Advances in these areas are giving scientists new methods for unraveling the complex biochemical processes occurring inside cells, with the larger goal of understanding and treating human diseases [4,5]. The ability to increase the number of printed biomolecules on a biochip while reducing the spot size surely increases the screening possibilities (thus the reliability of detection of diseases requiring multi cross-testing), and will allow devices for early diagnosis to be available in every home.

1.2.2. Emergence of new phenomena

The other benefit from the scale reduction of printed features is related to the limit of physical laws. Indeed, when reaching submicrometer sizes, new physical phenomenon appear and the classical laws describing the macro world are not necessarily valid anymore [6]. This is true in physics, as the behavior of electrons and particles in small and confined volumes undergo quantum effects. Magnetic materials can form single-domains and perfect dipoles when the dimensions of the deposited magnets are in the order of a few nanometers [7]. The same statement can be applied to optics, where photons behave differently when interacting with devices exhibiting features smaller than the light wavelength. The reduction in dimensions has also the particularity to increase the surface to volume ratio of microsystems. In this case, surface tensions and forces become preponderant regarding gravity and inertial forces. The reduction in size is also crucial in the biotechnological area because the dimensions of devices approach the size of cells and biomolecules [8]. It enables the manipulation of biological entities, the improvement of sensor selectivity and sensitivity and the study of a limited amount of molecules in controlled environments.

In order to take advantage of the scale reduction, the phenomena at small scale must be understood and new materials or thin film characteristics must be studied. This is necessary to allow accurate designs and simulations of new and small devices. Also, for progress to be made, enabling micro- and nanofabrication techniques as tools for experiments to understand the underlying science and engineering in the nanometer scale, easily accessible and flexible fabrication approaches are required. Figure 1.1 displays a scale chart providing natural and man-made objects found in the micrometer and nanometer worlds as a comparison means.

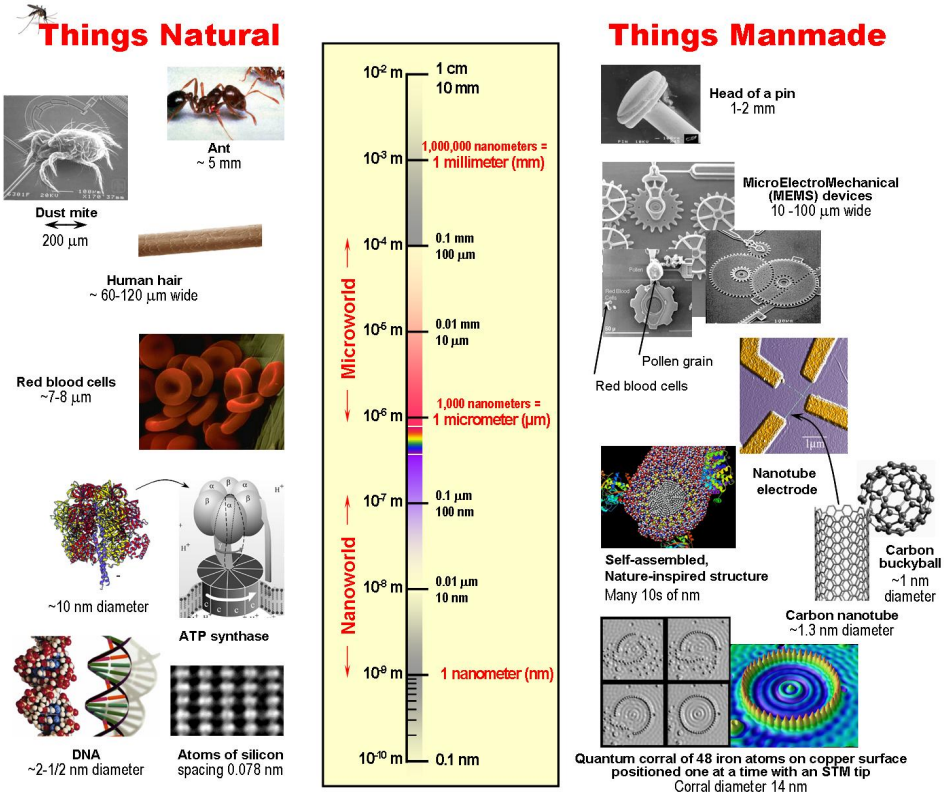

Figure 1.1: *Scale of things at the micrometer and nanometer scales [9].*

2. Applications

Surface patterning is the ability to structure a material in two or three dimensions at the micrometer and the nanometer scales. Because its definition is very open, the area of surface patterning encloses numerous techniques and materials and therefore is involved in a broad range of applications. Surface patterning is used for the fabrication of miniaturized devices, as well as for the biochemical surface functionalization. Hence, most applications are related to microelectronics and the associated technological fields, i.e. sensors and actuators. Only some examples are found hereafter.

2.1. Electronics

As stated above, surface patterning at the submicrometer scale has already been the base of the fast growing field of microelectronics. Complex processors, integrating complementary metal oxide semiconductor (CMOS) transistors and passive components onto IC chips are basic elements issued from the semiconductor industry. Obviously found in computers, cell phones and home electronics equipment, ICs are largely used in the automotive, the aerospace and the food industries as well as in the medical area. Millions of transistors are fabricated from silicon at the same time on large areas (large scale integration) thanks to optical lithography. The lithography technique basically consists in flashing a photosensitive polymer with UV light through an optical mask bearing the features to replicate. The polymer is developed so that the areas that have

been illuminated are removed (in the case of a positive resist). The patterned polymer is only used as a masking layer for post fabrication steps (etch of underneath layer, deposition of an additional layer followed by a lift-off process). Tricks have been used to print features with dimensions smaller than the light wavelength, so that UV lithography is still the surface patterning technique ruling the microelectronics industry [10]. However, other lithography techniques, using X-ray or electron beam, have been lately developed in order to reach smaller dimensions. These techniques rely on the same principle, i.e. the use of a sensitive layer to be removed, and are very time consuming and expensive. Thus, they can only be useful for large scale mass production or specific applications requiring strict characteristics, i.e. military or space applications.

Until now, silicon has been successfully used as the basic material in microelectronics, because of its semi-conducting properties, but also because it is cheap and its oxide is perfectly insulating. However it is very brittle and as novel applications become reality, such as flexible electronics that aim to introduce computer capability anywhere (for instance into clothing), silicon might not be the most suited material anymore. New materials, e.g. polymers [11], are to be used and new patterning techniques less expensive and adapted to small scale production are to be developed. Also the quest of faster and smaller devices might only be reached by using other materials or electronic building blocks because minimum feature sizes will soon reach the physical atom limit. Because materials with higher electron and hole mobility (some III-V compound materials) are very expensive to obtain and to process, nanosystems exhibiting specific electronic properties hold a promising way [12]. Improvements of surface patterning techniques are required to position these nanosystems, i.e. carbon nanotubes (CNTs), quantum dots, or molecules, at precise active locations.

Development of surface patterning techniques, leading to the reduction of feature sizes or the manipulation of new materials, could also impact other fields related to electronics, such as magnetic data storage (increase of memory capacity, improvement of reading and writing capabilities at the nanometer scale), nanoelectromechanical systems (NEMSs) for microwave applications (use of CNTs for new generations of switches, as shown in Figure 1.2) or chemical and physical sensors (integration of sensing elements, e.g. polymers or permanent magnets).

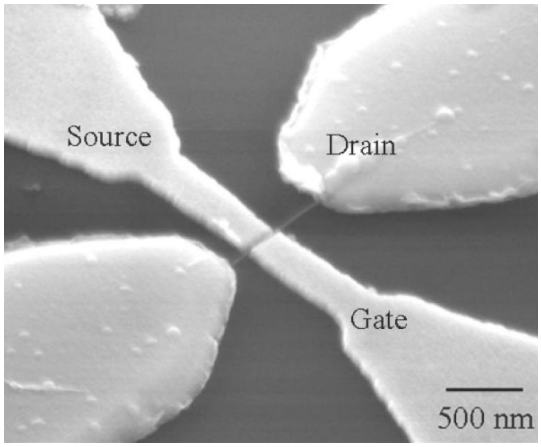

Figure 1.2: *Scanning electron microscope (SEM) image of a fabricated nanomechanical switch relying on a CNT [13].*

2.2. Photonics

Optics is an old scientific field that involves the generation, propagation and detection of light. Three major developments, which have been achieved in the last fifty years, are accountable for the renewal of optics and for its increasing importance in modern technology: the invention of the laser, the fabrication of low-loss optical fibers and the introduction of semiconductor optical devices [14]. As a result, electro-optics and optoelectronics devices are now essential in information and communication technologies, displays and sensors.

Because optical integrated circuits are based on the microelectronics industry, their fabrication relies on the use of patterning techniques. Thus, the advantage of optical integrated elements over their bulk counterparts are compact size, protection from thermal drift, moisture and vibration (thanks to the reliable and advanced packaging technology used for ICs), low power requirements, and low cost (due to the possibility of batch fabrication). Moreover, the alignment between the different optical elements, which is a critical problem for classical optical systems [15], can be simplified through the alignment possibilities offered by the microfabrication tools. To be used as a support of information, optical signals must be emitted, converted from/to electrical signals and transmitted over large distances. For this purpose, lasers and light emitting diodes (LEDs), wave guides and lenses, modulators, switches, multiplexers, filters, and other active optical functions are to be integrated with processors onto a same substrate. In optical integrated circuits, light is confined in thin film wave guides that are deposited and patterned on the surface or buried inside the substrate. The functions can be realized in many different ways, by passive or active elements. Passive elements, such as Bragg grating (to deflect and split), waveguides lenses (to image, collimate, focus, and so on), and grating couplers (to excite and take out a guided wave) can be obtained by coplanar periodic structures made of materials exhibiting appropriate optical indexes. Active elements can be realized with surface acoustic wave devices (acousto-optics Bragg cells), interdigital electrodes (electro-optic grating modulators), MEMSs (micropositioners, movable micromirrors), or monolithic devices (diodes, photodetectors). Among the various technical challenges faced by researchers and engineers, one consists in identifying materials which have both the right electro-optical properties along with reliable means of forming them into useful structures (i.e. patterning methods) on the integrated circuits.

An example of the newly central role played by structuration techniques in photonics concerns the fabrication and positioning of microlenses. Microlenses can be used as associated micro-optical components to enhance the performance of vertical cavity surface-emitting lasers (VCSELs) and to increase the coupling efficiency to optical fibers. After more than 20 years of development in microlenses fabrication, the major work today concerns polymer microlenses because of their low cost and ease of use. Several fabrication techniques are available: thermal photoresist reflow [16], LIGA process [17], photopolymerization [18], laser ablation [19], direct writing by electronic beam [20] and so forth. However, most of the above-mentioned techniques need a final assembling step on the VCSELs after fabricating the lenses, leading to strong alignment issues hardly suited for collective fabrication. Consequently, methods to fabricate a customized microlens directly on the VCSEL with a control on its dimensions have been recently proposed, such as ink-jet printing [21], or direct contact methods [22]. Figure 1.3 shows a row of microlenses realized by depositing polymer droplets with a MEMS-based contact technique.

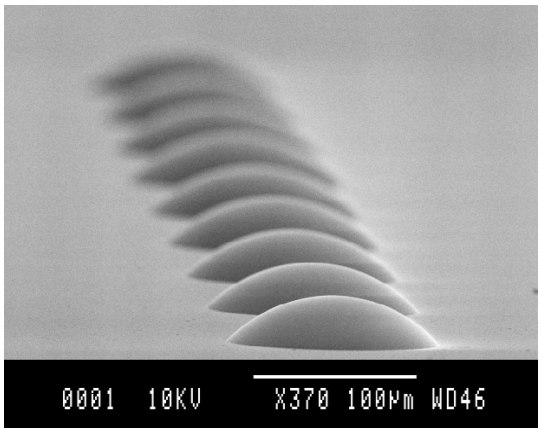

Figure 1.3: *SEM picture of an array of polymer microlenses deposited with a cantilever-based microsystem [22].*

Finally, optics is to be greatly impacted by further reductions in size, thus by nanotechnologies and advances in nanopatterning techniques [23]. The performance of optoelectronics systems based on two-dimensional (2D) quantum-confinements, already used in CD and DVD players/recorders (lasers and so on), can be improved by reducing the carrier properties to a zero-dimension with the use of self-assembled quantum dots. Three-dimensional (3D) photonic crystals can be obtained by microlithography or self-assembly to generate periodic structures. Patterning polymers at the nanometer scale, along with research efforts in new materials, are foreseen to impulse the breakthrough of organic optoelectronic nanostructures and to provide cheaper and flexible devices. LEDs made from small, conjugated organic molecules are already used as display elements in cell phones, car stereos and digital cameras for example. One can foresee that devices with higher complexity could also be realized.

2.3. Biotechnology and chemistry

The previously cited fields of applications have benefited from the improvement of surface patterning techniques to currently reach a fast development pace but there is much more to do in the area of biotechnologies. Surface patterning is promised to greatly impact the fabrication of bioarrays, biosensors, and lab-on-chip and indirectly to modernize medicine and consumer health.

Biochips, i.e. DNA and protein arrays, are respectively used in genomics and proteomics as useful and necessary tools for the comprehensive analysis of the molecular basics of cancer and other disease states, as well as for drug discovery, biomarker identification, gene-expression analysis and molecular profiling of cellular material [24,25]. Basically, DNA, and protein arrays consist of numerous spots of biomolecules (i.e. DNA, RNA, proteins, peptides or even drug molecules) immobilized onto a surface. Target molecules can bind specifically to these probe molecules with a specific affinity (nucleic acids with corresponding sequences or antibodies-antigens couples, for instance). Thus, by knowing the set of probe molecules one can deduce information concerning the presence or not of molecules in the sample to analyze (purified blood or urine samples, cells, and so forth) or directly concerning an unknown

target. Usually, probe molecules are immobilized on the microarray, but reverse phase arrays contain the analyte molecules. Detection of a binding event occurs by tagging either the probes or the targets with a fluorescent or a radioactive molecule and imaging the array with a dedicated scanner. In this case, the substrate is only used as a physical support providing a correct anchoring of the probe molecules thanks to appropriate chemical functionalizations of the surface. However, the in situ, real time detection of the binding event is possible if the substrate onto which the probes are grafted is used as a signal transducer. This is the case for biosensors that can use mechanical (silicon micromembranes and microbeams [26]), optical (surface plasmon resonance devices [27]), or acoustic (quartz microbalances [28] or SAW devices) transduction schemes. These latter signals are then usually converted to electrical ones, easy to handle and process. Thus biosensors can take advantage of the computing integration offered by the microelectronics industry to satisfy portable and multi-analysis applications. The immobilization of molecules on either the microarray or the biosensor surface obviously concerns the surface patterning technology. Chemical molecules (self-assembled monolayers) are usually used to covalently link the probe molecules onto inorganic substrates providing a correct anchoring (which is required to resist the numerous washing and incubating steps used in biological processes). The creation of molecule spots (or other features) is usually carried out by directly patterning molecules onto the chemically modified substrate (obtained by batch surface treatments, in liquid or vapor phase, and leading to the entire surface coverage). To keep their biofunctionality, the molecules to be immobilized are typically diluted in a solvent. The patterning tools suited for this application are thus based on the delivery of liquids, which happens either in a contact (quill, pin), or non contact mode (ink-jet).

The use of surface patterning methods is also of great interest for fabricating and functionalizing lab-on-chip and other microfluidic devices. These miniaturized systems that have emerged in the past few years, enable to handle, mix and analyze minute amounts of gazes or liquids. They are promised to replace conventional macrosystems and analysis platforms [29]. More than simply reducing the size of existing systems, microfluidics offer the advantage to reduce the amount of chemical or biological reagents and the power consumption (because of small heat dissipation), and to increase the reaction efficiency and the precision control of important parameters (such as temperature). Therefore microreactor chemistry is considered as a novel method on which to build new biochemical technologies and processes. It has been conclusively demonstrated that reactions performed within microreactors invariably generate relatively pure products in high yield. One of the immediate and obvious applications is therefore in combinatorial chemistry and drug discovery. The recent improvements related to microfluidics and microsensors have also led to the integration of the different operations necessary for bioanalysis in micro total analysis systems [30,31]. DNA purification, amplification, and separation can, for example, all be done on a single lab-on-chip. Thus one can imagine that complex, expensive, and time consuming analysis, currently carried out by laboratories, could be done at home. This could surely help early disease detection and treatments and would revolutionize the point-of-care and medical areas.

2.4. Material and surface sciences

The development of materials with improved mechanical properties (robustness, hardness, heat transfer, weight) is of great interest in multiple domains, such as aerospace, automotive, and civil engineering. Even though most of the significant progress concerns bulk materials, surface engineering is of importance for the control of interface properties (roughness, impermeability, resistance to corrosion and so on).

Recently, lots of research and industrial works have focused on the development of superhydrophobic surfaces to fabricate self-cleaning materials. Because the contact angle of water on superhydrophobic surfaces is very high (greater than 150°), water drops are unstable and do not adhere. Thus, impurities that accumulate on the surface are washed off by rolling drops, as their affinity with the liquid is higher (see Figure 1.4a). Surface wettability can either be tuned chemically (plasma treatments, deposition of polymer coatings), physically (change of roughness) or by a combination of both surface state modifications [32]. The increase of surface roughness is directly inspired from the lotus-leaf effect that is due to the unusual surface topography of the leaves (see Figure 1.4b). Structuration at the nanometer scale is thus a promising route to alter the wetting surface properties. For instance, the use of self-assembled nanoparticle monolayers as templates for surface structuration has already proved its efficiency, as seen in Figure 1.4c [33].

Surface patterning is also of great interest for bioengineering and for the development of new biomaterials. It is now well established that cellular growth and differentiation are directed by information exchanged between the cell and its surroundings [34]. Therefore, the components of the extracellular matrix and the surface state of artificial materials are of crucial importance in cell culture. By depositing specific molecules at precise locations on a substrate, cell growth can be promoted and spatially controlled (see Figure 1.5). For cell growth in vitro, bioengineered surfaces can be prepared by patterning peptide sequences. Such surfaces are very important in fundamental biology and medical research as they serve as scaffolds required for the culture of cells. Possibly in the future, they could also provide matrices for bioengineered artificial organs. The control of cell responses is also crucial in the case of engineered implants, and the challenges are exacerbated by the complexity of living systems. Improvements of artificial implants, such as artificial bones, joints, or heart valves, are due to advances in materials (metal alloys, ceramics) and devices mimicking organs but also to active research in bioengineered surfaces constituting the interface between the implant and the in vivo surrounding. In order to promote biocompatibility of an implant, the cell specificity of the implant surface can be realized by physical, chemical or biological functionalization. Engineered surfaces can be prepared by coupling anorganic functional groups with the intention to adsorb in vivo the right biomacromolecules which control cell adhesion in the sense of a specific auto-biocompatibilization of the material in situ [37]. This has the advantage in that the reaction of the immunological system (i.e. inflammation, foreign body reactions, etc.) can be minimized, thus avoiding any toxic effects on the hosts and damage of the implant. Local surface patterning may play an important role in the future of bioengineering with the intrusion of active sensors and complicated microsystems in the body (e.g. for the insulin level measurement and delivery). In this case, a specific functionalization of the active part of the implantable biosensor might be required and might differ from the rest of the device.

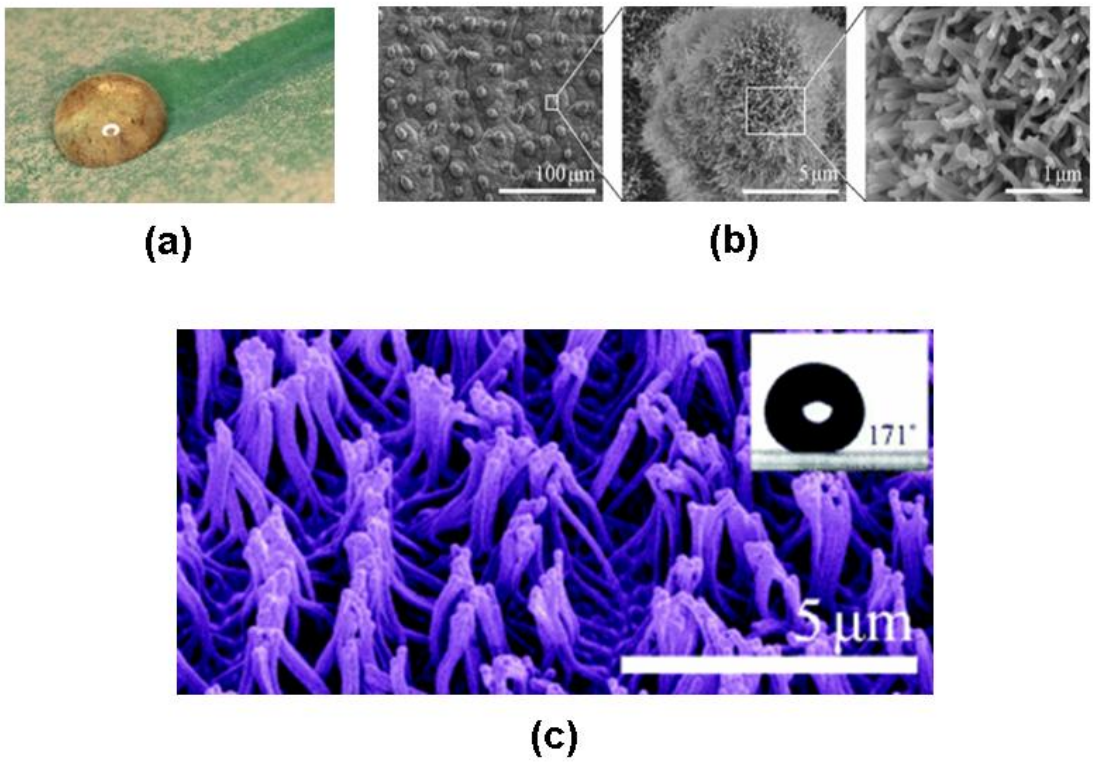

Figure 1.4: *(a) Droplet cleaning a lotus leaf. (b) SEM image of the surface structure of a lotus leaf at different magnifications. (c) SEM image of an engineered superhydrophobic surface made of perfluoropolyether derivative, the inset shows a water drop on the surface with an extremely high static contact angle [33].*

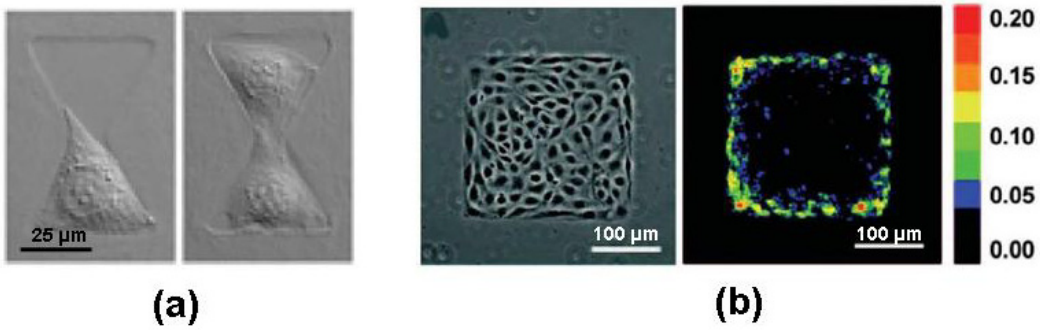

Figure 1.5: *Patterning of multicellular aggregates. (a) Single (left) and pair (right) of bovine pulmonary artery endothelial cells patterned in bowtie-shaped microwells [35]. (b) Phase image (left) and proliferation index (right) of cells patterned onto a large island of fibronectin [36].*

3. Characteristic elements and challenges

It makes sense that, regarding the variety of the fields of application, the specifications required for surface patterning can be very diverse. In order to dress a list of specifications, one must previously determine which are the important criteria describing the resulting patterns. This section provides characterization elements that need to be addressed for each application and that can differentiate the tools. For a given application, the more appropriate patterning method can be selected according to the desired characteristics. The aim here is also to introduce the challenges inherent to the combination of several requirements and that fabrication processes must face.

3.1. Minimum resolution and feature size

As previously stated, the quest for the size reduction of fabricated systems is already effective and has proven its significance for numerous applications. Thus, the minimum feature size that can be patterned onto a surface with a given technique is obviously very important. Care must be taken when talking about the size of the pattern itself or the size of the features created within the pattern. For instance, large scales micrometric patterns can be created by the arrangement of ordered colloids exhibiting nanoscale features. In any case, minimum feature size might be the first criteria taken into account when selecting a specific tool for a given application. Generally the complexity and the cost of fabrication inherent to a patterning technique increase with the reduction of printed patterns and their resolution. The nanometric resolution essential to fabricate complex microprocessors is not required for the fabrication of simple microfluidic devices designed to handle cells. In the latter case, channels exhibit geometries comparable to the cell size, i.e. typically several tens of micrometers. Besides, one must also consider the end user and its means. The fabrication of microprocessors is suited to industrial mass production with high throughput and large scale integration. Indeed, one type of chips can be incorporated in different brands of PCs that are large selling goods. Conversely, researchers might need to fabricate small numbers of microfluidic chips in a customized fashion.

3.2. Pattern uniformity and reproducibility of replicated patterns

The uniformity of printed features is of paramount importance for the reliability of fabrication processes. The difference in uniformity illustrates a loss of replication information and is a source of differences between the characteristics of a fabricated device and what is initially designed and expected. When referring to geometrical uniformity, not only the lateral dimensions of a pattern are to be considered, but also its thickness. This is obvious when the deposited layer is used as a part of a device. This is also important when the layer is used in a fabrication step, e.g. as a protective layer for an etching process. Non-uniformities can occur on a same substrate or from one sample to another. Both cases are particularly problematic when considering industrial applications. The uniformity issue is also a consideration when functionalizing surfaces and patterning biological compounds. For instance, in the case of bioarrays, the DNA or protein containing spots must be identical in shape, area and density in order to properly compare the emitted fluorescent signals. Failure to guarantee a good uniformity leads to the inability to carry on quantitative measurements and possible erroneous results.

Needless to say that this limits the power of these technologies for diagnosis applications, as no risk can be taken.

3.3. Combination of different feature sizes

The connection of miniaturized systems to the micro and the macro worlds is compulsory to enable exchange of information, send commands and read output signals. This issue, already addressed by various packaging technologies, is further complicated by the shrinkage of the dimensions. For instance, interdigited nanoelectrodes must be associated with microelectrodes built on the same chip to allow the connection of wire bonds through pads of appropriate dimensions (several hundred micrometers square). Nano and microelectrodes can be patterned during a single run with, for instance, e-beam lithography techniques which can be very time-consuming. Another approach to realize structures of different scale ranges consists in combining patterning tools in different fabrication steps (e.g. E-beam can be associated to optical lithography). This way, one can benefit from the advantages offered by both tools. However, the second set of electrodes must be aligned on the firstly fabricated pattern, which implies complexity in the pattern designs and more requirements concerning the tools. These comments are generally relevant concerning the integration of devices with different sizes on the same chip. The ability to replicate small features on large areas is also a serious issue for patterning methods, resulting in uniformity problems or long time processes. The use of prefabricated masters, which allow replicating patterns in one step, is thus preferable to direct writing techniques. However, to offer reliable solutions for large area patterning, techniques have to reach a mature state. This has been achieved by the microelectronics industry that has invested a lot on photolithographic tools to enable printing on 12" wafers with high yields.

3.4. Materials - Quality and functionality

The characteristics of a fabricated system are inherent to the geometry of the prints, as well as the materials that it is made of. Hence, the quality of patterned materials is of importance for microtechnologies. A lot of research work focuses on improving the properties of thin film materials. In the case of dielectric and ferromagnetic materials, the goal is to get as close as possible to the bulk properties. However, the fabrication processes of bulk materials impact their resulting properties, and the same applies to the microfabrication techniques that rely on molding, embossing or direct printing of thin films. Specific materials, such as photosensitive polymers, are only developed for dedicated tools, but can have different purposes, such as constituting a protective layer or an active part of a micromechanical system. The former case requires the polymer to withstand the strong acids used in etching processes, while the later case requires the polymer to exhibit good mechanical properties. Reproducing both these qualities is a challenge for the common technique (e.g. photolithography). Interface properties can also be altered by patterning. Methods based on the use of laser beams, for instance, change the chemical surface state while direct writing with a microstylus modifies the roughness. The main issue concerning the patterning of chemical and biological compounds is the preservation of a desired functionality. A chemical or biochemical pattern is effective only if the molecule reactivity is respected. This means that the first prerequisite for a tool dedicated to

deposit biomolecules is to keep them in a suitable environment to avoid their denaturation. For instance, as proteins are required to be in a liquid medium to be functional, the most appropriate tool to handle them should be based on liquid delivery.

3.5. Range and combination of materials

The strength of the patterning methods is strongly correlated to the huge library of materials that are available. It includes all the materials conventionally used in microelectronics (i.e. semiconductors, their oxides and compounds, glass, metals, dielectrics, magnetic materials, and polymers) and materials used in organic chemistry and in biology. Giving the fact that these materials are very different in nature, they can be formed and deposited on a substrate by various means. Only a few materials are suited for direct patterning during deposition (typically the ones that can be evaporated or that can be dissolved). The other materials must be patterned after being deposited onto the entire surface of the substrate. The wide range of materials that can be patterned opens unimaginable possibilities of combinations toward the realization of hybrid devices. However, one must keep in mind that a single patterning method might be restricted to the use of a limited number of materials. Furthermore, an important parameter to consider is the ability of any tool to deposit different materials onto the same substrate or device in a single step. Analogously to the challenges inherent to the realization of different feature sizes, printing different materials might require time. Thus, for the fabrication of genomic arrays, for instance, the possibility to print in parallel several types of oligonucleotides is preferable, regarding the thousand or million of sequences that must be explored.

3.6. Substrate state and pattern alignments

The substrate is an important element to consider in the patterning process. More than its size, geometry and nature, its surface state can dictate the patterning possibilities. In the microelectronics industry, substrates consist of large silicon wafers that are perfectly flat. Dedicated tools that are designed in consequence offer the optimum and the more reliable performances with these substrates. Other techniques are less restricting and enable to work on a wide range of substrates with various topographies and roughnesses. Besides, a patterning step is generally part of a fabrication process flow. Patterns are realized over existing structures and surface functionalization is desired on specific substrate locations. Thus, tools must enable the alignment of the new patterns regarding the features already existing on the surface. This usually requires to design and to fabricate specific zones containing alignment marks, which reduces the overall area dedicated to the useful devices. Tools must include the means to observe these zones and to achieve the spatial alignment with a desired resolution. Observations are usually carried out optically, but force sensors can also be used to deduce the relative tool position by screening the surface. Finally, actuating schemes are necessary to achieve the relative displacement of the tool on top of the surface with specific accuracies.

3.7. Concluding remarks

The specification elements discussed in the above sections must be used to describe the technological needs inherent to the fabrication of a system. The domain of application and the end user determine the volume of production and the time and cost constraints. The wide range of available feature sizes, resolutions, materials and substrates emphasizes the tremendous potential offered by the patterning technologies for the realization of complex hybrid systems. However, because of this large range of possibilities, the universal surface patterning tool does not exist. Thus, there is a need for a library of tools that allow reaching targeted specifications at various costs and complexity levels. The most suited method for a given application can then be selected from this toolbox.

4. Overview of the patterning tools and methods

The process of patterning has a long history, as human beings have always looked for means to transcript information, text and images, onto solid media. The fountain pen, the printing press and the serigraphy technique are among numerous examples illustrating the diversity of writing tools. The revolution of microtechnologies has generated a need to develop new writing apparatuses for the micrometer and nanometer scales. Most of these tools have been inspired from what is already available at the macro scale, leading to numerous types of techniques. These techniques can be classified according to their characteristics, requirements and aspects of emphasis. In this section, a short overview of the main methods allowing the fabrication of two-dimensional patterns is presented and logically organized in three categories: the direct writing, the self-assembly, and the replication techniques [38]. The first two techniques allow creating patterns from scratch, while the second technique allows duplicating patterns from prefabricated masks. A short discussion concerning these methods will be provided at the end of this section, raising the need for alternative versatile techniques based on ink deposition.

4.1. Direct writing techniques

Direct writing techniques enable one to generate arbitrary features on a surface. It is a serial process that is time consuming and only suited to fabricate few copies of original samples. Pattern generation by direct writing techniques is carried out either by locally modifying material properties, or by locally etching or depositing material. These results can be achieved by using beams of energetic particles, electric or magnetic fields, rigid styluses, or deposited inks. The latter method is detailed in section 5 of this chapter.

4.1.1. Laser, electron and focused ion beams

The beam writing techniques use a focused beam of photons, electrons or ions scanned across the surface to pattern. Chemical and physical reactions occur where the beam hits the sample surface, in and close to the illuminated spot. The resulting effects on the surface depend on the type of radiation, the dose, and the materials involved.

Focused laser beams are used as local ablation tools and work with different types of materials, i.e. inorganic materials (as shown on Figure 1.6a in the case of nickel) or polymers [39]. Commercial photomasks are often fabricated with this technique when the feature size is larger than a micrometer. Materials can also be deformed or melted at the focal spot due to thermal energy dumped by the beam. A laser beam lithography technique, based on near-field scanning optical microscopy (SNOM), allows higher resolutions by using a transparent, aluminum coated probe tip at the end of an optical fiber [40]. Electron beam (E-beam) and focused ion beam (FIB) techniques are used to create patterns with small feature size and high resolution, due to their short wavelength and large depth of focus. They are usually combined with powerful observation tools, such as SEMs. The E-beam technique is most often used with the poly(methyl methacrylate) (PMMA) resist, but is also compatible with a wide range of materials, such as polymers, inorganic materials, and self-assembled monolayers (SAMs) [41]. FIB offers the additional possibilities to carry out highly localized implantation doping, ion-induced deposition (see Figure 1.6b), ion-milling or etching [42]. E-beam is extensively used in nanofabrication, conversely to FIB that is in a less-developed state.

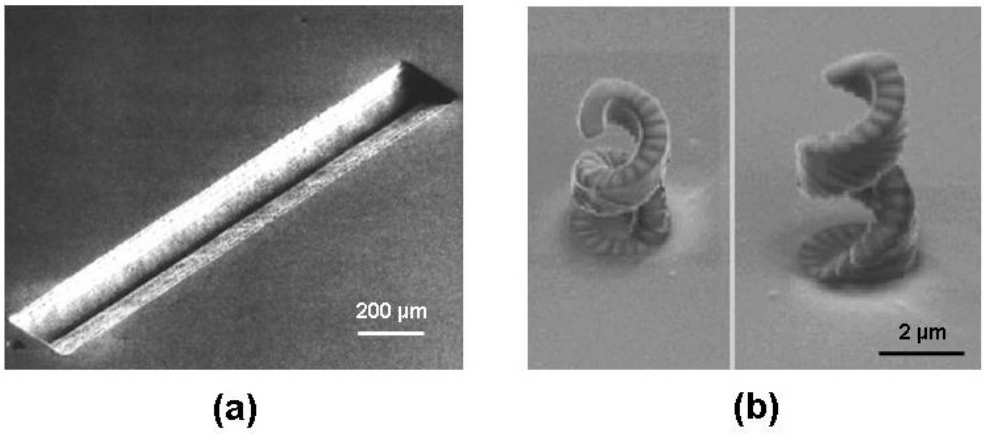

Figure 1.6: *(a) V-shaped groove in nickel machined by multiple scanning with a laser beam [39]. (b) Three-dimensional shaped ion-induced depositions with overhanging features [42].*

4.1.2. Electromagnetic field assisted techniques

Local electrical writing is based on the use of an auxiliary electrode situated nearby the surface that constitutes the counter electrode. The applied electromagnetic field affects the physiochemical properties of the species at the interface because of the field itself, the induced current or the redox reactions occurring at the tip or on the surface. Scanning tunneling microscopy (STM) and scanning electrochemical microscopy (SECM) are typical tools that can be used for local electrical writing [43,44]. The field-assisted method allows one to position precisely metal clusters, to create pits or holes and to manipulate individual molecules or atoms [45]. Electrochemical reactions are used to oxidize surface, to deposit metal islands, and to modify SAMs and organic thin films. Analogously, a magnetic field can be used to

change the magnetization of magnetic materials (i.e. polycrystalline magnetic alloys or iron oxide particles). In this case, the writing element is an inductive device fixed on a recording head. This technique, that is crucial for information storage technology, has the advantage to induce reversible modifications.

4.1.3. Surface engraving with solid tips

Mechanical stress and strain can be induced by a rigid stylus in contact with a surface. The displacement of the stylus on the surface is used to engrave patterns in relief and results in the creation of holes or trenches surrounded by walls formed by the displaced materials. A wide range of feature sizes can be achieved, depending on the dimensions and the sharpness of the tip. Macrometer size styluses are used to micromachine bulk materials. Sharp micrometer tips, such as the ones used for atomic force microscopy (AFM), are able to write nanometer scales features on a variety of materials including polymers, metals (see Figure 1.7), oxides and SAMs [47]. This technique is known as scanning probe lithography (SPL). An AFM-based data storage concept, relying on SPL principle, has been recently proposed [48]. It consists of an array of 32 × 32 AFM cantilevers, individually addressable, with integrated write/read capability. Area densities of 100-200 Gb/in.^{2} have been achieved on thin PMMA layers with this system.

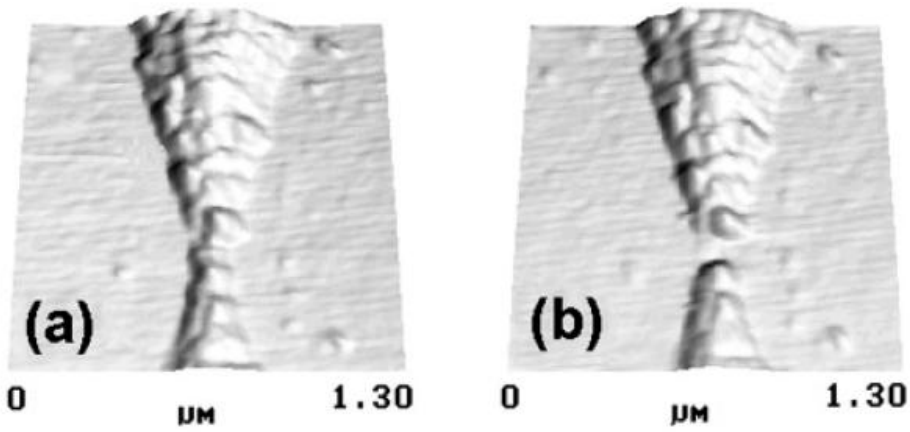

Figure 1.7: *Three-dimensional view of an aluminum stripe before (a) and after (b) directly removing the metal with an AFM tip in the thinnest region [46]. The resulting gap is 60 nm wide.*

4.1.4. Add-on processes

Add-on processes consist in directly depositing material at the desired location of a substrate. An important aspect of this technique is that the material to pattern does not have to cover the entire surface of the substrate prior to patterning. Thus, this helps to reduce the number of process steps, such as the deposition of the initial layer, and the waste of raw material (because it is only deposited in useful locations). The other

interesting advantage offered by this method is the direct fabrication of patterns with high biochemical functionality without the risk of material cross-contamination. Techniques belonging to the add-on category include laser-induced chemical deposition and FIB-based deposition that use gaseous precursors, plus numerous ink-based deposition techniques that use precursors in liquid medium. The advantages of the latter method as well as the description of the associated tools will be presented in the last section of this chapter.

4.2. Self-assembly

Self-assembly is used to create patterns from small entities, such as nanoparticles or molecules that have the ability to organize themselves in stable, well-defined structures. Unlike the other types of patterning methods, this is a bottom up approach inspired from the self-assembly mechanisms occurring in nature. The self-assembly process depends on the properties of the building-blocks, which include their topography, shape, surface functionality and electrical potential, as well as the properties of the medium in which they are dissolved.

The molecular self-assembly uses electrostatic, hydrophobic, or van der Waals' interactions between molecules, and hydrogen or metal-ligand bonds. The formation of SAMs, lipid monolayers, micelles and crystals is based on these principles. Chemical or biological layers are usually used in surface functionalization for bioengineering, biosensors and bioarrays, and the former can also be used in micromachining processes in order to avoid stiction problems occurring during the release of MEMS devices [49].

Self-organization of colloidal particles, nanowires and nanotubes is influenced by additional forces, such as gravitational, capillary or external electromagnetic forces. Layers of self-assembled nanoparticles can either be used as an active part of a device [50] or as a mask to pattern the surface underneath. For instance, regular metal patterns with pyramidal shapes can be obtained by evaporating metal in the void space left between the particles that are removed afterwards by a lift-off technique (see examples of shadow nanosphere lithography experiments in Figure 1.8). Particles can also be used as an etch mask during the reactive ion etch process of a silicon surface that leads to the fabrication of well-ordered silicon nanopillars [52].

Generally, self-assembly produces simple patterns that can be obtained over large areas. However, to control the location of the well-ordered features, self-assembly must be associated to other patterning techniques. For instance, beam or stylus writing techniques can be used to draw features in SAMs and particles can be removed from specific areas by a lift-off method, providing that a prior photolithographic step is done. As exposed in a following section, microcontact printing is extremely suited for the patterning of self-assembled monolayers. But the most straightforward techniques for the local deposition of SAMs and nanoparticles are based on liquid delivery.

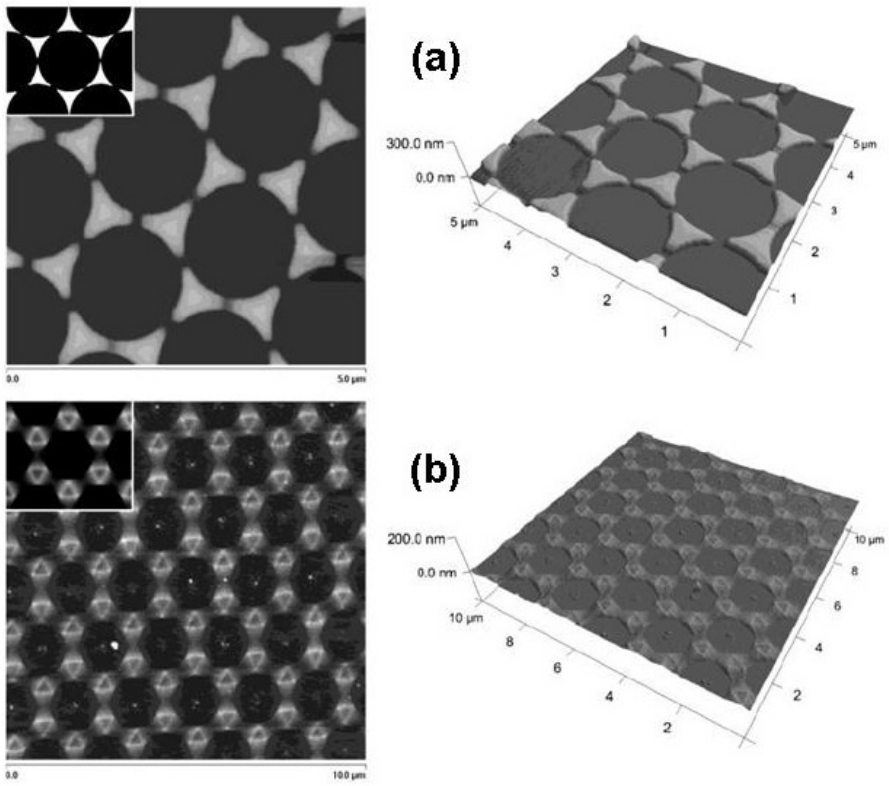

Figure 1.8: *Two-dimensional metallic structures fabricated using angle-resolved nanosphere lithography. Simulations and experiments of metal evaporation (40 nm of Ni) through a monolayer of latex nanoparticles (with 1710 nm radius) for different tilt angle values: (a) tilt angle of 0° and (b) tilt angle of 15°. The insets of the AFM pictures show simulated particle shapes [51].*

4.3. Replication of patterns

Replication techniques consist in duplicating patterns already created on a mask, a master or a stamp on a substrate with high fidelity and reliability. These methods enable the fabrication of multiple copies rapidly and are thus well suited for mass fabrication. The original mask must previously be realized by using direct-writing techniques. Information can be transferred by using a flux of photons or material passing through the apertures of a mask, by embossing or molding material with a master, or by printing ink with a stamp.

4.3.1. Optical and stencil lithography

Optical lithography, a technique previously introduced in this chapter, relies on the interposition of an optical mask between the source of photons and the substrate to pattern. The mask enables the selective illumination of the photoresist polymer on the substrate surface by bearing transparent and opaque regions. It is usually made of a piece of glass or quartz onto which a chromium layer is patterned with the features to replicate. Because this technique is limited by light diffraction, it is necessary to

continuously decrease the wavelength of the source in order to keep pace with the trend in downsizing the feature size. The numerous advantages offered by this technique, such as a minimum feature size as small as 65 nm, high resolution and the ability to create large and small patterns with arbitrary shapes in a single step, are balanced by its difficult implementation and its high cost. As already stated, it is the base of the microelectronics industry and it is extensively used to fabricate MEMSs, NEMSs and photonic devices. Lately, it has been adapted for the manufacture of DNA chips. Light exposure is used to create photochemical reactions at specific sites of molecules supported by a solid surface. The repetition of the reactions with different chemical reagents and appropriate masking enable the construction of oligonucleotide chains with different base pairs in desired sequences [53]. However, this method is only suited when a small number of sequences is involved.

The other masking technique, the stencil method, is based on the selective deposition of material evaporated (typically metals or complex oxides) through micro- and nanoapertures [54,55,56]. The main added value here is that the technique does not rely on photoresist processes, as the material is patterned during its deposition. The shadow evaporation technique typically uses miniature mechanical membranes with tiny apertures (see Figure 1.9). Nanometer scale features can be fabricated simultaneously with micrometer scale patterns in a single process step using this technique. The deposited structures can be used directly, transferred into a sub-layer, combined to lift-off processes or refined by self-assembly or growth processes.

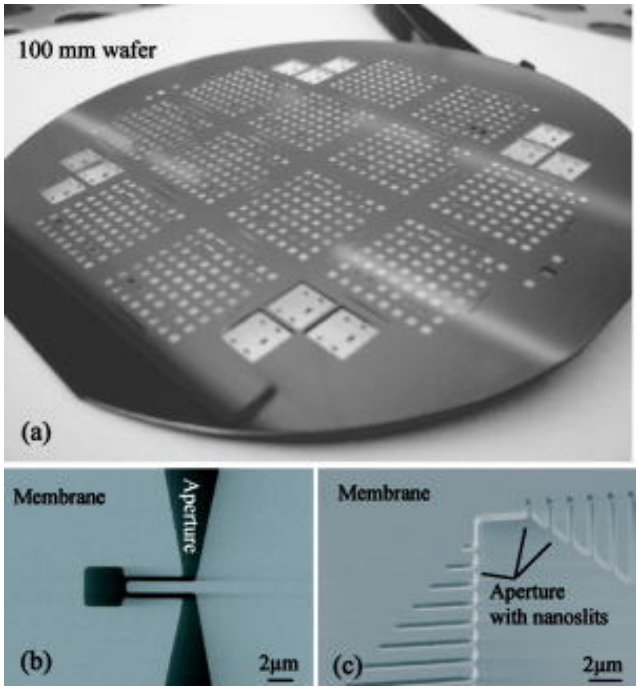

Figure 1.9: *(a) Optical image of a full wafer scale (100 mm) stencil containing various membranes, each containing numerous geometrical apertures [57]. (b), (c) Released SiN membrane containing simultaneous micro- and nanoapertures ranging from 350 nm up to 30 µm and 400 nm up to 300 µm, respectively.*

4.3.2. Imprint and soft lithography

Replication with a master includes the imprint lithography and the soft lithography techniques [58]. Both techniques are used to generate patterns either identical or complementary to those on the master at a relatively low cost. Imprint lithography is a polymer embossing process requiring a rigid mold, a polymer and temperature-pressure cycles. Generation of relief patterns is carried out by mechanically deforming the polymer (which is either thermoplastic, UV- or thermally-curable) with the rigid master. It has undergone a relatively fast development since it emerged in 1995, offering the possibility to create patterns with feature sizes below 10 nm [59,60]. However, residual films are most of the time present in the embossed grooves requiring subsequent etching steps, and the demolding process is not so trivial. Since the emergence of the laser-assisted imprinted technique, the range of imprinted materials is not limited anymore to polymers only. Indeed, silicon embossing has recently been realized with this method, as demonstrated in Figure 1.10 [61].

Soft lithography is a molding technique relying on the use of an elastomeric master, usually made of poly(dimethylsiloxane) (PDMS). The more straightforward procedure, replica molding, consists in pouring an organic polymer into the mold and curing it in order to retain the mold topography. Another approach (microtransfer molding), enables to print the mold replica on a surface and involves two more steps: after filling the mold with the polymeric precursor, excess material is removed from the mold surface, and finally, the mold is placed on a desired surface, the polymer is cured and the mold peeled off. Its immediate advantage is that it offers the possibility to achieve intimate, conformal contact with flat or curved surfaces over large areas. Small feature sizes can be replicated with high fidelity and accuracy without any damage.

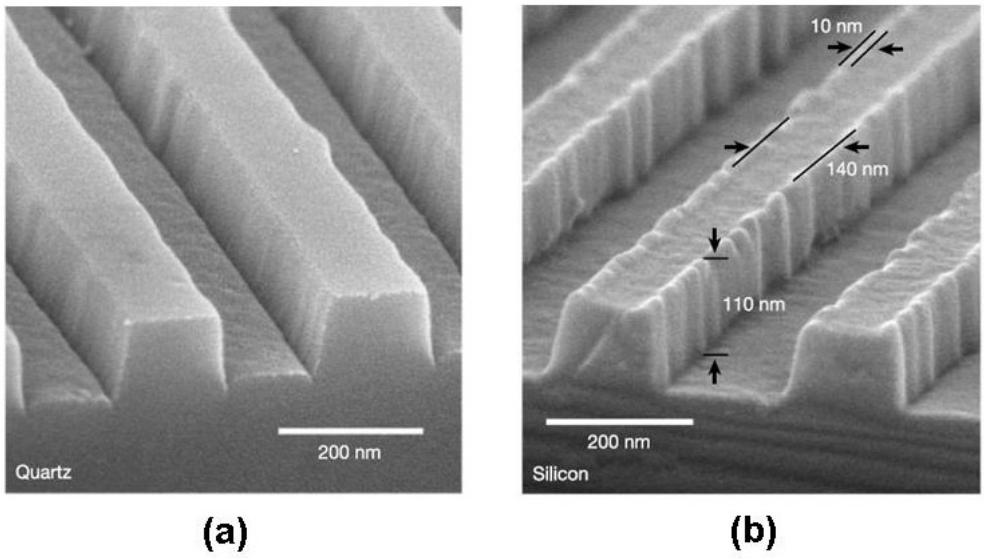

Figure 1.10: *SEM images of the cross-section of samples patterned using laser-assisted direct imprint [61]. (a) Quartz mold. (b) Imprinted patterns in silicon.*

4.3.3. Microcontact printing and fluidic patterning

Both techniques differ from the one previously presented in this section in the sense that they are especially well-suited for the patterning of entities dissolved in a liquid medium, i.e. chemical or biological compounds. Microcontact printing (μCP) relies on the use of an elastomeric stamp to transfer patterned ink onto a substrate in a very simple and convenient way [62]. It is inherently an additive technique. Soft stamps usually made of PDMS exhibit grooves patterned in a flat surface. The stamp is soaked in the solution of ink containing the species of interest and then dried. It is finally brought into contact with the surface of a substrate to allow the transfer of species from the flat surface of the stamp to the substrate, before being released from the surface. Because the material inside the groove does not contact the substrate, it is not transferred, resulting in the replica of the stamp pattern on the substrate. This technique has been demonstrated for SAMs and works well for other chemical species, such as catalysts, dendrimers, organic reactants, and conventional polymers, as well as colloidal particles. Elastomeric stamps provide an ideal interface between biological and non-biological entities. Thus it is especially suited for the deposition of lipid bilayers, proteins (see Figure 1.11) and DNA [63,64]. Soft lithography is a promising tool for the patterning and biochemical functionalization of large areas at a very low cost [65]. However, it lacks optimized materials for high resolution stamps, know-how for fabrication of accurate stamps/tools with overlay, and inks for high yield processes. Deformations currently preclude accurate patterning below 150 nm over areas larger than 100 mm.

Pattern replication and surface functionalization can also be realized by means of a microfluidic device [66]. Basically, an open channel fluidic network is placed on the surface to pattern so that the liquid flowing in the channels is in contact with the surface. The liquid serves as a transport and reaction medium that can be used to deposit material (by adsorption, specific recognition events, or sedimentation for instance), or to remove material or species (by chemical etching or dissolution, respectively) from a surface. Microfluidic patterning is a very interesting method to pattern cells and biomolecules because specific binding and recognition events can be simply and conveniently localized.

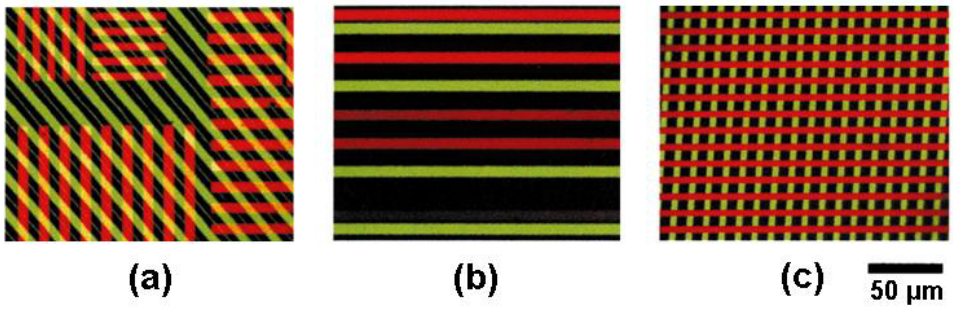

Figure 1.11: *Fluorescent images of microcontact printed proteins onto a substrate. (a) Two different proteins subsequently printed using different PDMS stamps [63]. (b) 16 different proteins patterned onto the polystyrene surface of a cell culture dish using a stamp inked by means of a fluidic network. (c) Three different proteins simultaneously printed onto a glass slide by a flash stamp.*

4.4. The need for alternative patterning techniques

The different techniques introduced in this section enable one to pattern a wide range of materials with feature characteristics specific to each method. According to the requirements of a targeted application, some tools are better suited than others. The production scale and the financial means are important parameters to take into account when selecting a tool. For industrial production, requiring the fabrication of a large number of similar devices with high yields, the use of replication techniques is definitely more appropriate. While projection mode lithography is perfectly adapted to the microelectronics industry, some newly emerged technologies, such as imprint or soft lithography, show great promises for more economically constrained industries and applications requiring less complexity. All these techniques must be associated with direct-writing tools to fabricate the original mask, mold or stamp that is to be duplicated. Self-assembly is a powerful technique, simple and cheap, but is limited in terms of patterns that can be created and must also be coupled with other methods in order to localize the patterned area. Direct writing techniques that allow to straightforwardly draw simple features, such as lines and dots, on a substrate in a serial fashion are suited for the fabrication of few devices (because of time issues) or for post-processing tasks. Direct writing is of paramount importance because it is always involved, even indirectly, in the fabrication of micrometer and nanometer scale patterns. However, most of the mature and high-performance direct writing tools are very pricey and high maintenance. For example, E-beam, FIBs and AFMs are expensive equipment that require highly qualified operators. Thus they are mainly accessible to specialized industries and important technological research laboratories.

The use of surface patterning for new applications requires the development of low-cost and simple direct patterning techniques. Add-on tools based on micromechanical systems (ink-jet print heads or microcantilevers) propose an interesting route toward this purpose, as they can benefit from low-cost fabrication (thanks to mass production) and they can be implemented in ready-to-use, user-friendly systems (such as ink-jet printers). Besides, the local functionalization of surfaces with biochemical molecules using subtractive direct writing techniques is difficult to achieve without cross contamination. Add-on tools based on liquid delivery are particularly suited for that intention, because each type of molecule can be printed at the desired location. These tools can also be used in combination with other printing techniques, e.g. microcontact printing (to ink the stamp with different molecules), thus allowing different species to be printed in a single run in a parallel manner [67]. Because of the versatility of printed materials (including all the ones that can be dissolved), the ease of implementation and the possibility of parallelization, we believe that tools relying on the local delivery of inks are extremely promising. An overview of those tools, including the one resulting from our work, is provided in the next section.

5. Liquid-based patterning tools

The ink-based direct writing techniques rely on the local delivery of materials onto a surface via a liquid meniscus or a droplet. The range of feature sizes that can be achieved is consequent, as attoliter to microliter volumes can be delivered. Figure 1.12 displays a scale that gives an idea of the dimensions involved in the description of these small volumes. Two different methods are generally used in ink-based patterning. The non-contact method consists in projecting liquid drops on the patterning surface from a droplet ejector (ink-jet like techniques). The contact method allows transferring droplets, molecules and species thanks to the liquid meniscus formed between a tip or a pen and the contacting surface (direct scanning probe lithography or micromachined fountain pen techniques). The tool developed in this thesis work belongs to the second category. The objective of this section is to provide a short overview of the ink-delivery methods, discuss their pros and cons, introduce foreseen applications and compare their performances.

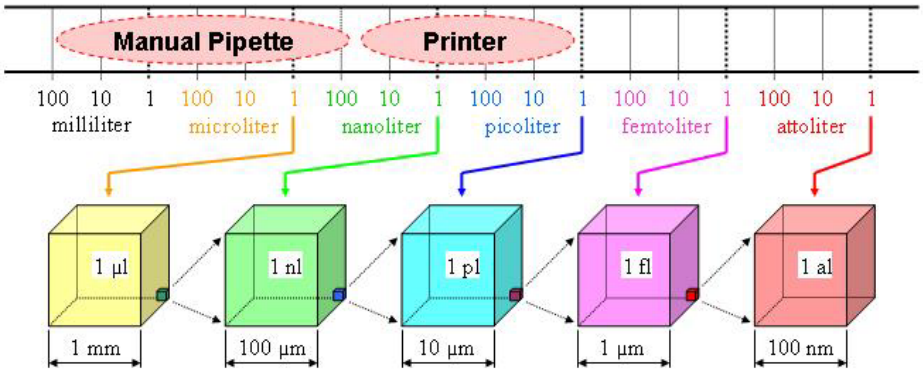

Figure 1.12: *Volume scale providing the dimensions involved in the description of small volume [68]. As a comparison means, the range of volumes of liquid handled by two of the most common drop dispensers are provided.*

5.1. Ink delivery by non-contact methods

The non-contact method consists in ejecting a droplet from a nozzle placed above the surface by different methods. It offers the advantage to be compatible with any type of support, especially those with irregular surfaces that are difficult to pattern with other tools, but the alignment with existing patterns can be quite challenging.

5.1.1. Ultrasonic micropipette

Manual pipettes have been extensively used in biology to deliver precise amount of liquids. Usually, they use plastic cones with inside diameters of more than several hundred micrometers, thus, the smallest volume that can manually be delivered is in the order of few tens of microliters. By using small glass capillaries, pipettes can be

fabricated with much smaller outlets (ranging from 0.1µm to 30µm). The principle of operation of the ultrasonic pipette relies on causing the tip of a capillary to vibrate in order to eject a stream of reproducible droplets [69]. The vibrations are provided to the pipette via a piezoactuator fixed on the capillary, and the droplet production rate equals the actuation frequency (typically a few hundred kHz). Hager et al. have imposed the flow rate inside the capillary by external pumping systems, in order to control the volume of the ejected droplets. They report the ejection of 1 pl to 2 pl droplets. Lee et al. have introduced a similar system relying on the resonant longitudinal motion-induced squeezing of a tapered volume that is free from any pumping mechanism, thus a lot simpler [70]. This drop dispenser is presented in Figure 1.13. The main interest of the PZT/tapered glass capillary ejector is that the formation of satellite droplets can be avoided by controlling the velocity of the tip displacement. This type of ultrasonically driven micropipette can also be used in contact mode [71]. In this configuration, the pipette is brought into contact with the surface, a pulse at the correct frequency and peak-to-peak voltage is sent to the piezoactuator during a given time to create a droplet, and the pipette is finally released from the substrate. Larson et al. have demonstrated that this method could lead to the deposition of droplets with controlled volumes. This tool is thus well suited for many printing applications, the contact mode operation being especially appropriate for the fabrication of biochips. However, the use of glass capillaries prevents high reproducibility in terms of tip diameter, proscribes any integration and parallelization.

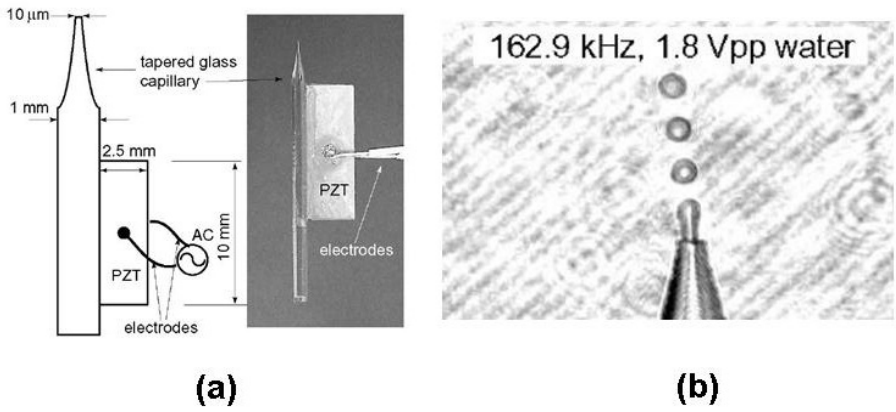

Figure 1.13: *PZT/Glass capillary actuator [70]. (a) Schematic drawing and picture of a fabricated device. (b) Picture of water drops ejected from the glass capillary.*

5.1.2. Electrospray

In the electrospray type of droplet generation, the stream of liquid coming out of a capillary is caused to split into numerous droplets upon the application of a direct current (DC) voltage. The generated electric field causes the formation of a Taylor cone, leading to a spray of fine ionized droplets. It was initially pioneered by Zeleny using glass capillary tubes [72]. Electrospray ionization was first applied in the 1980s for mass spectrometry using a stainless steel needle [73]. It is still almost exclusively used to prepare gas-phase ions in ionization mass spectrometry and for laser plasma X-

ray generation. However, Yogi et al. have used a similar method to realize a microarray of rhB molecules [74]. The difference with electrospray relies on the use of a pulsed-field to create on-demand droplets. Their droplet spotter permits the creation of pico- to femtoliter droplets from a glass capillary by using 1000 V and 10 ms pulse voltage (Figure 1.14). Recently, an electrospray ionization source based on a rectangular capillary slot, rather than a tube, has been presented [75]. This geometry is very interesting as it is compatible with the features that can be created when micromachining thin films. Thus new sources can be made out of silicon or polysilicon, enabling the fabrication of multiple in-plane sources on the same chip for parallel deposition. The same research group has also used FIB etching to create a nanofluidic capillary slot in the silicon source, as shown in Figure 1.15 [76,77]. The reduced dimensions of the capillary lead to the creation of droplets with nanometric diameters at reduced voltages. However, these silicon-based sources have not yet been used for surface patterning. Finally, it is important to notice that nanofibers can be fabricated with a similar field-assisted method. Instead of using liquid sources and capillary tubes, near-field electrospinning relies on the use of polymers and solid tips, respectively [78]. Applying a high voltage to the tip provokes the formation of a charged jet of polymer (Figures 1.16a and 1.16b). These results are particularly interesting as polymer fibers are difficult to obtain and pattern by other means. The electrospray technique is thus very attractive to deposit minute amounts of liquid; however, it requires complicated apparatuses and the generation of high-voltages to operate.

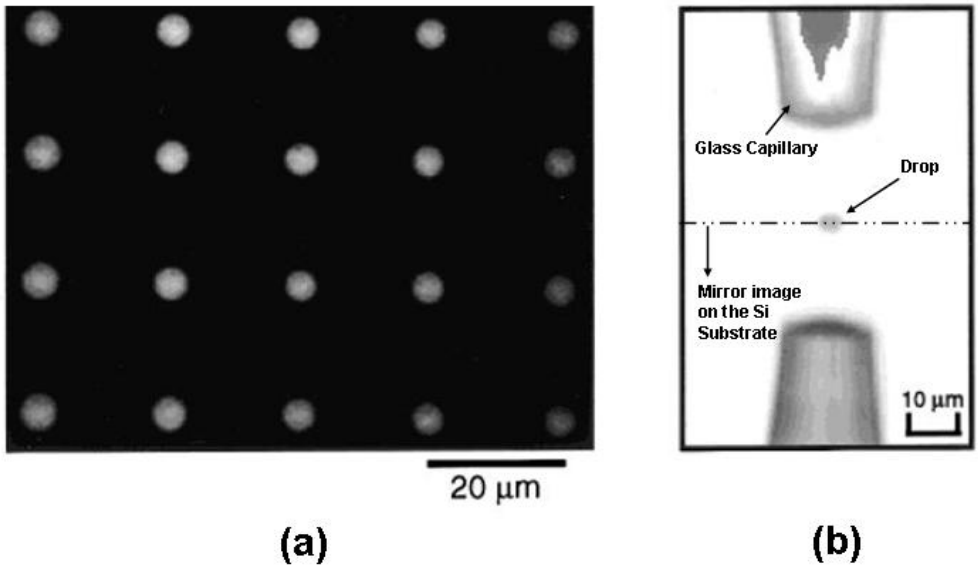

Figure 1.14: *(a) Microarray of rhB molecules deposited by the pulsed-field spotter and (b) side-view video image of a droplet of rhB solution in water after deposition [74].*

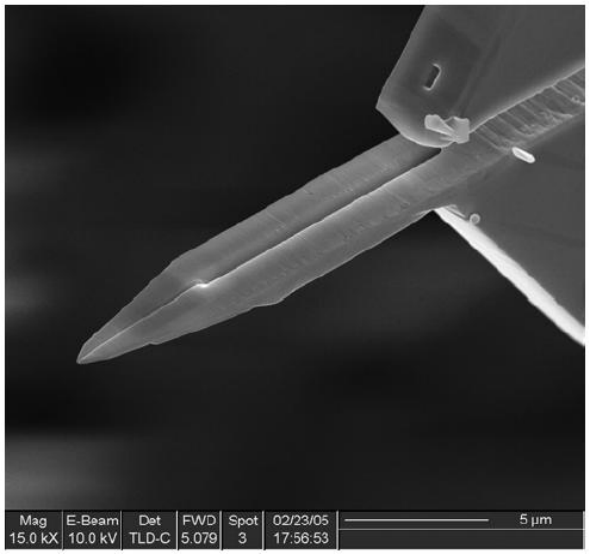

Figure 1.15: *SEM picture of a nanofluidic capillary slot fabricated by FIB etching [77].*

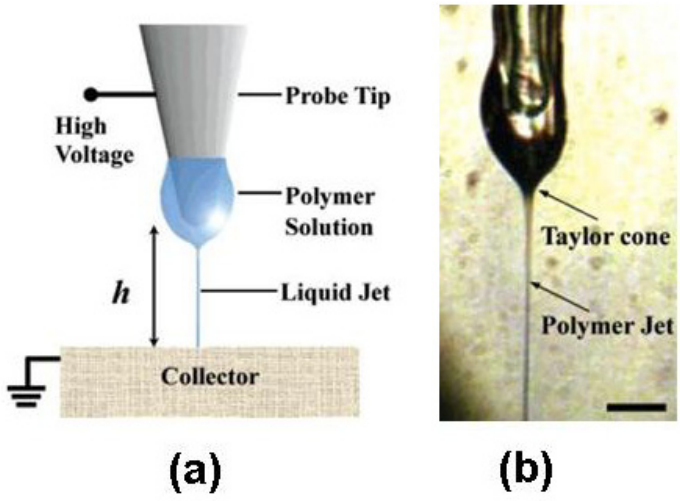

Figure 1.16: *(a) Principle of near-field electrospinning and (b) picture of a polymer jet ejected from the apex of a Taylor cone under applied electric field (scale bar is 25 µm) [78].*

5.1.3. Ink-jet printing

Ink-jet printing is a mature technology that is used in most commercial and professional computer printers. It is fairly inexpensive, pretty fast and many printers can produce high quality outputs. The original continuous jet printers used electrostatic plates to deflect an uninterrupted liquid jet on the surface to print or a reservoir for recycling, but these systems have largely been supplanted by drop-on-demand printers.

The ink-jet principle of operation is based on the ejection of liquid droplets from a chamber through a nozzle. In drop-on-demand systems, there are usually two means of expelling the drop. Either a heater is used to create a bubble in the closed chamber or a piezoactuator is used to compress the chamber until the liquid is propelled out of the nozzle. Piezoelectric ink-jet printing is usually more reliable in terms of jetting precisions and controlled volumes [79]. It allows printing a wider range of inks, as thermal ink-jet relies solely on water-based inks. Ink-jet has been lately used in surface patterning because of its low-cost, ease-of-use and flexibility regarding the variety of materials that can be deposited. Sol-gel materials, conducting polymers, epoxies, ceramic powders, nanoparticles and metals have been used for the fabrication of hybrid lenses, organic LEDs, organic transistors, solder bumps (see Figure 1.17a) for packaging applications and so on [80-83]. An interesting feature of ink-jet is the possibility to print liquids into polymer matrices. This enables the fabrication of complex 3D structures, e.g. sintered molds for metal casting, and the preparation of tablets with graded pharmaceutical contents to give predictable release profiles. Ink-jet printing is especially very promising for the deposition of biological compounds. DNA and proteins can be printed without alteration for the fabrication of functional bioarrays [84,85]. Xu et al. were able to print mammalian cells and showed that 90% of the deposited cells were not damaged during the nozzle firing [86]. These results will surely find interest in tissue engineering and cell culture. Another important use of ink-jet technology consists in functionalizing fragile MEMS structures, such as cantilever-based biosensors (Figure 1.17c) [87].

Other ejector devices have been recently proposed as an alternative to ink-jet print heads. For instance, Kang et al. have developed a microinjector using a microheater array for adjusting the ejected drop volume from 12 pL to 55 pL [88]. Demirci has proposed an interesting technique that relies on the use of acoustic waves generated in a liquid pool to eject drops from small apertures [89,90]. This technique avoids either the liquid heat or pressurization inherent to conventional ink-jets. It has been so far used to eject photoresist and etchant droplets. In addition to its proven versatility, the parallelization of ink-jet is straightforward and it can benefit from mass-fabrication techniques resulting in low-cost devices [91].

However, the drawback of ink-jet technology mainly concerns the requirement of inks with specific properties. Indeed, ink-jet is very sensitive to nozzle clogging, due to the solvent drying or particles aggregation, and to drop dripping. Thus the ink must satisfy combinations of a viscosity low-enough for droplet ejection and a surface tension high-enough for holding the liquid in the nozzle. Moreover, when printing inks that contain particles (of given size and surface properties), one must carefully select the particle concentration and the type of solvent avoiding any aggregation. The uniformity of the printed features is also a big concern because the formation of pinholes can easily occur. However, Bietsch et al. have recently proved that high quality SAMs could be patterned [92]. One can wonder to what extent the reduction in feature size can be achieved, as the smaller the expelled droplet is the more energy is required to overcome surface tensions corresponding to the formation of a drop with a

high surface to volume ratio. While droplet diameters can decrease from the current 20-30 µm, the constraints arising from viscous flow through a small hole seems to make unlikely the direct printing of features smaller than 10 µm [81].

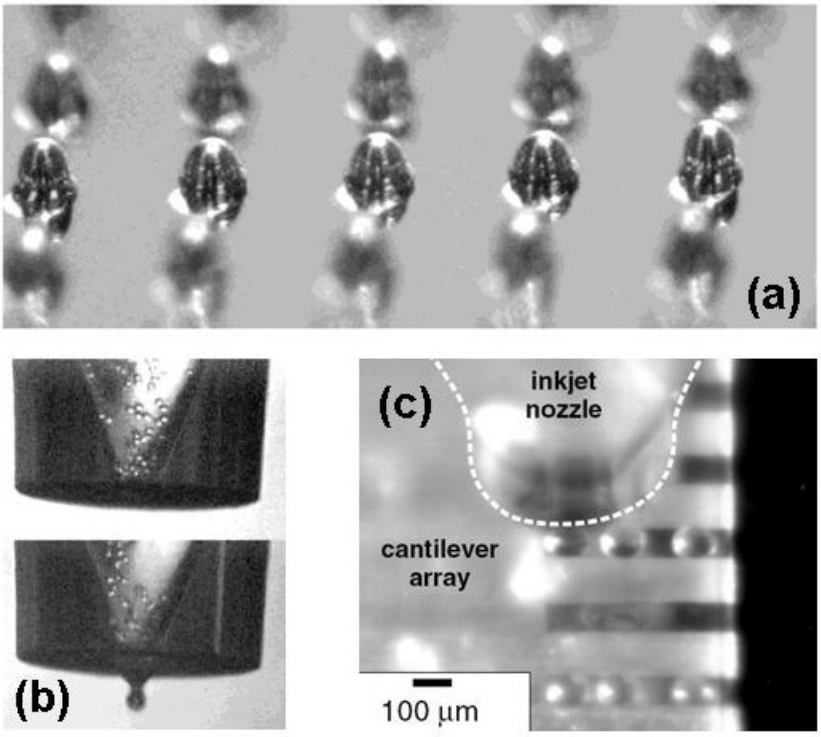

Figure 1.17: *(a) 100 µm solder drops placed onto 250 µm pitch pads at a rate of 400 s^{-1}, and (b) human liver cells being jetted in a phosphate buffer [81]. (c) Ink-jet printing of individual droplets onto a cantilever array [87].*

5.1.4. Capillary-free jetting mechanism

The capillary-free jetting technique, proposed by Barron et al., is based on the use of a focused laser pulse to transfer material from a target support onto a substrate [93]. The target support comports microwells filled up with the material to deposit. The laser hits the back of the target at a location of a specific well, inducing the heat-up of the material via a laser absorption layer, and leads to the formation of a jet. The jet breaks up into a droplet that is projected onto the substrate. Several spot diameters can be achieved by adjusting the laser fluence. This technique has been successfully used to fabricate BSA protein arrays. Immunoassays with anti-BSA have been carried out, demonstrating the immunoreactivity of the proteins. This result shows that the energy transfer induces little heating. Capillary-free jetting has the potential to be extremely well-suited for protein array applications. Indeed, because protein solution can be highly viscous, can adhere to a variety of surfaces and tend to agglomerate at high concentration, their deposition can be problematic with ink-jet and quill-pin

technologies. However, up to now, the application of the capillary-free jetting mechanism has been only demonstrated for the patterning of proteins and cells.

5.2. Ink delivery by contact methods

In contact methods, a solid tip or the extremity of a capillary touches the surface to pattern, allowing species to be transferred or liquid drops to be deposited, respectively. The advantages of having a direct contact between the patterning tool and the surface are numerous. First of all, because the transfer occurs thanks to capillary forces acting on the liquid, the contact method is a passive delivery technique. Thus there is no need for liquid actuation means and tools are greatly simplified. Sensors can be incorporated to the tool itself to have a direct control of the deposition process and direct information on the tool position. However, this method depends greatly on the physical and chemical states of the surface to pattern.

5.2.1. Micro- and nanopipettes

Pipettes can be used in contact mode for the local deposition of liquids. Any capillary in contact with a surface, providing the substrate is not too hydrophobic, leads to the formation of a drop. The ultrasonic pipette, presented in the previous section and designed for non-contact operation, has been used in contact mode [71]. Because of the passive nature of liquid transfer, the actuation system, i.e. the ultrasonic vibrations, is only used for the control of the delivered volume. A very interesting patterning solution relying on the use of a double-barrel nanopipette, fabricated from a glass capillary, has been recently presented [94]. The main strength of this method is the ability to deliver independently two different species from each barrel of a single tip. The use of electrodes placed inside each barrel enables the selection of the depositing barrel and the voltage control of deposition parameters such as the distance between the tip and the surface and the volume of liquid delivered. Moreover, it has been demonstrated that volumes could simply be added to an existing droplet with this tool, as shown in Figure 1.18. Microfabricated tools that mimic the capillary pipettes have been also lately introduced [96]. They consist in silicon or polymer tubes arranged on a surface. Liquid is provided on one side of the device, and flows into the tubes to reach the depositing surface. These tools have several advantages over conventional pipettes. The tube inner and outer diameters, which control the size of the deposited drop, can be fabricated with high precision and can exhibit very small dimensions. Moreover, the microfabrication approach easily allows the parallelization of the deposition technique, as several tubes can be fabricated on the same device. However, these tubes are usually not flexible and can not undergo large stresses and strains, thus microfabricated pipette arrays have to be very carefully operated. Alignment with pre-fabricated patterns can also be an issue.

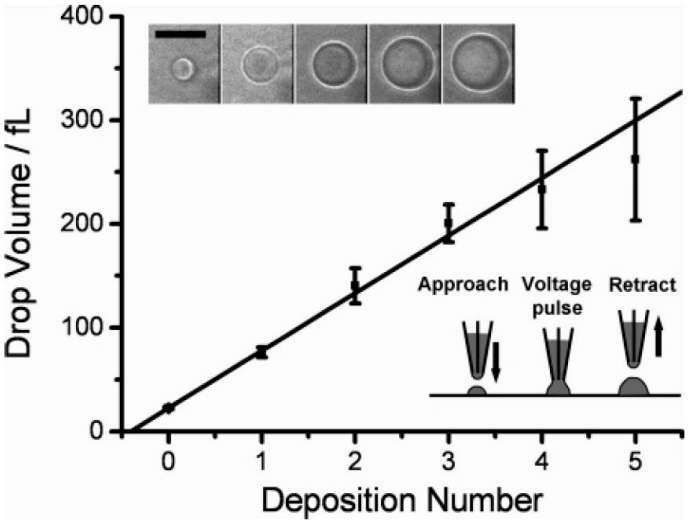

Figure 1.18: *Linear fit to the increase in drop volume deposited subsequently with the double-barrel nanopipette [95]. The top inset shows representative optical images of an initial drop and its increasing size with four subsequent addressing pulses (scale bar is 5 µm). The bottom inset shows the process of sequential addressing of a droplet.*

5.2.2. Scanning probe lithography

Scanning probe techniques are based on atomic force microscopy, for which silicon cantilevers with sharp tips are scanned across a surface to create an image of the surface topography with nanometric precision. The original idea of the scanning probe lithography (SPL) technique is to use the cantilever tip to deposit chemical and biological materials. The interesting feature of SPL is that the same tip can be used to write patterns and to image them. SPL methods take advantage of the high resolution of AFMs resulting so far in the minimum feature sizes patterned by add-on processes (sub-100 nm). This high resolution is balanced by the long writing times necessary to pattern microareas. There are two approaches in SPL techniques, detailed hereafter.

5.2.2.1. Dip-pen lithography

Butt et al. have first demonstrated the use of a scanning force microscope (SFM) tip to deposit organic material [97]. In their experiments, a SFM tip was covered with octadecanethiol (ODT), by dipping it into liquid ODT, and then brought into contact with a mica surface. Upon contact with the surface, ODT was transferred from the tip onto the surface. This technique has been further developed (and popularized) by Mirkin under the name dip-pen nanolithography (DPN) [98]. In this technique, the ink loaded onto the AFM tip is delivered to the substrate via a water meniscus that forms between the tip and the surface (see Figure 1.19). This meniscus serves as a medium for ink transport with nanometric precision and is thus fundamental for the success of ink delivery. This requires working in a suitable humid environment with enough water vapor to allow proper condensation on the tip. Importance to control the humidity level is necessary for reproducible patterning results [99]. DPN has been initially used to

pattern alkylthiols (e.g. MHA and ODT) onto gold films with an overwriting capability and a 15 nm resolution [100,101]. Its writing potential has rapidly been extended to numerous SAMs and surfaces (e.g. HMDS on semiconductor surfaces [102]), allowing the indirect patterning of bigger entities. The indirect method consists in firstly patterning the surface with functional chemistry via DPN to generate a template for the subsidiary grafting of colloids [103,104], DNA strands [105,106] or proteins [107-109]. Because only the template fabrication is carried out locally (unlike the immobilization procedure), it is difficult to produce patterns of different compounds on the same surface. For this purpose, the direct patterning of large molecules has been demonstrated. DNA and proteins, adsorbed on tips, have been deposited without altering their biofunctionality [110-112]. Thanks to the rising attention paid by the scientific community to DPN and the increasing research work focusing on that subject, the direct patterning of a lot of other materials have been investigated: nanoparticles, metal-salts, sol-based inks, colored inks and polymers have been successfully used targeting various applications [113-116].

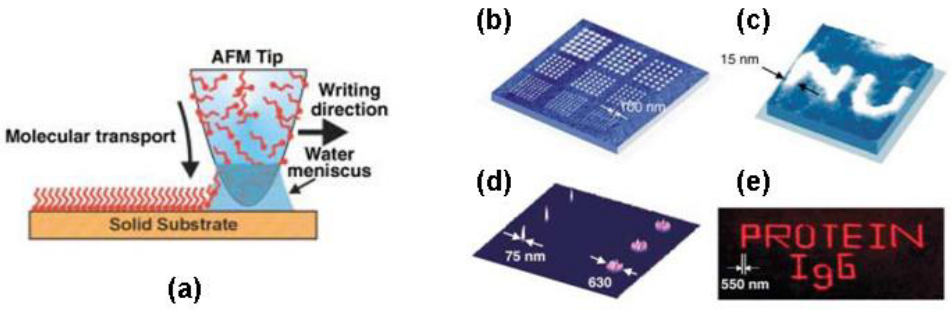

Figure 1.19: *Dip-pen lithography, principle of operation and fabricated patterns [98]. (a) Schematic representation of the DPN process. (b) Nanoscale dot array written on a polycrystalline Au surface with MHA. (c) Nanoscale letters written on an Au (111) surface with MHA with DPN. (d) AFM image of 25- and 13-nm gold nanoparticles hybridized to surface DNA templates generated with direct-write DPN. (e) Fluorescence image of direct-write DPN patterns of fluorescently labeled immunoglobulin G (IgG) on* SiO_x.

Several recent feature enhancements added to DNP promise to extend its functionality. For instance, the possibility to carry out electrochemical reaction by using the conductive tip as the working electrode was lately explored. Electrochemical DPN has been used to deposit platinum, to oxidize the surface, or to change the local surface chemistry [117-119]. Moreover, by heating the tip, Sheehan et al. have succeeded in depositing continuous metal nanostructures and solid inks [120,121]. However, the most important improvement is the integration of thermal actuators in order to control the bending of the cantilever, i.e. the height of the tip related to the depositing surface [122]. Because AFM tips are fabricated with standard micromachining processes, the fabrication of numerous DPN on the same chip is easily achievable [123], and force sensors can be integrated to the cantilevers. The possibility to address each cantilever of an array is an essential characteristic to produce arbitrary features and to control the

writing process. DPN is a tool ideally suited for nanofabrication and shows great promise for fundamental research seeking better understanding of phenomena at the nanoscale and technological breakthroughs. Because of the size of the tip and the writing process, deposited volumes can only be small and the coverage of micrometric areas leads to very long process times [124].

5.2.2.2. Scanning probe contact printing

In scanning probe contact printing (SPCP), the cantilever tip is made of an elastomeric material (a tip is shown in Figure 1.20). It is used to print chemicals onto surface analogously to a microcontact stamp. The tip is usually made of PDMS and the dimensions of the tip can be controlled during the fabrication of the cantilever. The initial fabrication process of these tips was proposed by the Mirkin group [125], and a simpler fabrication approach, developed by NanoInk Inc., consists in dip-coating the tip of a regular AFM cantilever with PDMS [126]. In SPCP, a chemical ink is firstly absorbed into the PDMS tip. Each contact of the tip on the surface leads to the transfer of molecules onto the surface and creates a pixel print. Arbitrary patterns can thus be formed in a dot-matrix manner. Unlike DPN, SPCP can be operated at ambient conditions and features are inherently larger. Thus it can be considered as a brick bridging the gap between: i) the lower resolution but massively parallel μCP method and ii) the higher resolution but lower throughput DPN process.

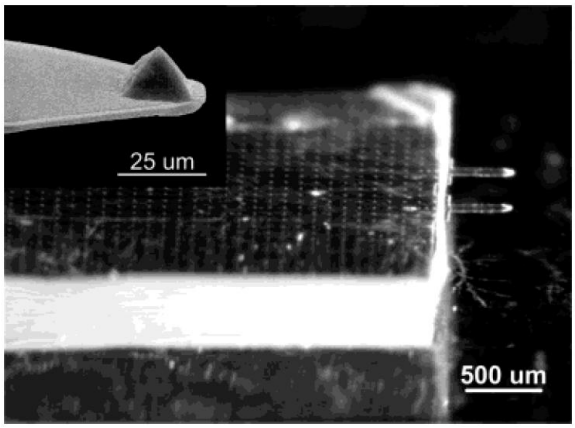

Figure 1.20: *Optical micrograph of a probe chip having two SPCP probes. The inset shows a SEM picture of the integrated PDMS tip on a cantilever [125].*

Because both DPN and SPCP techniques rely on the use of AFM probes, they can all be integrated on the same chip, including printing and imaging capabilities. Wang et al. have demonstrated the fabrication of such an integrated device (displayed in Figure 1.21), with probes being able to perform a dedicated function [127]. To take advantage of the combination of different tools, thermal electric actuators have been integrated to each cantilever, allowing an individual addressing. This multifunctional probe array is therefore capable of performing a rich variety of operations with minimal chemical crosstalk and high registration accuracy. It is extremely well-suited for the

fabrication of nanometer scale patterns with high resolution and in situ characterization means. However, inherently to the dip-pen and SPCP principle of operation, only small areas can be patterned in a time consuming process. Moreover, because of the tiny amount of ink material that a probe can carry, writing steps must often be alternated with necessary reloading procedures.

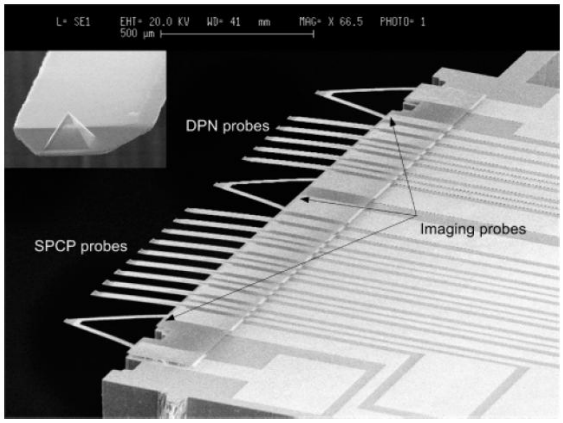

Figure 1.21: *SEM micrograph of a multifunctional probe array including 5 DPN probes, 9 SPCP probes and 3 imaging probes [127].*

5.2.3. Nanofountain pen based on modified AFM tips

In order to extend the printing capability of AFM-based techniques, a fluidic capillary and a liquid reservoir can be added to the cantilever tip. This trick offers the main advantage to solve the issue of the rapid ink depletion observed with dip-pen and SPCP. For this purpose, Lewis et al. have proposed a nanofountain pen system based on the use of cantilevered quartz micropipettes mounted onto the probe of an AFM [128]. They have previously demonstrated that these cantilevered pipettes could be used as a force sensing microscope for scanning microscopy with high resolution [129]. The deposition of different materials has been carried out with this system: local delivery of chromium etchant for mask repair applications [128], local printing of proteins [130], and formation of polymer droplets for microlenses fabrication [131]. However, despite its interesting capability, this system is not suited for parallelization and integration.

Lately, a very promising approach has been proposed within the NaPa framework by Meister et al. to overcome these drawbacks. The key feature of their nanodispensing system (NADIS) is the deposition of liquids through apertured scanning force microscope probe tips. The first probes were fabricated using a dedicated process allowing the creation of an open reservoir on top of the cantilever with a nanochannel at the apex [132]. An alternative fabrication method relying on the modification of commercial AFM tips by FIB milling (see Figure 1.22) has also been proposed [133]. Nanodrops of 20 nm polystyrene particles were deposited with this system. The open reservoir on top of the cantilever raises two important issues. The loading of the cantilever is very delicate, and giving the small volume of the drop reservoir, only liquids with a low evaporation rate can be used as solvent mediums. Hence, Deladi et al. have recently fabricated a cantilever with a close channel allowing a continuous liquid

supply to the cantilever tip (Figure 1.23) [134]. Kim et al. presented a similar device that was used to pattern 40 nm wide lines of MHA on gold substrates [135]. The same volcano tip (shown in Figure 1.24) was used to write and successfully image the patterns. However, these closed-channel configuration tools can experience clogging, thus leading to a failure to write. Besides, simple cleaning procedures are difficult to foresee. Still, these devices can benefit from the advantages of using microfabricated cantilevers (listed for the SPL tools).

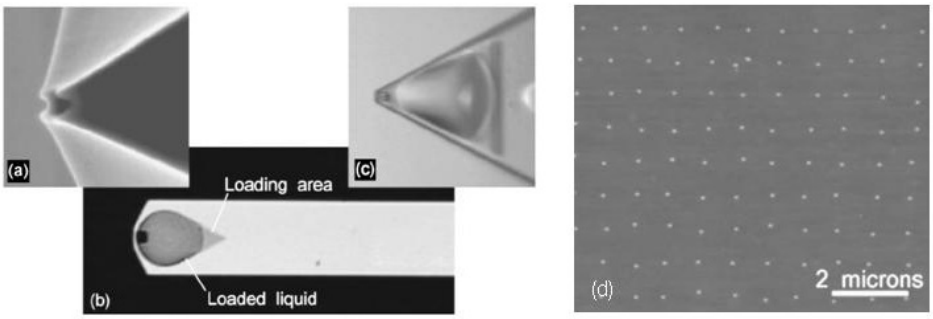

Figure 1.22: *NADIS dispensing tool fabricated by FIB etching [133]. (a) SEM of a tip with a 200 nm aperture at its apex. (b) Optical photograph of a cantilever with the loading area partially filled with liquid. (c) Close-up view of the loading area. (d) Topographic tapping AFM micrograph of an array of dots made of the nonvolatile residue formed after the evaporation of glycerol droplets deposited by NADIS.*

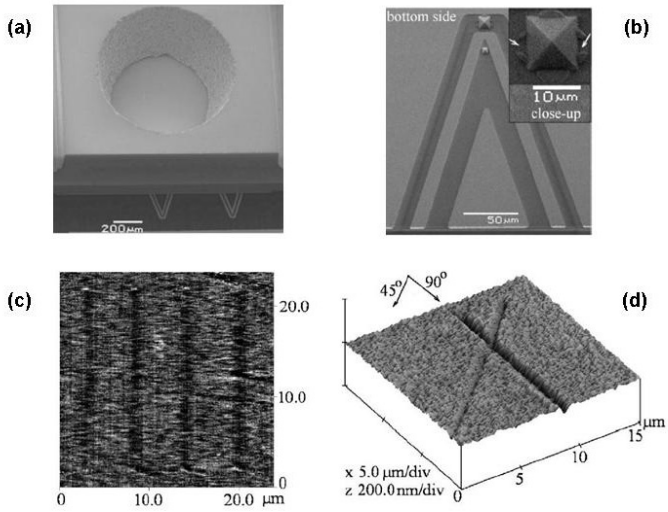

Figure 1.23: *Micromachined fountain pen (MFP) [134]. (a) Fabricated MFP with one inlet reservoir for the channels in the V-shaped cantilever. (b) Bottom view of a MFP with a close-up view of the tip (outlet holes are shown with arrows). (c) Friction image of patterns generated with ODT on a gold sample. (d) Lines etched with chromium etchant directly deposited with MFP on sputtered Cu.*

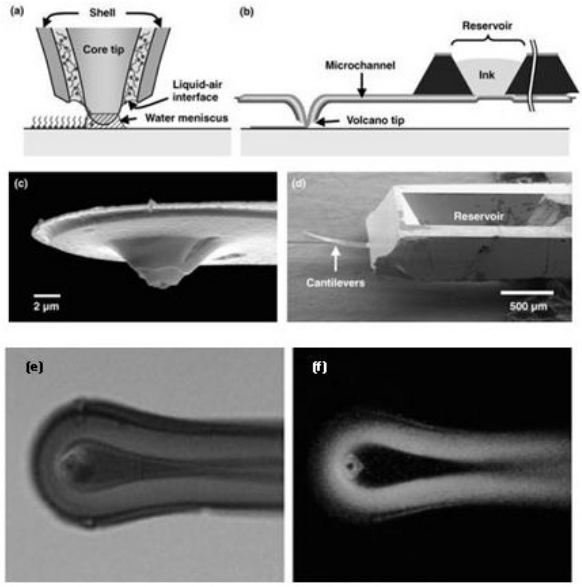

Figure 1.24: *Nanofountain probe (NFP) [135]. (a), (b) Writing mechanism of the NFP device. (c), (d) SEM images of a volcano dispensing tip and an on-chip reservoir. Flow test with a fluorescent solution: (e) transmission optical photograph with empty channel, (f) transmission fluorescence photograph showing the liquid in the fluidic channel.*

5.2.4. In-plane microcantilevers for liquid delivery

Recently, direct liquid delivery techniques inspired from the stainless steel pins currently used to fabricate biochips have been proposed. Systems based on commercial quills and pins allow printing spots with 60 µm diameters [136]. The needles are machined in a serial fashion and are usually very expensive. Besides, because the pins are made of stainless steel and the deposition occurs by a direct contact of the pin tip with the surface, the tips are easily damaged, causing inconsistent drop sizes. Finally, parallelization can only be obtained by manually placing several needles on the same support (as shown in Figure 1.25).

The idea of using silicon microcantilevers as printing pins has emerged from Bergaud and its team at LAAS-CNRS [137] quickly followed by other research groups in the U.S.A. [138,139], leading to very similar devices (Figure 1.26). This idea offers several advantages: thanks to the microfabrication techniques, arrays of cantilevers can be realized on the same chip resulting in cheap and disposable devices. Due to the micrometric precision of photolithography, these cantilevers can be made very small, enabling the deposition of smaller droplets, typically with diameters of several tens of micrometers. Unlike the dip-pen technique, the tip used for liquid transfer is in the plane of the cantilever, and can directly be fed by a fluidic system placed on top or in the cantilever. Usually the fluidic system consists in an open channel etched in the cantilever, thus solving any clogging issue (however this usually requires one to work with low evaporation rate solvents). The size of the channel is usually large enough to allow printing hundreds of spots without reloading the cantilever that can be thus loaded

with an external chip. However, a liquid reservoir can also be incorporated on the chip bearing the cantilevers. Similarly to DPN, the droplet size is controlled by the contact time between the tip and the surface, but deposited volumes are much bigger. Because the targeted application of these devices is the fabrication of biochips, they have only been so far used to print DNA or proteins. These cantilever pins are very attractive for the delivery of picoliter droplets because of their simplicity and low-cost, however, the deposition of other materials needs to be carried out to prove their versatility.

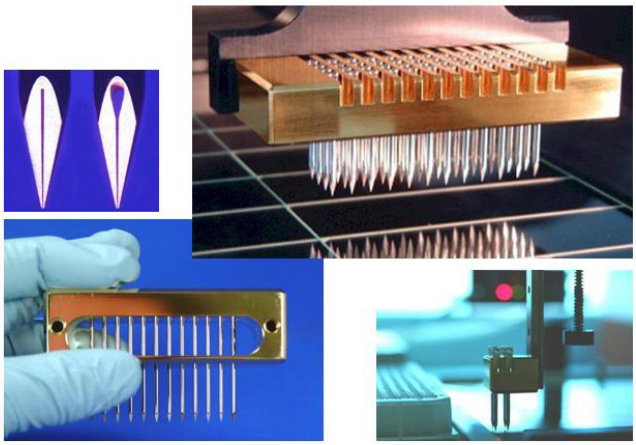

Figure 1.25: *Pictures of a commercial spotting system for biochip fabrication [136].*

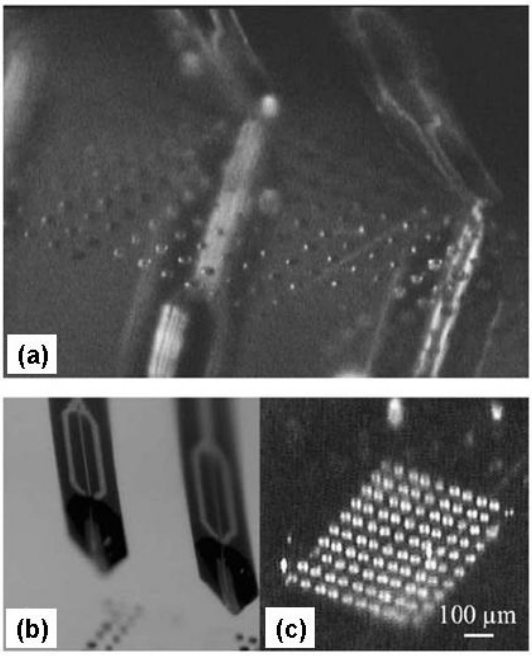

Figure 1.26: *Spotting system developed at LAAS-CNRS. (a), (b) Two silicon-based microcantilevers during the deposition process. (c) Resulting spots on a glass slide.*

5.3. Summary

The direct writing tools based on liquid delivery propose an interesting alternative way to pattern a wide range of materials by add-on processes. Unlike other direct writing techniques, most of them are simple to operate and offer in situ controls during the deposition at a low cost. These tools cover a wide range of printed feature sizes, and are all very complementary because they exhibit different specificities. Table 1.1 summarizes the characteristics of some of the above-mentioned direct patterning tools. This table provides elements of comparison and is to be used to choose the best-suited tool for a given application. However, it is necessary to keep in mind that this choice results in tradeoffs between the desired characteristics: high resolution is not compatible with high writing speed!

Tool	Ultrasonic pipette	Electrospray	Ink-jet	Dip-pen	Nano-fountain pen	In-plane cantilevers
Type	Non-contact	Non-contact	Non-contact	Contact	Contact	Contact
Environment	Atmospheric conditions	Atmospheric conditions	Atmospheric conditions	High Humidity	Atmospheric conditions	Atmospheric conditions
Resolution/ Volume	>10 µm 1-2 pL	5 µm 30 fL	>20 µm 10 pL	15 nm X	70 nm 1 aL	10 µm <1 pL
Deposited Area	Very large (>10 cm²)	Large (>1 cm²)	Very large (>10 cm²)	Very small (≈ mm^2)	Very small (≈ mm^2)	Large (>1 cm²)
Deposition rate	>10^5 drops/s ejected	<100 drops/s	<10^3 drops/s	Very low	2 drops/s	>10 drops/s
Volume available	Very large	Very large	Very large	X	Very small (>100 al)	Small
Materials	Acetone Water	Water Dye solution Polymers	Polymers Particles Biological solutions Cells	SAMs Biological entities Particles	SAMs Particles	Biological solutions Polymers
Substrates	No restriction	?	No restriction	Very flat surface	Very flat surface	Flat surface
Controls	Volume ejected	Volume ejected	Volume ejected	Force	Force	Force
In situ characterization	X	X	X	AFM	AFM	X
Pros	- High speed drop ejector	- Si-based tips very promising	- Mature technology - Available on market - Simple - Inexpensive - Parallel	- Mature technology - Available on market - Electro-chemistry - Parallel	- Parallel - Resolution	- Parallel - Inexpensive - Simple - Disposable
Cons	- Fragile - Bulky - Not parallel - Alignment	- H-voltage - Complex apparatus - Alignment	- Accuracy - Alignment - Limited viscosities	- Very slow	- Slow	- H-boiling point solvent required

Table 1.1: *Overview of the characteristics of some of the liquid-based direct patterning tools.*

5.4. Toward a highly functional micro dispensing system: Bioplume

There is obviously a gap that needs to be addressed between the resolution of tens of micrometers offered by fast direct writing techniques, such as ink-jet printing, and the nanometer scale resolution offered by slow processes, such as SPL tools. We believe that this gap can be filled by silicon pins because they are suitable to a further size reduction and they still allow depositing consequent amounts of materials. Thus they are perfectly suited for the fabrication and the functionalization of the next generation of highly integrated biochips and biosensors, respectively. Moreover, silicon pins combine numerous advantages over other presented techniques, i.e. the ease of implementation, the possible parallelization and the incorporation of sensors for position and deposition controls. However, work remains in order to demonstrate the extended capabilities of these devices in terms of function integration and range of materials deposited. In this thesis we propose to design, fabricate and prove the functionality and versatility of an in-plane cantilever liquid delivery method with enhanced functions. Because silicon pins show great promise for bioarray application and surface functionalization, we choose to put our attention on the following added features:

- Incorporation of force sensors for position monitoring and deposition control
- Proposition of an active loading scheme of the fluidic channel to reduce wasted material
- Implementation of an electrospotting means to allow performing local electrodepositions of materials

Along with these optimizations, we prove the downsizing possibilities and the flexibility to work with other materials, i.e. colloids, metals and polymers, in order to bring this tool to a mature and competitive level. In addition to be ready to use for specific applications, we aim to show that this deposition technique is a promising tool for the fundamental study of electrochemical or self-assembly phenomena in picoliter and femtoliter volumes, at the micrometer scale.

6. Conclusion

Technology today is an essential part of our economic, physical and societal environment, and its importance will continue to increase. Within the past 40 years, the transformation of scientific knowledge into commercial products has reached a pace unimaginable in the 1960s. This involves a transfer of basic scientific knowledge into products. There is now a worldwide agreement that science and technology at the micrometer and nanometer scales will revolutionize and transform information technology, biotechnology and materials technology. Scientific and technological advances in physics, molecular biology, chemistry, engineering and computer science today are all emerging from science at small scales. Patterning methods, enabling to structure and functionalize surfaces, is foreseen to play a major role for the future technological developments. The study of novel materials and understanding phenomenon on a small scale is also a prerequisite for new technological breakthroughs. More than to be only dedicated to industrial production, patterning techniques have the capability to be powerful research tools.

The variety of existing techniques that are now available allows patterning a wide range of materials by different means, with specific feature sizes and resolutions. The cost and time of processing also differ a lot from one tool to another. This variety of tool characteristics and application requirements results in the need to select the most appropriate technique for a given application. To satisfy the increasing interest in biology and the need for inexpensive and easy-access direct writing tools for research environments, new methods based on the local delivery of liquid are a promising solution. The direct contact patterning tools relying on the use of silicon cantilevers exhibit very interesting advantages: disposable and cheap devices are inherent to the fabrication techniques, tool parallelization is straightforward, and incorporation of in-situ position monitoring and deposition controls is possible. Implementation of deposition via electrochemistry is also feasible as the liquid meniscus bridging the tool to the surface can be used as a support medium for induced reactions. This advanced function is a key to print new materials in a controlled fashion.

Because the feature sizes addressed by the current tools are either several tens of micrometers or tens of nanometers, there is a micrometer gap to be filled. We thus propose in this thesis to design, fabricate and test an improved liquid delivery tool able to print micrometer size droplets. The goal is to extend the versatility and functionality of silicon devices inspired from stainless steel pins. By varying the nature of the liquid, various applications can be envisioned, such as the production of bioarrays by using protein solutions, rapid prototyping by using etch resistant liquids or SAM materials, or nanoelectronics by using conductive liquids or suspensions of metallic nanoparticles.

References

[1] R. P. Feynman, Journal of Microelectromechanical Systems, 1 (1), p. 60 (1992).
[2] G. E. Moore, Electronics, 38 (8), p. 114 (1965).
[3] M. Lynch et al., Proteomics, 4, p. 1695 (2004).
[4] G. MacBeath, and S. L. Schreiber, Science, 289, p. 1760 (2000).
[5] C. G. Fathman et al., Nature, 435, p. 605 (2005).
[6] M. Wautelet, European Journal of Physics, 22, p. 601 (2001).
[7] S. Y. Chou et al., Journal of Applied Physics, 79 (8), p. 6101 (1996).
[8] G. M. Whitesides, Nature Biotechnology, 21 (10), p. 1161 (2003).
[9] http://www.er.doe.gov/bes/scale_of_things.html
[10] G. L.-T. Chiu, and J. M. Shaw, IBM Journal of Research and Development, 41 (1/2), p. 3 (1997).
[11] A. Dodabalapur, Materials Today, 9 (4), p. 24 (2006).
[12] R. V. Seidel, Nano Letters, 5 (1), p. 147 (2005).
[13] S. N. Cha et al., Applied Physics Letters, 86, 083105 (2005).
[14] B. E. A. Saleh, and M. C. Teich, "Fundamentals of photonics", 1st ed. John Wiley and Sons, Inc. (1991).
[15] H. Wong, Proceedings of the 23rd International Conference on Microelectronics, 12-15 May, 2002, Niš, Yougoslavia, vol. 1, p. 285 (2002).
[16] Z. Popovic, R. Sprague, and G. Connell, Applied Optics, 27 (7), p. 1281 (1988).
[17] P. Ruther et al., Pure and Applied Optics: Journal of the European Optical Society Part A, 6, p. 643 (1997).
[18] C. Croutxé-Barghorn, O. Soppera, and D. J. Lougnot, Applied Surface Science, 168, p.89 (2000).
[19] K. Naessens et al., Applied Optics, 42 (31), p. 6349 (2003).
[20] M. T. Gale, M. Rossi, and J. Pederson, Optical Engineering, 33 (11), p. 3556 (1994).
[21] D. J. Hayes et al., Proceedings of SPIE, vol. 4809 Nanoscale Optics and Application, p. 94 (2002).
[22] V. Bardinal et al., Proceedings of SPIE, vol. 6185 Micro-Optics, VCSELs, and Photonic Interconnects II: Fabrication, Packaging, and Integration, p. 618510 (2006).
[23] M. Di Ventra, S. Evoy, and J. R. Helfin, Jr., "Introduction to nanoscale science and technology", Springer (2004).
[24] M. C. Pirrung, Angewandte Chemie International Edition, 41, p. 1276 (2002).
[25] V. Espina et al., Proteomics, 3, p. 2091 (2003).
[26] M. Calleja et al., Ultramicroscopy, 105, p. 215 (2005).
[27] P. Guedon et al., Analytical Chemistry, 72 (24), p. 6003 (2000).
[28] H. Sota et al., Analytical Chemistry, 74 (15), p. 3592 (2002).
[29] R. F. Ismagilov, Angewandte Chemie International Edition, 42, p. 4130 (2003).
[30] R. H. Liu et al., Analytical Chemistry, 76 (7), p. 1824 (2004).
[31] V. Srinivasan, V. K. Pamula, and R. B. Fair, Lab on a Chip, 4, p.310 (2004).
[32] L. Feng et al., Advanced Materials, 14 (24), p. 1857 (2002).
[33] L. Zhang et al., Langmuir, 22 (20), p. 8576 (2006).
[34] W. F. Liu, and C. S. Chen, Materials Today, 8 (12), p. 28 (2005).
[35] C. M. Nelson et al., Molecular Biology of the Cell, 15, p. 2943 (2004).
[36] C. M. Nelson et al., Proceedings of the National Academy of Sciences of the United States of America, 102 (33), p. 11594 (2005).
[37] R. Thull, Materialwissenschaft und Werkstoffechnik, 22, p. 949 (2001).

[38] M. Geissler, and Y. Xia, Advanced Materials, 16 (15), p. 1249 (2004).
[39] A. Stephen et al., RIKEN Review, 43, p. 56 (2002).
[40] S. Wegscheider et al., Thin Solid Films, 264 (2), p. 264 (1995).
[41] A. Gölzhäuser et al., Journal of Vacuum Science and Technology B, 18 (6), p. 3414 (2000).
[42] S. Reyntjens, and R. Puers, Journal of Micromechanics and Microengineering, 11, p. 287 (2001).
[43] S. Kondo et al., Journal of Applied Physics, 78 (1), p. 155 (1995).
[44] G. Wittstock, and W. Schuhmann, Analytical Chemistry, 69 (24), p. 5059 (1997).
[45] D. M. Eigler, and E. K. Schweizer, Nature, 344, p. 524 (1990).
[46] A. Notargiacomo et al., Nanotechnology, 10, p. 458 (1999).
[47] S. Krämer, R. R. Fuierer, and C. B. Gorman, Chemical Reviews, 103 (11), p.4367 (2003).
[48] P. Vettiger et al., IBM Journal of Research and Development, 44 (3), p. 323 (2000).
[49] U. Srinivasan et al., Journal of Microelectromechanical Systems, 7 (2), p. 252 (1998).
[50] M. Achermann et al., Nano Letters, 6 (7), p. 1396 (2006).
[51] A. Kosiorek et al., Nano Letters, 4 (7), p. 1359 (2004).
[52] C. L. Cheung et al., Nanotechnology, 17, p. 1339 (2006).
[53] M. Schena et al., Trends in Biotechnology, 16 (7), p. 301 (1998).
[54] G. M. Kim, M. A. F. van den Boogaart, and J. Brugger, Microelectronic Engineering, 67-68, p. 609 (2003).
[55] C.-V. Cojocaru et al., Applied Physics Letters, 86, 183107 (2005).
[56] S. Egger et al., Nano Letters, 5 (1), p. 15 (2005).
[57] M. A. F. van den Boogaart et al., Journal of Vacuum Science and Technology B, 22 (6), p. 3174 (2004).
[58] Y. Xia, and G. M. Whitesides, Angewandte Chemie International Edition, 37, p. 550 (1998).
[59] S. Y. Chou, P. R. Krauss, and P. J. Renstrom, Applied Physics Letters, 67 (21), p. 3114 (1995).
[60] S. Y. Chou et al., Journal of Vacuum Science and Technology B, 15 (6), p. 2897 (1997).
[61] S. Y. Chou, C. Keimel, and J. Gu, Nature, 417, p. 835 (2002).
[62] Y. Xia, and G. M. Whitesides, Annual Reviews of Materials Science, 28, p. 153 (1998).
[63] A. Bernard et al., Advanced Materials, 12 (14), p. 1067 (2000).
[64] S. A. Lange et al., Analytical Chemistry, 76 (6), p. 1641 (2004).
[65] J. A. Rogers, and R. G. Nuzzo, Materials Today, 8 (2), p. 50 (2005).
[66] D. Juncker et al., Journal of Micromechanics and Microengineering, 11, p. 532 (2001).
[67] J. D. Gerding, D. M. Willard, and A. Van Orden, Journal of the American Chemical Society, 127, p. 1106 (2005).
[68] A. Meister, "Nanoscale dispensing of single ultrasmall droplets", Ph.D. thesis, Universität Basel (2004).
[69] D. B. Hager, and N. J. Dovichi, Analytical Chemistry, 66 (9), p. 1593 (1994).
[70] C.-H. Lee, and A. Lal, IEEE Transactions on Ultrasonics, Ferroelectrics, and Frequency Control, 51 (11), p. 1514 (2004).
[71] B. J. Larson, S. D. Gillmor, and M. G. Lagally, Review of Scientific Instruments, 75 (4), p. 832 (2004).

[72] J. Zeleny, The Physical Review, 3 (2), p. 69 (1914).
[73] M. Yamashita, and J. B. Fenn, The Journal of Physical Chemistry, 88 (20), p. 4451 (1984).
[74] O. Yogi et al., Analytical Chemistry, 73 (8), p. 1896 (2001).
[75] M. Brinkmann et al., Applied Physics Letters, 85 (11), p. 2140 (2004).
[76] S. Arscott, and D. Troadec, Applied Physics Letters, 87, 134101 (2005).
[77] S. Arscott, and D. Troadec, Nanotechnology, 16, p. 2295 (2005).
[78] D. Sun et al., Nano Letters, 6 (4), p. 839 (2006).
[79] N. Reis, C. Ainsley, and B. Derby, Journal of Applied Physics, 97, 094903 (2005).
[80] J. Bharathan, and Y. Yang, Applied Physics Letters, 72 (21), p. 2660 (1998).
[81] P. Calvert, Chemistry of Materials, 13 (10), p. 3299 (2001).
[82] B.-J. de Gans, P. C. Duineveld, and U. S. Schubert, Advanced Materials, 16 (3), p. 203 (2004).
[83] H.-H. Lee, K.-S. Chou, and K.-C. Huang, Nanotechnology, 16, p. 2436 (2005).
[84] T. Goldmann, and J. S. Gonzalez, Journal of Biochemical and Biophysical Methods, 42, p. 105 (2000).
[85] T. R. Hughes et al., Nature Biotechnology, 19, p. 342 (2001).
[86] T. Xu et al., Biomaterials, 26, p. 93 (2005).
[87] A. Bietsch et al., Nanotechnology, 15, p. 873 (2004).
[88] T. G. Kang, and Y.-H. Cho, Journal of Microelectromechanical Systems, 14 (5), p. 1031 (2005).
[89] U. Demirci, Applied Physics Letters, 88, 144104 (2006).
[90] U. Demirci, and M. Toner, Applied Physics Letters, 88, 053117 (2006).
[91] S. C. Chen et al., Sensors and Actuators A, 127, p. 241 (2006).
[92] A. Bietsch et al., Langmuir, 20, p. 5119 (2004).
[93] J. A. Barron et al., Proteomics, 5, p. 4138 (2005).
[94] K. T. Rodolfa et al., Angewandte Chemie International Edition, 44, p. 6854 (2005).
[95] K. T. Rodolfa et al., Nano Letters, 6 (2), p. 252 (2006).
[96] O. T. Guenat et al., Journal of Micromechanics and Microengineering, 15, p. 2372 (2005).
[97] M. Jaschke, and H.-J. Butt, Langmuir, 11, p. 1061 (1995).
[98] D. S. Ginger, H. Zhang, and C. A. Mirkin, Angewandte Chemie International Edition, 43, p. 30 (2004).
[99] M. Su et al., Langmuir, 21 (24), p. 10902 (2005).
[100] R. D. Piner et al., Science, 283, p. 661 (1999).
[101] S. Hong, J. Zhu, and C. A. Mirkin, Science, 286, p. 523 (1999).
[102] A. Ivanisevic, and C. A. Mirkin, Journal of the American Chemical Society, 123 (32), p. 7887 (2001).
[103] L. M. Demers, and C. A. Mirkin, Angewandte Chemie International Edition, 40 (16), p. 3069 (2001).
[104] X. Liu et al., Advanced Materials, 14 (3), p. 231 (2002).
[105] L. M. Demers et al., Angewandte Chemie International Edition, 40 (16), p. 3071 (2001).
[106] H. Zhang, Z. Li, and C. A. Mirkin, Advanced Materials, 14 (20), p. 1472 (2002).
[107] H. Zhang et al., Nanotechnology, 14, p. 1113 (2003).
[108] K.-B. Lee et al., Nano Letters, 4 (10), p. 1869 (2004).
[109] S. Woo et al., Advanced Materials, 18, p. 1133 (2006).
[110] J.-H. Lim et al., Angewandte Chemie International Edition, 42, p. 2309 (2003).

[111] S.-W. Chung et al., Small, 1 (1), p. 64 (2005).
[112] K.-B. Lee, J.-H. Lim, and C. A. Mirkin, Journal of the American Chemical Society, 125 (19), p. 5588 (2003).
[113] J. C. Garno et al., Nano Letters, 3 (3), p. 389 (2003).
[114] M. Su et al., Journal of the American Chemical Society, 124 (8), p. 1560 (2002).
[115] M. Su, and V. P. Dravid, Applied Physics Letters, 80 (23), p. 4434 (2002).
[116] A. Noy et al., Nano Letters, 2 (2), p. 109 (2002).
[117] Y. Li, B. W. Maynor, and J. Liu, Journal of the American Chemical Society, 123 (9), p. 2105 (2001).
[118] G. Agarwal, R. R. Naik, and M. O. Stone, Journal of the American Chemical Society, 125 (24), p. 7408 (2003).
[119] Y. Cai, and B. M. Ocko, Journal of the American Chemical Society, 127 (46), p. 16287 (2005).
[120] P. E. Sheehan et al., Applied Physics Letters, 85 (9), p. 1589 (2004).
[121] B. A. Nelson et al., Applied Physics Letters, 88, 033104 (2006).
[122] D. Bullen et al., Journal of Microelectromechanical Systems, 13 (4), p. 594 (2004).
[123] K. Salaita et al., Small, 1 (10), p. 940 (2005).
[124] J. R. Hampton, A. A. Dameron, and P. S. Weiss, Journal of Physical Chemistry B, 109, p. 23118 (2005).
[125] X. Wang et al., Langmuir, 19 (21), p. 8951 (2003).
[126] H. Zhang et al., Nano Letters, 4 (9), p. 1649 (2004).
[127] X. Wang, and C. Liu, Nano Letters, 5 (10), p. 1867 (2005).
[128] A. Lewis et al., Applied Physics Letters, 75 (17), p. 2689 (1999).
[129] K. Lieberman et al., Applied Physics Letters, 65 (5), p. 648 (1994).
[130] H. Taha et al., Applied Physics Letters, 83 (5), p. 1041 (2003).
[131] M. Sokuler, and L. A. Gheber, Nano Letters, 6 (4), p. 848 (2006).
[132] A. Meister et al., Microelectronic Engineering, 67-68, p. 644 (2003).
[133] A. Meister et al., Applied Physics Letters, 85 (25), p. 6260 (2004).
[134] S. Deladi et al., Applied Physics Letters, 85 (22), p. 5361 (2004).
[135] K.-H. Kim, N. Moldovan, and H. D. Espinosa, Small, 1 (6), p. 632 (2005).
[136] http://www.arrayit.com/
[137] P. Belaubre et al., Applied Physics Letters, 82 (18), p. 3122 (2003).
[138] J. G. F. Tsai et al., Proceedings of the 16th Annual International Conference on Micro Electro Mechanical Systems (MEMS'03), 19-23 Jan, 2003, Kyoto, Japan, p. 295 (2003).
[139] J. Xu et al., Biomedical Microdevices, 6 (2), p. 117 (2004).

Chapter II

Implementation of the Bioplume Liquid Dispensing System

1. Introduction

1.1. Background

There are numerous direct writing methods that allow patterning surfaces from scratch with various materials. Direct patterning tools that are based on the delivery of liquids are particularly attractive for applications involving biochemical compounds and nanoparticles in solutions. However, the main drawback of the direct writing technique is its serial nature. As a result, the printing process can be extremely time-consuming if the size of the printed patterns is much bigger than the tool feature size. Thus, to promote the versatility of the liquid delivery method and its competitiveness regarding other techniques, development of a number of tools is required in order to address various feature sizes, from the nanometer to the millimeter scale. In this chapter, we present a simple and mature tool based on the local delivery of liquids that creates controlled micrometer size patterns, thus suited for applications requiring more precision than ink-jet technology while able to deposit more material than dip-pen.

1.2. Presentation of the initial system

The LAAS deposited system, originally proposed by Bergaud and co-workers [1], is a direct patterning method inspired from stainless steel slit pins (currently used to fabricate biochips) that relies on the deposition of liquid drops on substrates. Analogously, droplet delivery occurs by a contact method between the tool and the surface to pattern, allowing liquid transfer by capillary forces. Unlike stainless steel quills, the LAAS tool consists of a silicon chip bearing pen-shaped microcantilevers. A simple PC-controlled automated motion stage is used to position the chip and execute the loading and deposition steps. Patterns are created from the superposition of deposited drops that act as liquid pixels.

The manufacture of the cantilevers is based on conventional microfabrication techniques which enable to realize cantilevers with micrometer dimensions for picoliter droplet deposition and chips with several cantilevers for parallel patterning. The other advantage inherent to the cantilever fabrication is the ability to fabricate multiple chips on a single wafer, thus lowering the cost of a single chip. This also permits the depositing chip to be disposable, i.e. to be changed between the deposition steps of different materials, if a risk of contamination is proscribed. Each microcantilever

incorporates a fluidic channel in its tip for liquid deposition. In order to avoid having a complicated fluidic system on the chip for liquid supply to the channel, the loading of the cantilever is carried out by external means. In addition, the cantilever can also bear a reservoir to increase the storage capacity and to allow depositing more spots without reloading. In order to facilitate the cantilever fabrication process and the possible cleaning of the fluidic system (allowed and more appropriate for some applications), the channel and the reservoir are open. This solves any clogging issue but raises evaporation problems that result in a decrease of liquid concentration with increasing number of prints. A high evaporation rate even prevents the deposition process to occur as no liquid remains in the channel by the time the chip is moved from the loading to the deposition point. Rather than working in a humid environment, a simple solution consists in adding high-boiling-point solvents to the deposited liquids.

1.3. Motivation for this work

The original deposited system described above, is compact, simple, and well-suited for low scale production, prototype manufacturing or post-processing steps (such as the functionalization of biosensors). However, it exhibits several drawbacks limiting its printing capabilities. In order to reach a mature state, it is important that the tool allows monitoring the cantilever position regarding the surface to pattern and controlling in situ the deposition process and the size of the printed drops. Also the printing versatility of the system, e.g. the possibility to deposit several entities in parallel, must be demonstrated. In this work, we propose to improve the initial LAAS depositing system by incorporating position sensors, as well as active loading and deposition schemes to the cantilevers. The main challenges we must face and the proposed technical solutions are described in the following section. Then, the design and the fabrication of the new generation of cantilevers, so-called bioplume, are introduced. After presenting the characterization results and the spotter implementation, this chapter ends with deposition tests aiming at proving the functionality of the developed system.

2. Challenges and solutions

2.1. Monitoring cantilever position and contact time and force during deposition

2.1.1. Significance

As the cantilevers are used in contact mode for the printing process, measurement of their bending provides information on important parameters during deposition, such as the contact time and force. It is necessary to control such parameters because the contact time influences the size of the printed droplets and the force exerted can prevent the printing process (if too low), or can lead to surface scratching (if too high). Moreover, measuring the cantilever bending can also be used to estimate the position of the cantilevers regarding the surface to pattern or the loading area. More generally, it provides alignment means via relative positioning. Such a detection scheme is particularly important when working with an array of cantilevers because non-uniform depositions occur when the array is not perfectly parallel to the surface (i.e. when the cantilevers do not contact the surface evenly). The trim of the array in relation

to the surface can simply be deduced and corrected by knowing the displacement of two cantilevers of the same array.

2.1.2. Detection methods

The rapid development of scanning probe techniques, such as atomic force microscopy (AFM), and the use of micromachined cantilevers as biosensors have led to the introduction of several displacement detection methods that allow measuring the bending of silicon microcantilevers with high sensitivity and resolution [2]. The most widespread method is the optical lever technique that relies on the reflection of a laser beam onto the cantilever [3]. The reflected beam hits a position sensitive photodetector and the bending of the cantilever is measured by the change of beam position on the detector. This method is highly accurate but necessitates the complex alignment of the optical devices and can not be integrated to the cantilever. It can be adapted to measure several cantilever displacements in parallel but requires precise knowledge and know-how because a beam and its optical setup are required for each cantilever. The capacitive sensors that measure the bending as a change in capacitance of a plane capacitor can be integrated and provides absolute displacement [4]. However, it is not appropriate to measure large displacements, and the fabrication process used to realize such devices can be complicated. Finally, piezoelectricity can be used to sense the bending of a cantilever by integrating piezoelectric materials into the cantilever beam [5]. Under stress conditions, i.e. the bending of the cantilever, an electric field is created inside the material and measurement of the voltage difference in the layer provides the cantilever displacement. This approach is very interesting and efficient, but requires specific knowledge and fabrication tools in order to integrate good piezoelectric materials on the cantilever.

2.1.3. Piezoresistive cantilevers

The variation of bulk resistivity with applied stress is known as the piezoresistive effect. A resistance made of piezoresistive material built onto a cantilever changes when the cantilever is stressed under displacement, providing a simple means to measure the bending [6]. The interesting advantage of this approach is that doped silicon exhibits a strong piezoresistive effect. Thus, the integration of a piezoresistor on the cantilever is simply achieved by adding a few fabrication steps. Moreover, measurement of the resistance change can be easily carried out with a Wheatstone bridge. Because piezoresistive elements are sensitive to light and temperature changes, stress measurement can be carried out by using a differential signal between a sensing cantilever and a reference one. Due to its numerous advantages and giving the fact that piezocantilevers have already been developed in our research group [7], the piezoresistive approach is the one selected for our application.

2.2. Parallelization of printed materials

The approach of using several cantilevers on a single chip for parallel deposition is relevant only if each cantilever can print a different material. The principal advantage is to lower the time of the overall deposition process by skipping numerous loading and

printing steps. The parallelization of printed materials can be achieved by loading each cantilever with a specific solution preferably in a single run. For this purpose, a loading fluidic chip must be associated with the cantilever chip. Such a delivery apparatus has already been proposed to simultaneously load an array of dip-pen [8,9]. This chip is an important link between the large volumes dispensed by manual pipettes and the small volumes used to load the microcantilevers. It must provide millimeter size fluidic inputs to load the chip with the different solutions and micrometer size outputs, i.e. inkwells, to allow liquid delivery to the cantilevers. In between, complex fluidic operations can be useful to address each cantilever with the desired fluid and have a possibility to change the delivered liquid without having to fully reload the chip. The choice of an external loading chip is dictated by versatility, a simple fabrication process and ease-of-use requirements.

2.3. Reduction of wasted material

Because the channel consists of two silicon walls facing each other (corresponding to a slit in the cantilever tip) with a square section and a rough and hydrophobic surface state (inherent to the fabrication procedure), the resulting capillary forces exerted on the liquid are too weak to induce any rise of a liquid column in the channel. Hence, the loading of the device is currently done by immersing the fluidic system (channel plus reservoir) of the cantilever in the liquid, requiring an important dead volume. In order to reduce this dead volume, an active liquid loading method must be incorporated to the cantilevers such that only the tip extremity has to contact the liquid during the loading process. The implementation of such a scheme has another advantage: it allows loading the required volume of liquid to be deposited, thus reducing some possible wasted liquid remaining on the cantilever after the printing process. Those are pertinent improvements when using biological solutions that are expensive or are only obtained in very small quantities. For its ease of implementation and use, as it does not require any mechanical moving parts, the electrowetting phenomenon is best appropriate for liquid actuation. Electrowetting consists in bringing electrostatic charges at a liquid/solid interface, resulting in a change of liquid contact angle thus modifying the spreading of the liquid [10]. This phenomenon is widely used on the microscale to move liquid droplets or columns on planar electrodes [11,12], and to induce the rise of liquid columns between a set of vertical electrodes [13]. In order to implement the electrowetting actuation scheme on the cantilevers, the channel walls must be electrically conductive. Actuation can then take place by applying a DC or low-frequency voltage between the walls and the liquid, resulting in liquid motion inside the channel.

2.4. Active control during deposition with electro-assisted methods

Liquid delivery by direct contact between the deposition tool and the substrate is a passive method governed by the spreading of the liquid onto the surface. Variation of contact time is usually used to adjust the size of the patterned area. However, this method strongly depends on the surface wettability, does not allow the three-dimensional (3D) control of the pattern and can be time-consuming [14]. Electro-assisted methods can provide an efficient active means for the control of the deposition process. First of all, as previously described, the electrowetting phenomenon can be

used to tune the contact angle of a drop onto a surface, thus leading to a change in contact area. The only prerequisite for this scheme implementation is to provide electrodes onto the surface and in the cantilever channel. With the same set of electrodes, redox reactions can be induced in an electrolytic drop used as an electrochemical cell. Electrochemistry is a powerful means to deposit or etch various materials allowing a precise control of the reactions by monitoring the number of charges supplied to the cell [15]. We believe that the incorporation of these electro-assisted methods to our deposition technique greatly enhances the printed performances without complicating much the fabrication process of the tool.

3. Design and fabrication of the bioplume chip

3.1. Design of the cantilevers

The geometry of the cantilevers developed in this thesis work is very similar to the first generation of cantilevers, i.e. it consists of a flexible beam ending with a sharp tip. The fluidic part of the cantilever comprises a slit that opens out into the extremity of the cantilever tip and a reservoir in the beam body. The main difference with the original design is the incorporation of a piezoresistor in the cantilever and a metal electrode in the channel. A schematic of the bioplume cantilever is displayed in Figure 2.1.

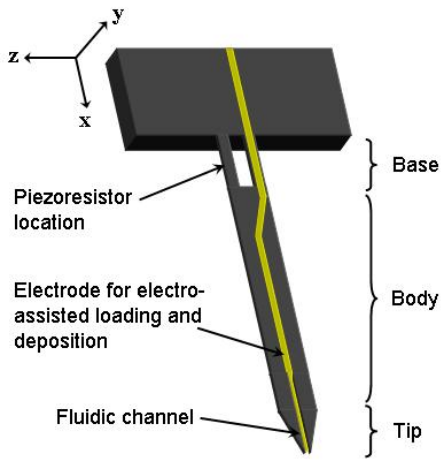

Figure 2.1: *3D schematic of the bioplume cantilever showing the working coordinate system used in the following calculations.*

The piezoresistor is located at the cantilever base, where the stress caused by the bending is maximum. The cantilever base exhibits a U-shape that permits the current to flow in one leg and out the other: this avoids possible shortage of the resistance and facilitates the overall fabrication process because the shape of the piezoresistor is defined during the cantilever fabrication without alignment issues. A metal electrode is

patterned in the channel of the cantilever for electrowetting and electrochemistry implementations. The electrode must be located inside the channel so that the spreading of the liquid occurring onto the electrode allows filling the channel. This configuration also enables the electrode to contact the liquid drop during deposition, thus permitting electrochemical and electrowetting reactions to occur on the substrate. The working principle of these electro-assisted methods is based on the application of a potential difference between the cantilever and the substrate surface. Thus, shortage between the cantilever electrode and the contacting surface is to be avoided. For that purpose, the electrode is required to be shorter than the channel length. This ensures a constant distance between the electrode and the deposition surface.

The cantilever is solely made of silicon and electrical connections are realized with metal lines. Passivation layers are used to electrically insulate each part of the cantilever. The base of the cantilever is a critical part because it hosts the piezoresistor and provides electrical contact to the channel electrode. Two designs are proposed for the cantilever base: a simple U-shaped base with the electrode connection passing over the piezoresistor or a double U-shaped base that allows separating the piezoresistive region and the electrical line on different legs. Two designs are as well proposed for the fluidics: one comprising a channel only, the other one with an additional reservoir. Figure 2.2 provides a schematic of the cantilever showing the four different design configurations: 2R, 2C, 4R, and 4C (the numbers 2 and 4 refer to the simple U-shaped base and the double U-shaped base, respectively, and the letters C and R refer to a cantilever with a channel only and a cantilever incorporating a channel and a reservoir). The choice of the cantilever dimensions is governed by the feasibility offered by the fabrication tools, the size of the drop to deposit, the resulting stiffness coefficient and the value and sensitivity of the piezoresistors. These design elements are provided in the next sections.

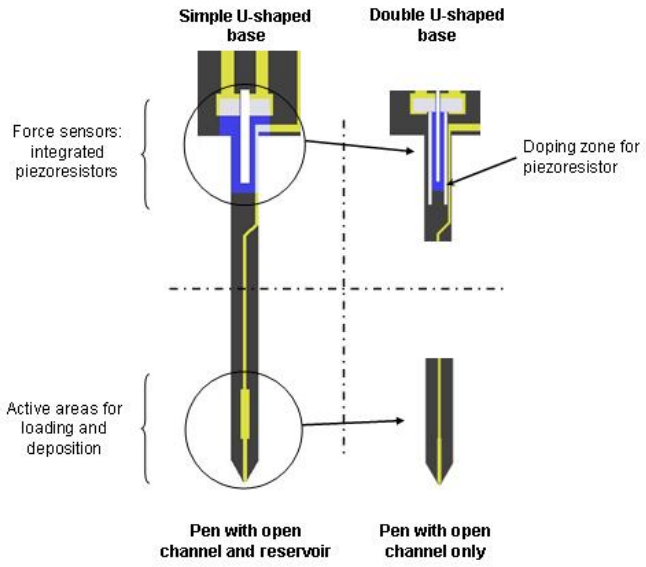

Figure 2.2: *Drawing of the four design geometries of the cantilevers.*

3.1.1. Fabrication possibilities

The fabrication of the cantilever is based on classical techniques used in the microelectronics industry and relies on photolithographic steps. The lateral dimensions of the cantilever are thus determined by the precision of the photolithography. With the classical photoresists and aligners used in our clean-room facility, the reasonable minimum feature size is 2 µm. The thickness of the cantilever is set by the layer of silicon into which the cantilever is patterned. In order to precisely control this thickness, the starting substrate is a silicon-on-insulator (SOI) wafer with top silicon layer thickness that can range between several micrometers to tens of micrometers.

3.1.2. Fluidic requirements

The section of the channel and the sharpness of the tip dictate the range of deposited drop sizes. Because the tip is in the plane of the cantilever, deposition is carried out with the cantilever almost perpendicular to the surface (but not perfectly perpendicular to avoid the buckling of the beam). This configuration allows achieving the smallest drop size. To deposit drops with diameters ranging from several micrometers to tens of micrometers, the channel must exhibit micrometer dimensions. Besides, the slit must almost have a square cross-section for the formation of circular droplets. The channel length and the size of the reservoir are chosen accordingly to the number of drops that are to be deposited without reloading. Our goal is to print more than 50 droplets with sub-picoliter volumes. Giving those facts, we chose the following dimensions: the channel is 4 µm wide, 5 µm thick (specifying the thickness of the top silicon layer of the SOI wafer) and 200 µm long; the reservoir is 24 µm wide, 5 µm thick and 200 µm long. Because the thickness of the deposited layers (silicon dioxide and metal) constituting the patterned electrode is very thin (submicrometer), the volume of liquid loaded in the channel and the reservoir can be estimated from the dimensions given above. The approximated corresponding volumes are thus 4 pL and 24 pL. Finally, the length of the electrode must be chosen considering the size of the electrochemical cell and taking into account alignment issues during fabrication. We arbitrarily decide to work with a cell having roughly a cubic shape: the electrode is 6 µm above the depositing surface.

3.1.3. Mechanical considerations

The stiffness coefficient of the cantilever is an important parameter to take into account in the cantilever design. The spring constant correlates the force applied on the cantilever to the displacement of the tip. Because there is no simple analytical expression of the axial stiffness coefficient k_x (describing the deposition configuration), the lateral coefficient (k_y, coupling the force and the displacement along the y axis) is used as a comparison means: regarding the proper behavior observed with the previous generation of cantilevers, a similar value of the lateral spring constant is chosen for this new design. This allows avoiding the sticking of the cantilever on the deposition surface or in the loading droplet (i.e. the cantilever is not too compliant) while preventing the scratching of the surface (i.e. the cantilever is not too stiff). Figure 2.3 shows a schematic of a simple U-shaped cantilever with a slit, and gives the geometrical dimensions used in the calculation of the stiffness coefficient. In the case of linear beam

behavior, i.e. for small displacements, the spring constant of such a cantilever is approximated by the following relation (the slit and the tip are not taken into considerations):

$$k_y = \frac{3EI_1I_2}{I_1l_2^3 + I_2(l_1^3 - l_2^3)} \tag{2.1}$$

with

$$I_1 = \frac{2w_1t^3}{12} \tag{2.2}$$

and

$$I_2 = \frac{w_2t^3}{12} \tag{2.3}$$

I_1 and I_2 are the quadratic moments of inertia of the cantilever (for the base of the cantilever and the bulk beam, respectively), E is the elastic modulus of silicon, t, the thickness of the cantilever, and w_1, w_2, l_1, and l_2, are the geometrical parameters defined in Figure 2.3. Taking into account the electrical requirements specified hereafter, we chose the following dimensions for the cantilever: the total length of the beam is 1500 µm with a width of 120 µm, and each arm of the base is 200 µm long and 42 µm wide. These dimensions lead to a stiffness coefficient of about 0.16 N/m (for E = 169 GPa). The arms of the double U-shape cantilever carrying the electrode and the piezoresistor are 20 µm and 22 µm in width, respectively, and have approximately the same length. This results in an expected similar spring constant for the double U-shaped cantilever.

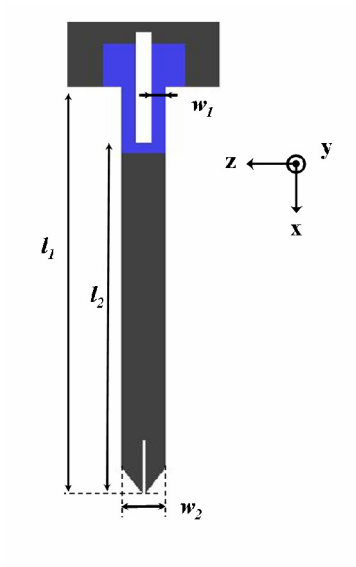

Figure 2.3: *Illustration of the cantilever with annotated geometrical parameters.*

3.1.4. Electrical considerations

The piezoresistor is integrated to the silicon cantilever by locally doping the initial substrate. The design of the piezoresistive element relies on the initial value of the piezoresistance and its expected sensitivity. Piezoresistive coefficients are used to correlate the change in resistivity of a piezoresistive material to the applied stress. The variation of resistivity in the direction parallel to the stress is the longitudinal piezoresistive effect, while the change in resistivity in the direction perpendicular to the stress is the transversal piezoresisitve effect. When applying a lateral (y-directed) or an axial (x-directed) force at the cantilever tip, the cantilever bends up or down and the stress is maximum at the cantilever base. Along the piezoresistor path, this region corresponds to the two legs where the current flows in a direction parallel to the stress gradient. As a result, only the longitudinal component is taken into consideration in the calculation of the piezoresistor sensitivity. Moreover, the highest stress regions are localized at the surface of the cantilever. Thus, the piezoresistive element must be confined at the surface to exhibit a high sensitivity. The expression of the resistance value is:

$$R = \frac{\rho l_R}{A} \tag{2.4}$$

for the simple U-shaped cantilever, the resistor cross-section is:

$$A = w_1 \times t_R \tag{2.5}$$

where ρ is the resistivity of the fabricated piezoresistor, and l_R, w_1 and t_R are its length, width and thickness, respectively. Because the piezoresistor fabrication relies on a doped silicon layer, its thickness is equal to the doping junction depth, x_j. In a first and simple approximation, the resistance of the piezoresistor is estimated by the contribution of the two legs only, i.e. $l_R = 2 \times (l_1 - l_2)$. An initial value of several kΩ is required to meet the specifications of the output electronics dedicated to the piezoresistance measurements. The value of the piezoresistor fabricated on the double U-shaped cantilever is expected to be twice that of the piezoresistor of the simple U-shaped cantilever. Indeed, the base legs are half wider in the case of a double U-shaped cantilever (see Figure 2.2). The expression of the relative change in resistance due to an applied lateral load, F_y, at the tip of the cantilever, is provided below [16]:

$$\frac{\Delta R}{R} = \frac{3\pi_L F_y (l_1 + l_2)}{2 w_1 t^2} \tag{2.6}$$

where π_L is the longitudinal piezoresistive coefficient. Equation (2.6) is obtained by considering only the contribution to the change in resistance given by the two legs and assuming a resistor perfectly confined at the cantilever surface. Knowing the stiffness coefficient from equation (2.1), we can express the theoretical lateral piezoresistor sensitivity (i.e. the fractional change in resistance for a unit displacement at the free end of the cantilever, u_y):

$$\left(\frac{\Delta R}{R}\right)\frac{1}{u_y} = \frac{3\pi_L k_y (l_1 + l_2)}{2w_1 t^2} \tag{2.7}$$

The intrinsic properties of the piezoresistor (π_L and x_j) are dictated by the doped layer fabrication and the orientation of the cantilever toward specific crystal axes. The other design parameters, i.e. the dimensions of the cantilever and the piezoresistor, are chosen in order to obtain the required resistance value, to maximize the sensitivity, while resulting in a beam with a suitable stiffness.

3.2. Design of the bioplume chip

A schematic of the 5 mm x 5 mm bioplume chip is shown in Figure 2.4. The chip is designed to incorporate 10 cantilevers for parallel liquid deposition (separated from each other by 320 µm). Two of these cantilevers incorporate a force gauge to measure and monitor the contact time and force during deposition. Two similar sensing force cantilevers are added on each side of the array for the trim control. These two cantilevers are placed forward on the chip, so that they touch the surface before the depositing cantilevers when moving the chip down to the surface. This design trick allows us to correct the array misalignment and to detect the deposition surface without proceeding to any deposition. An additional piezoresistive cantilever is integrated in the body of the chip for reference purpose: this cantilever undergoes the environmental changes (such as temperature, light, humidity) but is free from contact with a surface. Measuring the differential signal between any sensing cantilever and the reference one leads to the compensation of resistance change due to the environmental parameters. Finally, electric lines and bonding pads are designed to allow simple connections between the chip and its package.

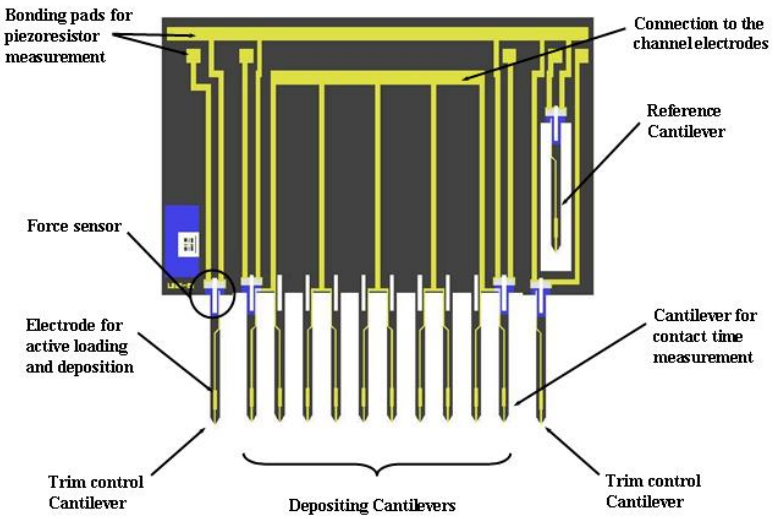

Figure 2.4: *Schematic of the bioplume array.*

3.3. Fabrication of the cantilever array

The fabrication of the bioplume cantilever array, depicted in Figure 2.5, is based on standard micromachining techniques. The process includes 8 photolithographic steps. The starting substrate is a 100 mm, (100), n-type SOI wafer, with a 1 µm thick buried oxide layer and a 5 µm thick top silicon layer (resistivity of 7 Ω.cm).

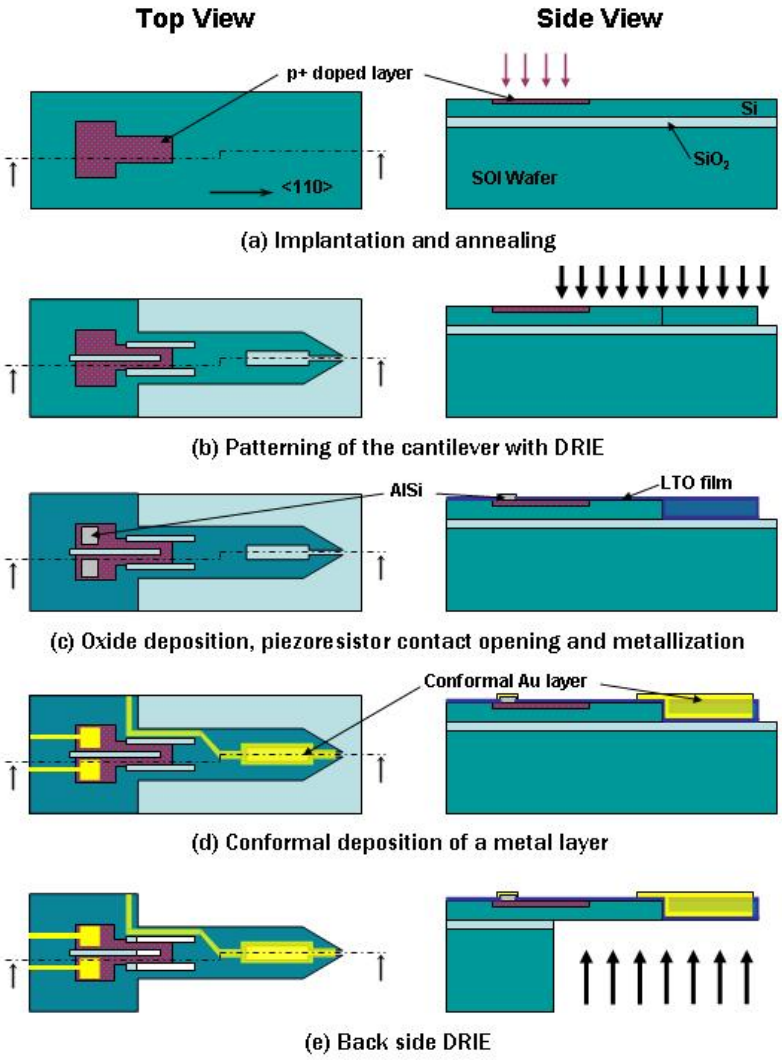

Figure 2.5: *Fabrication process of the bioplume chip. (a) Implantation of BF_2 to create the piezoresistor. (b) DRIE of the front side silicon wafer to pattern the cantilever. (c) Passivation of the cantilever and the piezoresistor and contact realization. (d) Evaporation of Ti/Au layers for electrode fabrication. (e) DRIE of the back side of the wafer to release the cantilever.*

The first step consists in creating the piezoresistor in the bulk silicon (Figure 2.5a). In order to optimize the piezoresistor sensitivity, the cantilevers are patterned along crystal axes for which the longitudinal coefficient is maximum, i.e. along the <110> direction in the case of a p silicon piezoresistor [17]. The fabrication method,

proposed by Bergaud et al., relies on the implantation of germanium (Ge) and boron fluorine (BF_2) in order to obtain an ultra-thin piezoresistor [18]. The localization of the piezoresistive layer at the anchored edge of the cantilevers is achieved by using silicon dioxide as a masking layer. For that purpose, 300 nm of silicon dioxide is thermally grown and patterned with a photolithographic step. Ge is implanted with energy of 60 keV and a dose of 5×10^{14} ions/cm^2 through a 6 nm silicon dioxide layer to create a preamorphized layer. This layer avoids channeling effects during the boron implantation and leads to a very thin doped region. BF_2 is then implanted with energy of 15 keV and a dose of 1×10^{16} ions/cm^2. Owing to the heavier mass of the boron fluorine molecule relatively to boron, the use of BF_2 results in a thickness reduction of the p+ doped region. The implantation process is followed by a rapid thermal annealing at 1000 °C for 15 seconds to minimize boron diffusion during the recrystallization of the amorphized layer and the electrical activation. This is followed by a conventional annealing at 850 °C during 20 minutes.

After removing the oxide masking layer in buffered oxide etch (BOE), the cantilever shape is created by a deep reactive ion etch (RIE) of the top Si layer (Figure 2.5b). The final shape of the piezoresistor is realized with this anisotropic dry etch process. The channel and the reservoir are also fabricated during this step. A 200 nm thick oxide layer is deposited by plasma enhanced chemical vapor deposition (PECVD) in order to protect the piezoresistors and to electrically insulate the bulk silicon from the metal lines to be patterned. Contact holes are opened and a 200 nm thick AlSi layer is sputtered and patterned in order to obtain electrical contacts for the resistors. Metal annealing is then performed at 450 °C for 20 min (Figure 2.5c).

Once the shape of the cantilever is created, the electrodes required inside the channel for the electro-assisted methods are fabricated (Figure 2.5d). For this purpose, metal is evaporated and a lift-off process is used. The connecting metal lines and bonding pads are fabricated along with the metallic electrodes. To allow a proper electrical connection between the metal patterned inside the channel and the one on the cantilever, 100 nm titanium and 700 nm gold layers are deposited in a conformal way with an electron beam evaporator. The metal annealing step is realized at 250 °C during 20 min.

The cantilevers are finally released by a deep reactive ion etch (DRIE) of the back side of the silicon wafer, followed by a RIE of the buried silicon dioxide layer (Figure 2.5e). Subsequent electrode passivation can then be optionally carried out by depositing two silicon dioxide layers of 200 nm, on the front and the back sides of the cantilevers, respectively.

Figure 2.6 shows a processed wafer before the final backside DRIE. Each wafer includes 192 bioplume chips. Scanning electron microscope (SEM) pictures of a fabricated array, including a close-up view of the channel at the tip of a cantilever, are shown in Figure 2.7. Each microfabricated silicon-based cantilever is 1500 µm long, 120 µm wide and 5 µm thick. The channel is 4 µm wide and 200 µm long, and the reservoir is 24 µm wide and 200 µm long.

The bioplume chips are then packaged to allow fixing it to the positioning apparatus and connecting it to the piezoresistor readout electronics. For that purpose, the chips are glued and bonded to a printed circuit board (PCB). Figure 2.8 shows a packaged device ready for testing.

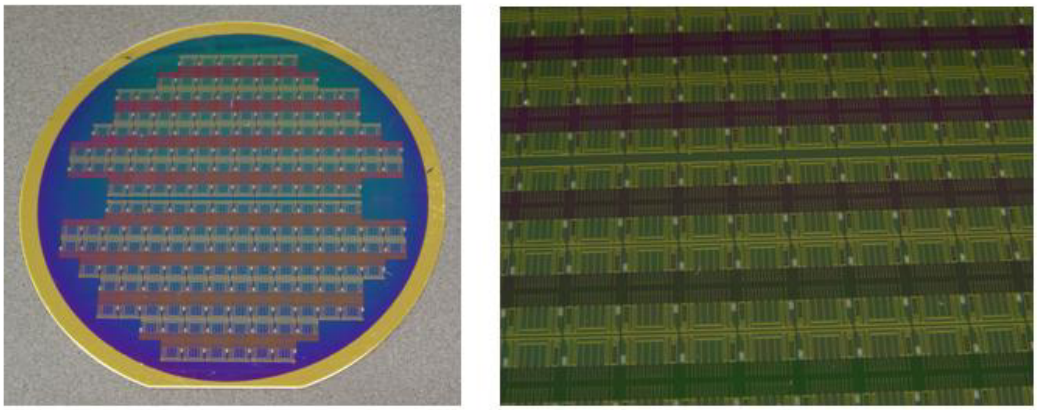

Figure 2.6: *Photograph of a processed wafer (left) and close-up view (right).*

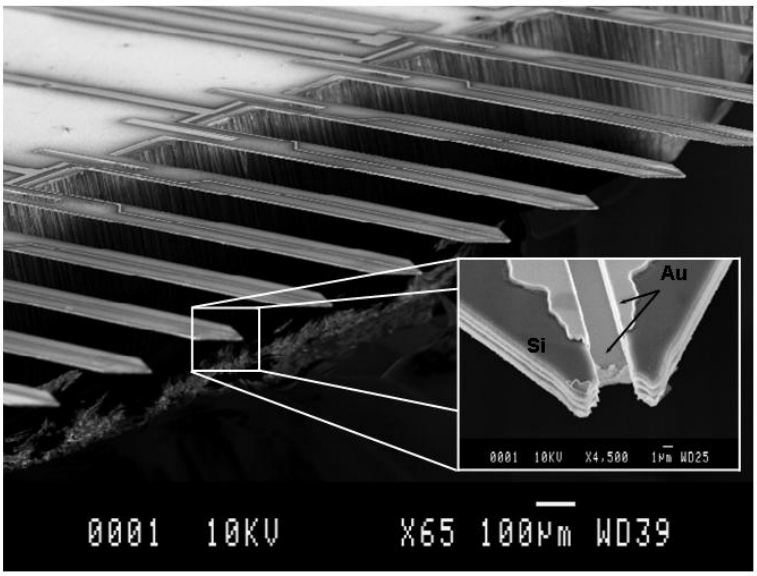

Figure 2.7: *SEM picture of a cantilever array with SEM close-up view of the silicon tip showing the electrode inside the fluidic channel.*

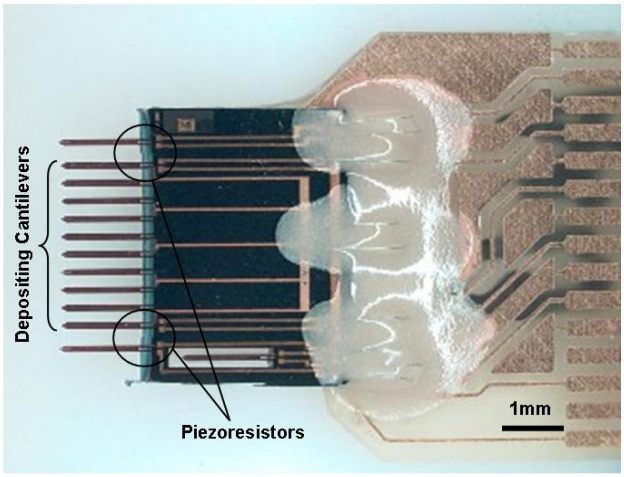

Figure 2.8: *Optical photograph of the silicon cantilever array bonded onto a PCB support.*

4. Piezoresistive cantilever measurement and characterizations

4.1. Readout electronics

4.1.1. Principle of operation

A conventional Wheatstone bridge is generally used to measure the static variation of a piezoresistor. However, a Wheatstone bridge does not lend itself to measurement optimizations. Indeed, this method is efficient under specific conditions (proper resistor dispersion ratio) that are not easily obtained when working with piezoresistors fabricated in laboratories.

Thus, a method relying on a modified Wheatstone bridge was recently proposed by our research group [19]. It consists in replacing the two static resistors of the bridge with controlled current generators, as shown in Figure 2.9. This solution offers several advantages. Firstly, the current generators enable the compensation of the bridge by monitoring biasing voltages. Secondly, the transfer function of the system results in a twofold gain compared to the one of the Wheatstone bridge. The noise balance is equivalent in both methods, since the signal to noise ratios are equivalent. From Figure 2.9, the output voltage of the bridge is expressed as follows:

$$V_{bridge} = \Delta RI + RI - R_{ref} I_{ref} \tag{2.8}$$

Because the change in resistance is usually negligible compared to the initial resistance value, the voltage bias due to the initial reference and measured resistances have to cancel out: this compensation is achieved by adjusting the currents I and I_{ref} so that $IR = I_{ref}R_{ref}$. In this case, the output voltage of the bridge can directly be expressed as a function of the resistance change and the power of operation:

$$V_{bridge} = \frac{\Delta R}{R}\sqrt{PR} \tag{2.9}$$

with

$$P = (R + \Delta R)I^2 \approx RI^2 \tag{2.10}$$

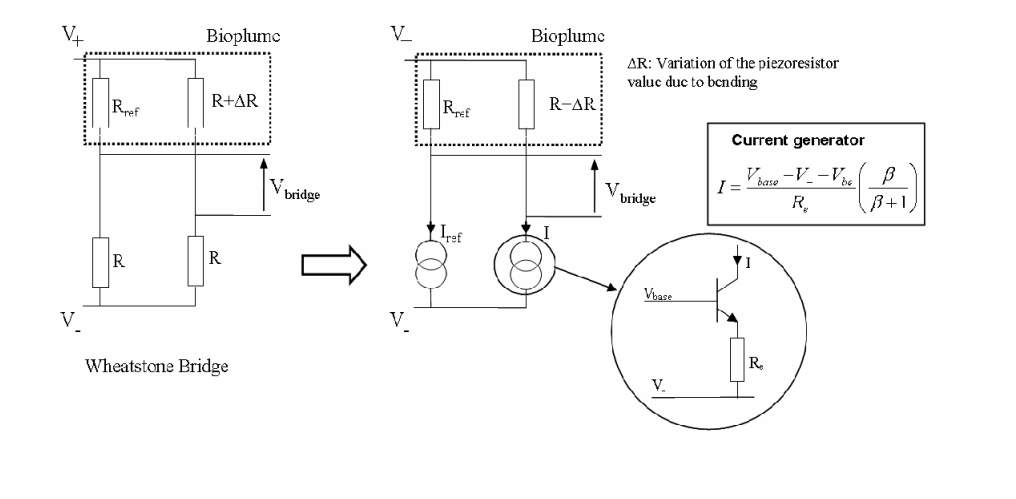

Figure 2.9: *Principle of the modified Wheatstone bridge.*

4.1.2. Electronic circuit implementation

The electronics designed for the bioplume chip incorporates one bridge per piezoresistive cantilever, using the reference cantilever as the reference resistance in the four bridges. The current generators are made of NPN transistors in a common emitter configuration with an accurate resistor connected to the transistor emitter. Base voltage is set by a reference voltage at a constant potential. Under these conditions, the current generated in each branch is a function of the negative bias voltage (and is equal). A differential amplification is used to generate the output signal of each bridge. The electronic components used in the realization of the parallel bridges are incorporated to a detection board onto which the packaged bioplume chip is directly connected: this allows the measurement to be carried out very close to the sensors, thus avoiding electromagnetic perturbations. Figure 2.10 shows the electronic diagram of the detection board. For packaging issues, this electronic board does not incorporate all the electronic components and is then connected to a main driving board. This board includes a final amplification stage, means to compensate the resistance dispersions (using offset voltages on the second amplification stage), the bias driving, and A/D converters for the measurement of each piezoresistive cantilever. It also includes a microcontroller that allows the operator to fix the voltages and currents required for an optimized operation. The output of the driving board provides a voltage proportional to the fractional change of resistance of the piezoresistor. Because, the overall amplification of the bridge output voltage is 110, the expression of the electronic board output voltage is:

$$V_{out} = 110 \times \sqrt{PR}\,\frac{\Delta R}{R} \tag{2.11}$$

By replacing, in the latter equation, the resistor fractional change calculated in equation (2.6) or (2.7), the output voltage of the electronic system can be expressed as a function of the applied force or the displacement of the cantilever tip. As expected, the output voltage provides direct means to estimate the bending of the cantilever. In the case of a simple U-shaped cantilever, the displacement of the tip under a lateral load is extracted from the following relation:

$$u_y = \frac{2w_1 t^2}{330 \times \sqrt{PR} \times \pi_L k_y (l_1 + l_2)} V_{out} \qquad (2.12)$$

A picture of the overall electronic set up is shown in Figure 2.11.

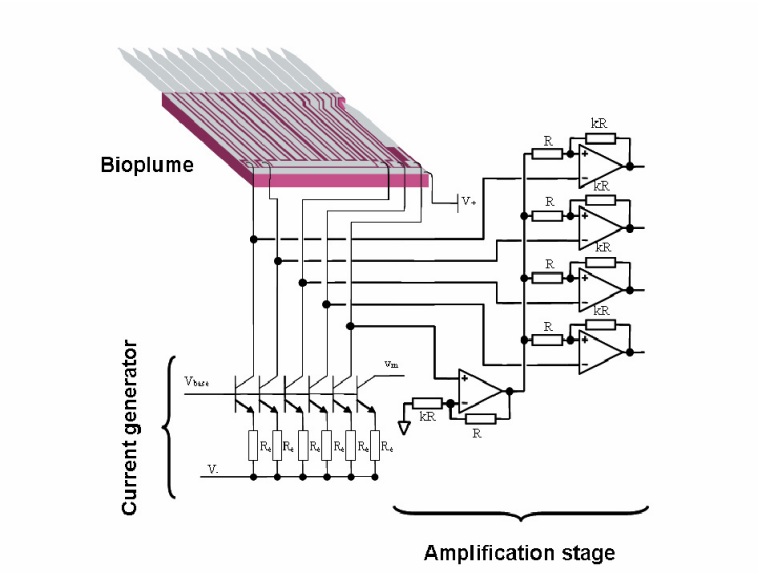

Figure 2.10: *Diagram of the detection board.*

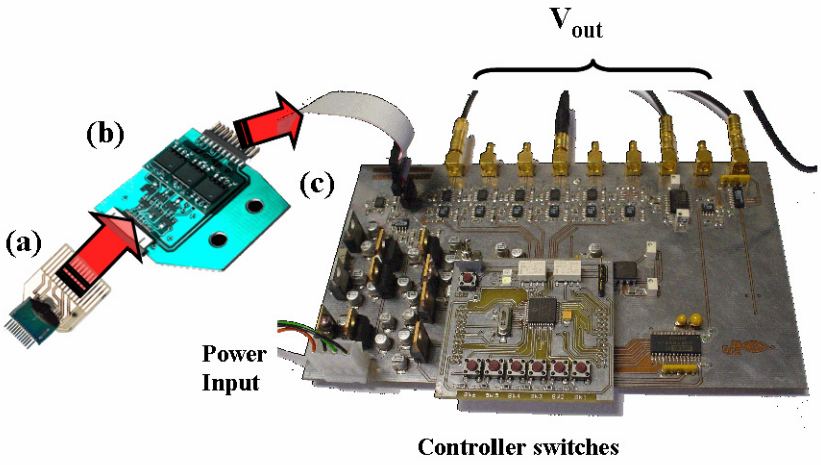

Figure 2.11: *Complete electronic setup including: (a) the bioplume chip on a PCB, (b) the detection board, and (c) the main driving board.*

4.1.3. Output characteristics and electrical response of the cantilevers

To characterize the sensitivity of the fabricated cantilevers and the output of the electronic circuit, bending experiments were conducted. The bioplume chip was attached to a positioning apparatus via the detection board: the chip was connected to the detection board, which was then used as a chip holder. For this purpose, the design of the detection board allowed directly mounting it onto a ceramic piezoactuator thanks to dedicated mechanical parts. The chip could be positioned in parallel or almost perpendicularly to the displacement axis and bending experiments were carried out by moving the cantilevers toward a fixed surface, as shown in Figure 2.12. The output voltage was recorded as the cantilevers bent on the surface.

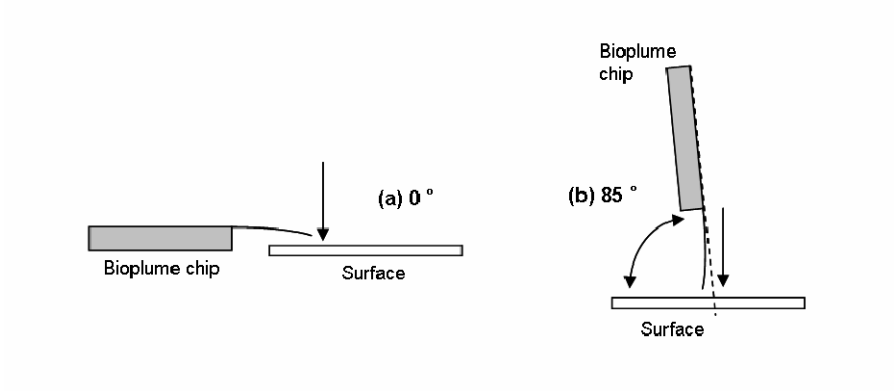

Figure 2.12: *Lateral (a), and axial (b) bending conditions. The axial condition corresponds to the deposition configuration.*

Figure 2.13 shows the resulting voltage output for two types of cantilevers (2C and 4R) experiencing a lateral displacement. Figure 2.14 displays the response of the four types of cantilevers to an axial displacement. The injected power was approximately set to 500 µW in all the experiments. The estimated output noise was less than 30 mV (effective voltage), but significantly higher than the 10 mV theoretical noise of the electronics. This experimental noise was attributed to mechanical vibrations within the system and room lighting. After proper filtering, the noise value could be reduced to almost 10 mV.

Under lateral loads, the response of the piezoresistive cantilevers is linear in the range of the induced displacements since the cantilevers do not experience large bending (the maximum free end displacement stays under ten percent of the total length of the cantilever). The slope of the resulting line is the piezocantilever sensitivity in terms of output voltage per unit displacement. In this configuration, the cantilever bending can directly be obtained by reading the output voltage value.

The response of the cantilevers bending under axial loads is strongly non-linear and the resulting sensitivities are much higher than the ones observed for lateral displacements. This is consistent with the fact that higher stresses are induced in this configuration for a given tip displacement. This result is also very interesting because it means that the deflection precision is better in the deposition configuration. However, because the voltage output saturates around 11 V (due to the electronics design), no more than 10 to 20 µm of tip displacements can be detected with this technique.

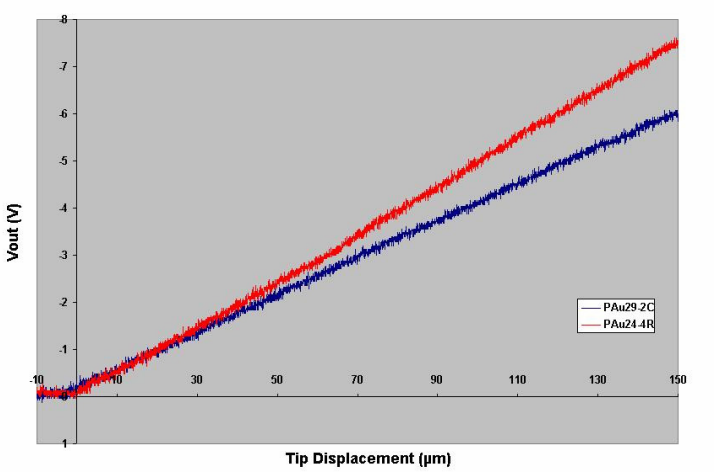

Figure 2.13: *Voltage output of the electronic board for the 2C and 4R cantilevers under lateral bending.*

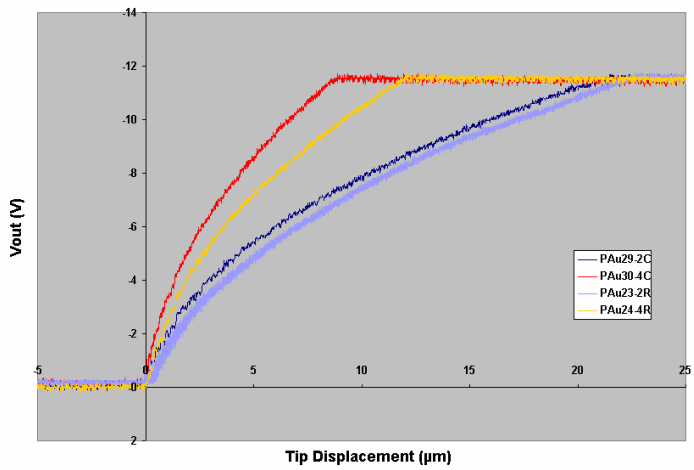

Figure 2.14: *Electrical response of the four types of cantilevers as a function of the axial displacement of the tip.*

4.2. Characterization of the piezoresistive cantilevers

4.2.1. Quality of the fabricated piezoresistors

4.2.1.1. Characterization of the doped layer

The electrical parameters of the doped layer constituting the piezoresistors, i.e. the junction depth and the resistivity, were measured to provide reliable inputs for the theoretical model describing the piezoresistor. The sheet resistivity was firstly measured with a four point probe. The resulting value is 205 Ω. Secondary ion mass spectrometry (SIMS) analyses were then conducted to obtain the doping profile of the implanted layer. The doping profile, shown in Figure 2.15, leads to the estimation of the metallurgic junction depth. By extrapolating the profile to the initial atom concentration

of the substrate, i.e. 10^{15} cm^{-3}, the junction depth is found to be around 200 nm. The electrical junction depth was taken as the metallurgic junction depth, hypothesizing the implanted ions were all electrically activated. The resistivity of the implanted layer, which is equal to the sheet resistivity times the junction depth, is thus 4.1×10^{-3} Ω.cm.

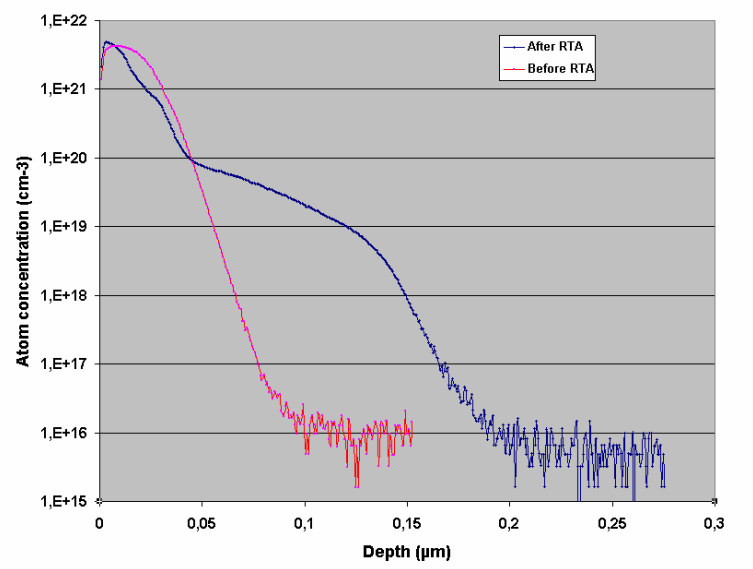

Figure 2.15: *SIMS analyses carried out on a fabricated piezoresistive layer before and after completing the rapid thermal annealing (RTA) process.*

4.2.1.2. Estimation of β

The evaluation of the quality of the fabricated piezoresistor is carried out by comparing the measured and the theoretical fractional change of resistance. The ratio between these sensitivities is:

$$\beta = \frac{\left(\Delta R / R\right)_{Measured}}{\left(\Delta R / R\right)_{Theoretical}} \tag{2.13}$$

β is a number related to the doping profile and the thickness of the cantilever. As previously stated, the theoretical sensitivity is calculated in the case of a resistor perfectly located at the surface of the cantilever. Thus $\beta = 1$ in the case of a surface resistor. The piezoresistor sensitivity decreases with its thickness and reduces to zero for a resistor integrated into the entire thickness of the cantilever because equal and opposite stresses are present in regions of the cantilever symmetric with respect to the neutral axis. In this later case, $\beta = 0$.

Because the theoretical sensitivity can only be expressed for lateral deflections, the measured voltage sensitivity is extracted from Figure 2.13. The resistor sensitivity (for 1 µm tip displacement) is obtained by using equation (2.11) and the measured initial resistor value. The theoretical sensitivity is calculated using equation (2.7) for a simple U-shaped cantilever (with $\pi_L = 50 \times 10^{-11}$ Pa^{-1}). For the 2C cantilever with an

initial resistance value of 5.7 kΩ, the theoretical and measured sensitivities, i.e. $\Delta R/R$ for a 1 µm displacement, are 3.2×10^{-4} and 2×10^{-4}, respectively. This results in $\beta = 0.63$. This value seems pretty low (regarding the SIMS profile and the thickness of the cantilever) but means that the effective sensitivity of our piezoresistors could easily be improved by adjusting the implantation parameters.

4.2.2. Sensitivity and minimum detectable deflection in the depositing configuration

In the depositing configuration, the output voltage varies non-linearly with the tip displacement, as shown in Figure 2.14. Thus, the piezoresistor sensitivity depends on the deflection in the tens of micrometer displacement range, before reaching the saturation of the electronics. The sensitivity can still be considered linear in the first micrometers of displacement, where it exhibits its maximum values, ranging from 1 V/µm to more than 3 V/µm. Considering an output noise of about 30 mV, the corresponding minimum tip displacement that can be detected lies in the range of tens of nanometers. This information is sufficient for surface detection applications. However, in order to estimate the bending force from the output voltage, one must be able to relate the tip displacement to the applied force. This is the aim of the following section.

4.3. Relation between the voltage output and the contact force during deposition

4.3.1. Mechanical simulation of bioplume for spring constant estimation

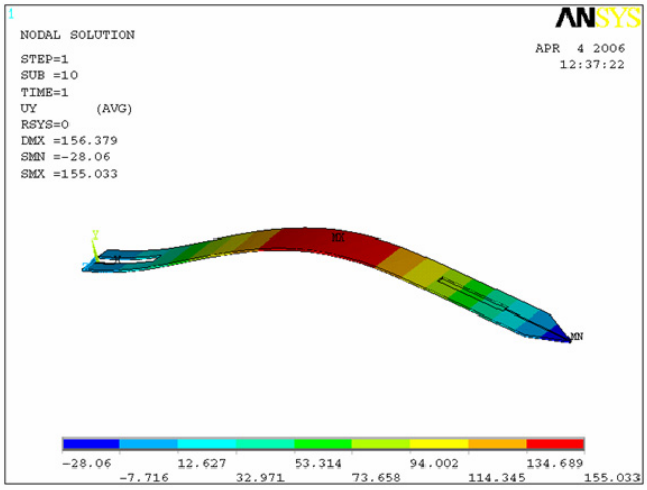

Figure 2.16: *Simulation result of a 2R bioplume cantilever with an applied axial force.*

As previously stated, it is very difficult to obtain an analytical expression of the axial stiffness coefficient. As a result, finite elements modeling (FEM) was carried out by our colleagues of the Computational Modeling Group at the Tyndall National Institute (within the NaPa framework) in order to estimate this coefficient. The ANSYS

simulation software was used for that purpose. The model of the bioplume cantilever was built based on the fabrication process previously described and the material parameters found in the literature. The accuracy of the material parameters, especially the value of the residual compressing stress of the silicon dioxide layers, were checked by comparing the simulation results of the initial bending of the cantilever with the shape of the fabricated cantilever at rest. Loads were then applied at the tip of the cantilever and numerous simulations were conducted with increasing applied forces. An example of simulation results showing the bended shape of a cantilever under an axial load is seen in Figure 2.16. For each load value, the axial displacement of the tip was extracted in order to calculate the spring constant of the cantilever. Modeling was realized for the four types of cantilevers, i.e. 2C, 2R, 4C, and 4R (2 or 4 for simple or double U-shaped cantilevers, C or R for cantilevers with fluidic channel only or with an additional reservoir).

4.3.2. Model validation with bending tests

To validate the accuracy of the mechanical model of bioplume, the predicted shape of the bended cantilevers were compared to displacement measurement results. Loads were applied at the tip of fabricated cantilevers and the side of the bended beams was imaged providing the lateral deflections, u_y, induced by the axial load. Experimentally, this was achieved by vertically moving the bioplume chip toward a horizontal surface, as shown in Figure 2.12. A CCD video-microscope was placed on the side of the device and the lighting was adjusted to obtain a contrasted image of the edge of the cantilever. Bending of the cantilever occurred when touching the surface: from the contact point (determined using the piezoresistor sensors) the chip was further moved down, with displacement steps of either 1 µm (from 0 to 10 µm tip displacement) or 5 µm (from 10 to 50 µm total tip displacement). For each step, a picture was taken and stored on disk. The pictures were processed by means of an image processing software in order to obtain the value of the lateral bending along the beam. The superposition of the cantilever profiles is plotted in Figure 2.17, illustrating the different shapes of the cantilever during its bending.

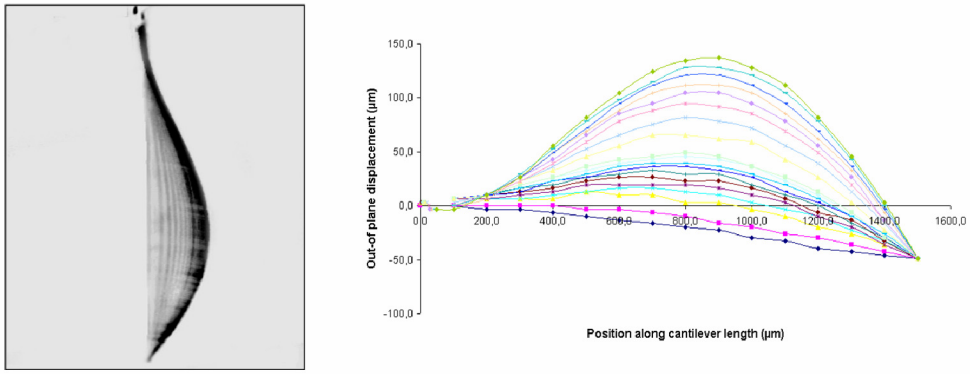

Figure 2.17: *Superposed images of a cantilever during the bending process cause by an axial force. Left: pictures. Right: graph displaying the measured data.*

These profiles were then compared to the simulation results: the simulated and experimental initial and final shapes of the four different cantilevers are plotted in Figure 2.18, while the shape of the four types of cantilevers for a maximum lateral displacement (50 µm), along with the corresponding force values, are given in Figure 2.19 as a comparison means. As expected, the differences in cantilever design do not affect much the mechanical properties. The fit between the predicted and experimental bended shapes proves that our model describes accurately the mechanical behavior of the cantilevers.

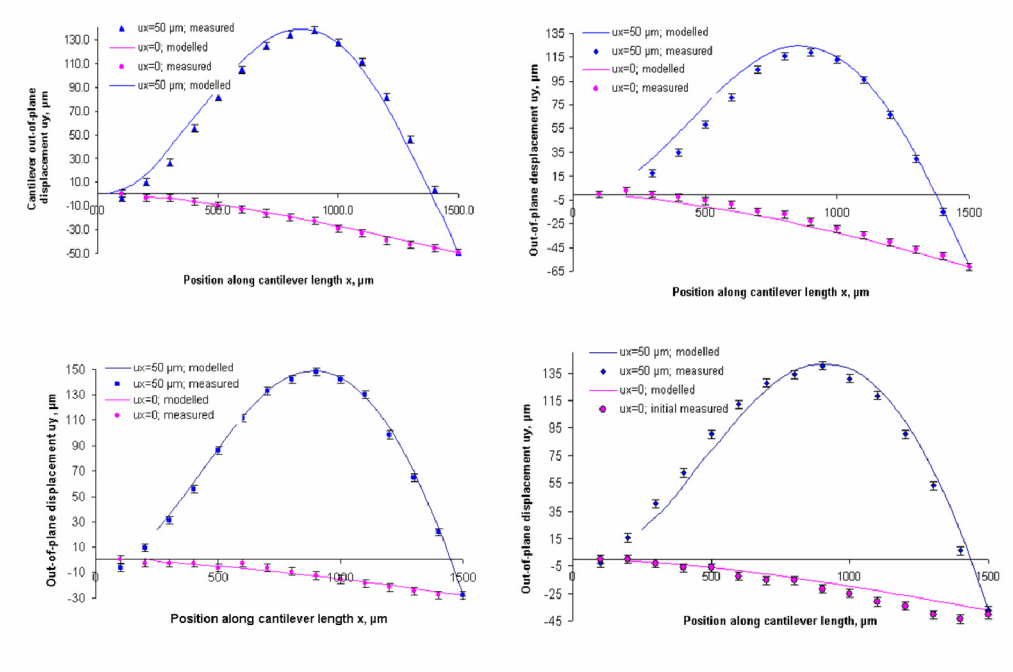

Figure 2.18: *Comparison between the simulations results and the experiments for the initial and the final shapes of the bioplume cantilevers. Top left: Cantilever 2C. Top right: Cantilever 4C. Bottom left: 2R. Bottom right: 4R.*

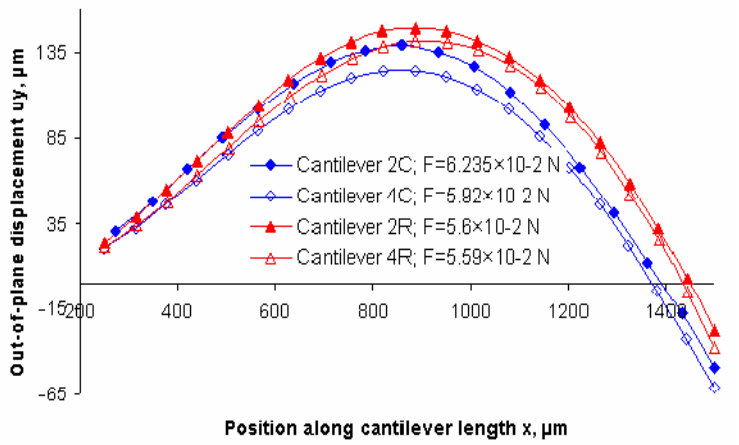

Figure 2.19: *Shape of the 4 types of cantilevers for a maximum lateral displacement. The corresponding applied forces are provided.*

4.3.3. Force exerted on the surface during deposition

The spring constant of the cantilevers, estimated by simulation means, was extracted by plotting the load applied at the tip of the cantilever as a function of the tip in-plane displacement. The plots are given in Figure 2.20 for the four types of cantilevers.

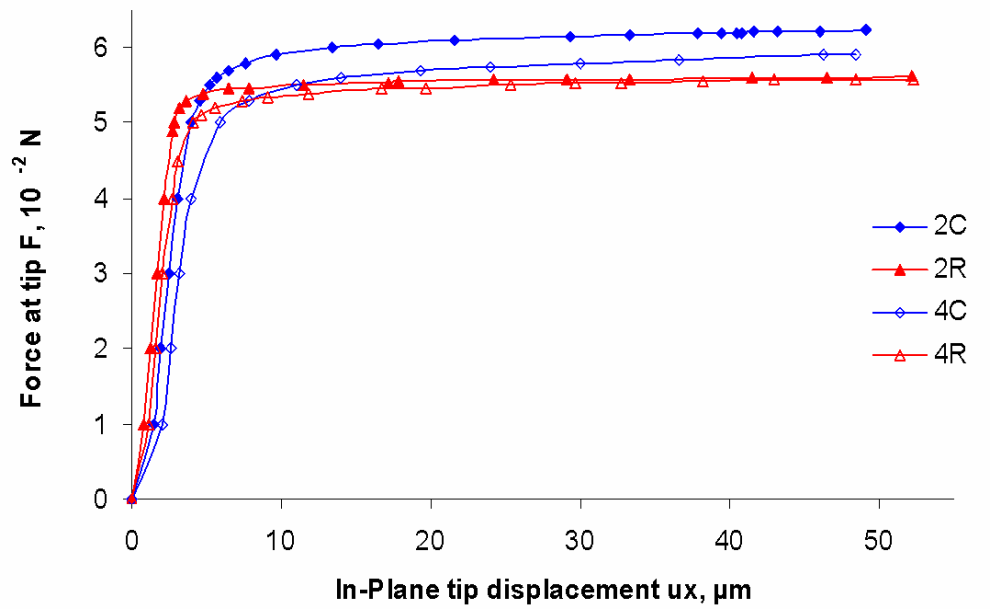

Figure 2.20: *Force applied at the cantilever tip versus in-plane tip displacement.*

The stiffness coefficient, which is simply obtained by dividing the applied force by the tip displacement, gives rise to interesting results. As expected, the four cantilevers exhibit the same behavior. The comparable plots obtained for the simple and double U-shaped bases make sense because the quadratic moment of inertia is similar in both cases. This also confirms that the addition of the reservoir does not modify the overall mechanical properties of the cantilever. In all cases, the spring constant varies with the bending of the cantilever. During the first micrometers of displacement, when the cantilever begins to bend on the surface, the force applied to the surface increases rapidly: the cantilever is very stiff (the spring constant is larger than 10^4 N/m) and gets stiffer with increasing tip displacement. This stiffening phenomenon might be due to the fact that the cantilever is initially pre-stressed. Then, after a given bending, the cantilever behavior changes drastically and it becomes very compliant: the beam experiences buckling and reaches a "soft-spring" state. This means that the force exerted on the surface by the cantilever tip increases very slightly with further displacement of the chip. However, the spring constant remains in the range of 10^3 N/m.

5. Automated spotter in closed-loop configuration

5.1. Principle of operation

The complete automated bioplume spotter comprises the silicon chip associated to the electronic circuit, a four-degree-of-freedom automated displacement system and a PC. The electronics is dedicated to the measurement of the piezoresistor and the motion stage is used to position the cantilever array. The stage supporting the loading and deposition surfaces can be moved in the X, Y, and Z directions by means of step motors, whereas the vertical (X) displacement and the tilt (θ) of the array are respectively done by a piezoactuator for fine positioning and a step motor. Each axis is controlled by the PC thanks to specifically written LabWindows/CVI software. The output of the electronics is connected to the PC so that the microsystem is in a closed-loop configuration: the cantilever bending occurring when touching a solid surface or a liquid droplet leads to the determination of contact points thanks to a specific algorithm, which is then used to control the displacement of the array. Via a graphic user interface (GUI), the operator specifies the deposition parameters to carry out automated experiments. A schematic of the closed-loop automated spotter is shown in Figure 2.21.

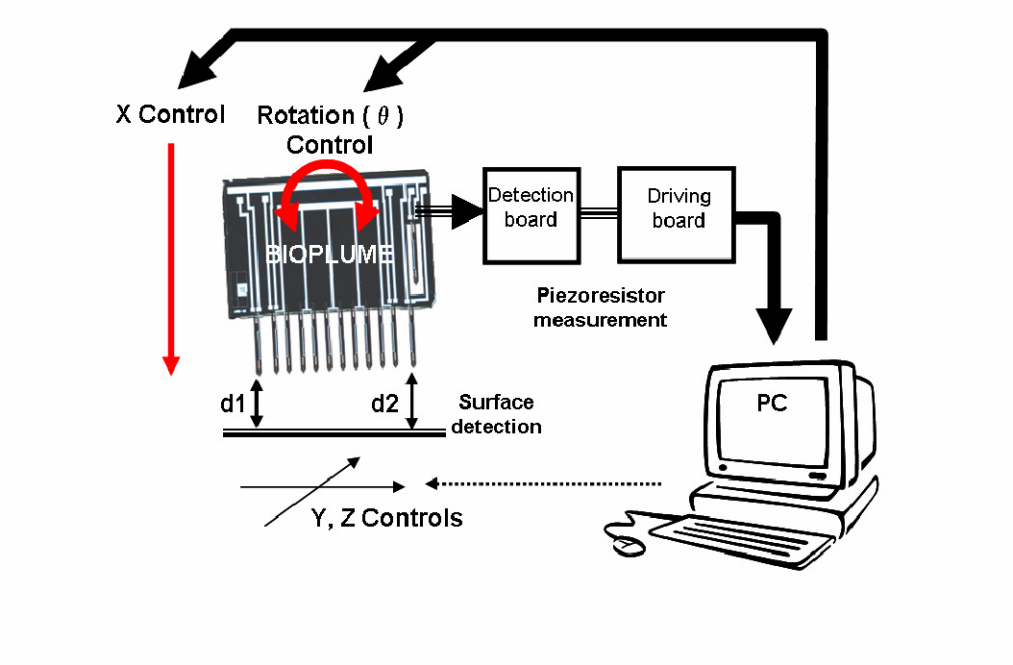

Figure 2.21: *Diagram of the closed-loop bioplume spotter.*

5.2. Positioning apparatus

For bioplume chip positioning, a specific automated spotter based on a four-degree-of freedom robot has been designed and fabricated. It comprises a XYZ stage onto which the loading and the deposition areas are located, along with a chip holder used to displace the bioplume array. The stage displacement is achieved by means of PC-controlled step motors with micrometric accuracies. The holder includes a nanoscale motion actuator (along the X direction) combined with an accurate rotating

device (for θ control). The mechanical drawing of the holder system is shown in Figure 2.22 and a picture of the overall set up is presented in Figure 2.23. The holder permits to directly attach the detection electronic board onto which the bioplume chip is connected.

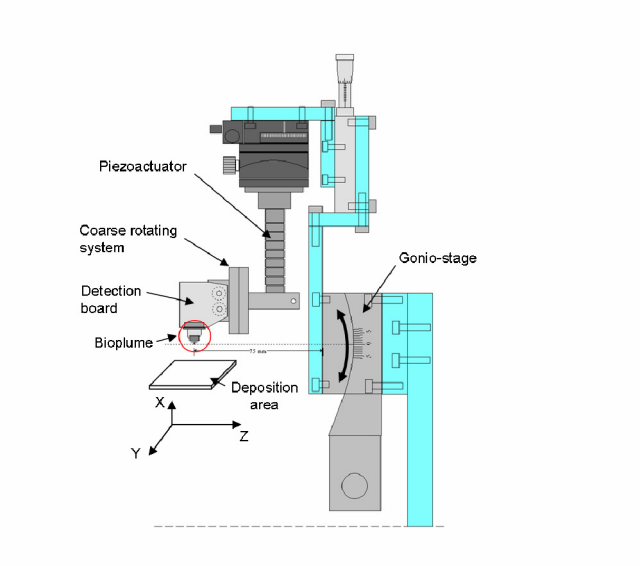

Figure 2.22: *Mechanical drawing of the bioplume holder allowing the angular and the vertical motion of the chip.*

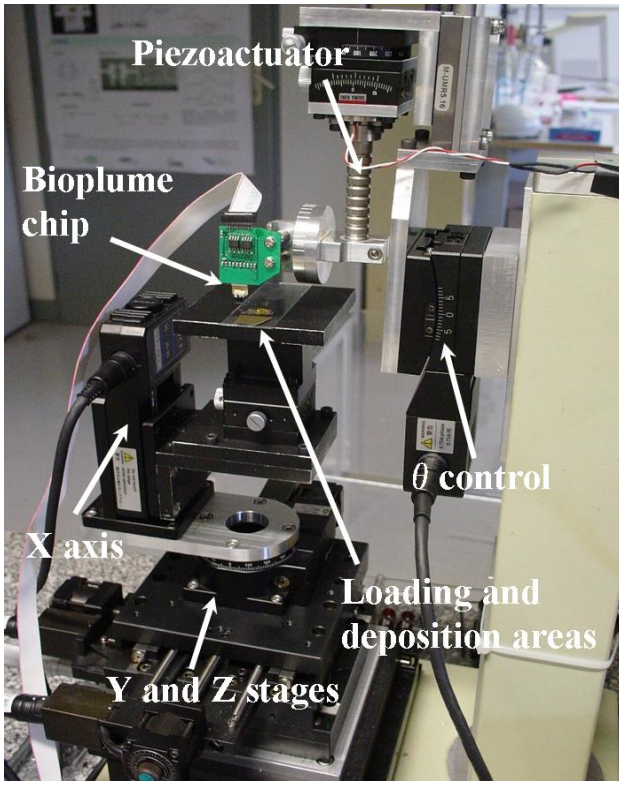

Figure 2.23: *Picture of the four-degree-of-freedom depositing spotter including the cantilever array.*

The precise control of the vertical position of the cantilevers above the surface is carried out by a metal sealed multilayer type piezoelectric actuator. The actuator length is typically 72 mm and a maximum displacement of 50 µm is achieved when applying 150 V. The actuator is controlled by using a high voltage controller inserted in the PC. Giving the fact that the controller has a 12-bit digital to analog converter, 12 nm displacement steps can be achieved. The goal of the rotation actuator system is to adjust the angle of the cantilever array with the deposition surface located on the stage. The actuator is a controlled gonio-stage with a typical rotation radius of 75 mm. Additional mechanical parts and manual position stages have been added in order to allow positioning the rotation centre in the middle of the line joining the tips of the bioplume cantilevers. The motorized gonio-stage exhibits ± 5° capability and 1/1000° accuracy. Because the cantilevers used for the tilt adjustment (placed on each side of the array) are separated from each other by 3700 µm, the 1 thousandth degree accuracy corresponds to a maximum error in height difference of $\Delta X = 64$ nm (see Figure 2.24). The bioplume holder also allows the adjustment of the deposition angle via a coarse rotating system. This angle is usually set to 85° during the deposition process, i.e. the cantilevers are almost vertical to the deposition surface.

Finally, a CCD camera connected to the PC is used to monitor the displacement of the chip regarding to the loading and deposition areas.

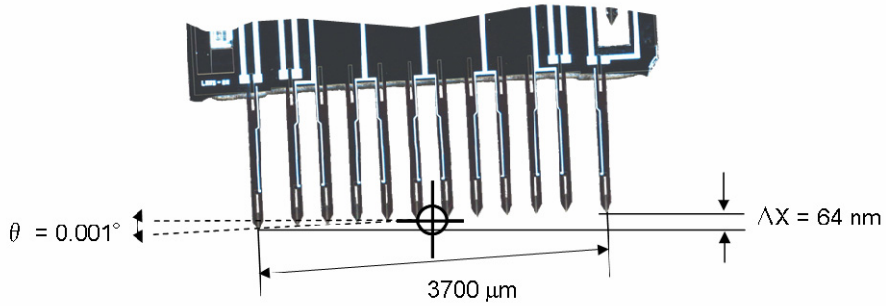

Figure 2.24: *Tilt of the bioplume array illustrating the maximum positioning error corresponding to the tilt accuracy.*

5.3. Response of the piezoresistive cantilever array in the deposition configuration

The deposition surface detection, the tilt measurement, and the contact time and force control are carried out using the electrical response of the four piezoresistive cantilevers of the bioplume chip. We follow the same experimental procedure used to characterize a single cantilever (described in section 4.1.3) to simultaneously obtain the response of the four cantilevers bending onto the deposition surface. Figure 2.25 shows the amplified output of a 4R cantilever chip when the chip is perfectly aligned to the surface (a) and after a 0.1° rotation of the array (b).

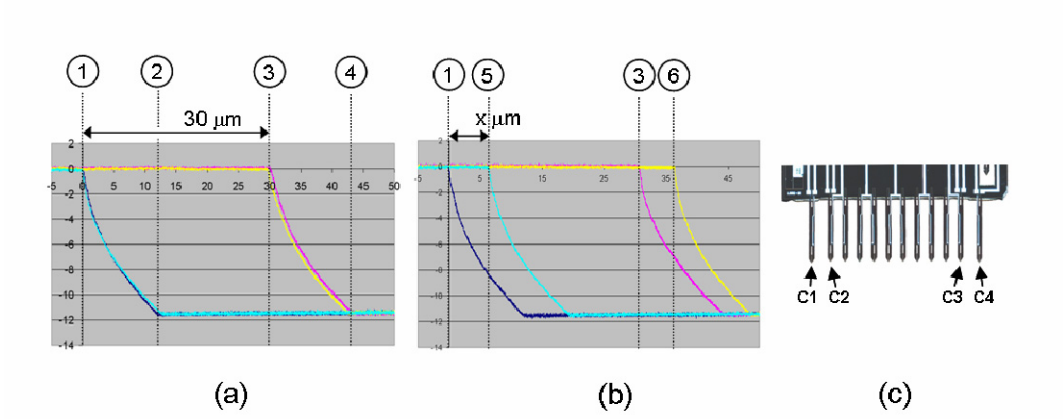

Figure 2.25: *Voltage output versus displacement (piezoactuator motion) of the four active cantilevers of bioplume. (a) Array parallel to the deposition surface, and (b) for a 0.1° tilt value. (c) Corresponding cantilever denominations.*

On the signal diagram shown on the left, four events are highlighted. When starting the chip movement, the cantilevers do not touch the surface and the voltage remains equal to zero (this null value is obtained with the compensation mode of the electronics). Once the outside cantilevers C1 and C4 contact the surface and bend (position 1) their output signal increases until reaching the electronics saturation (position 2). After 30 µm of chip displacement, the cantilevers C2 and C3 touch the surface as well (position 3). The 30 µm distance difference between the positions 1 and 3 is consistent with the chip design: C1 and C4 are 30 µm longer than C2 and C3. Finally, the response of the cantilevers C2 and C3 reach the voltage saturation as well upon further chip displacement.

On the plots seen in the center of Figure 2.25, two other events happen: because of the angle difference between the array and the surface, the cantilever C1 touches the surface and bends before the cantilever C4 (that contacts the surface in 5). The distance difference labeled x in the Figure, which is the same between the two inner cantilevers (positions 3 and 6), is used to measure the tilt of the array. As expected, the outside cantilevers respond before the inner cantilevers in both cases. They can thus be used to adjust the tilt of the array without inducing any deposition, even starting with a 0.1° angle difference. During deposition, the inner cantilevers can then be used to monitor the force and time of contact.

5.4. Control of the positioning system using the piezoresistor response

5.4.1. Surface detection

A schematic explaining the method used to precisely detect the sample surface with the piezoresistive cantilevers is shown in Figure 2.26. This method relies on the voltage output of the electronic board and the SDAPPLIN (surface detection by approximated lines intersection) software [20]. The idea is to determine the parameters of the cantilever response before and after contact and to use the intersection of the two resulting parametrical curves to precisely determine the contact point. During the non-contact phase, the output voltage given by the force sensor remains constant (see L1 in

the Figure). Once the cantilever touches the surface and experiences bending, the voltage output increases (line L2): line fitting is used because the response can be considered linear for small displacements. The software extracts the parameters of the lines L1 and L2, allowing the estimation of the contact point at the intersection of the two lines. The advantage of this method relies in the precision of the surface detection which is higher than the minimum step used to displace the chip.

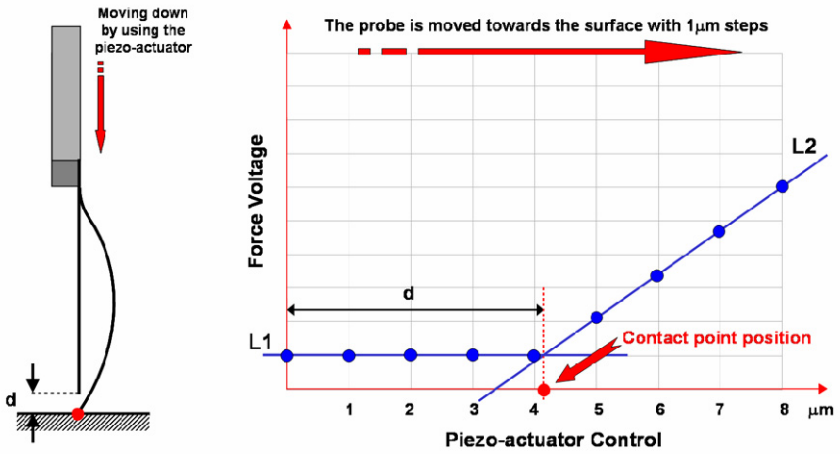

Figure 2.26: *Principle of operation of the surface detection using SDAPPLIN.*

5.4.2. Tilt error measurement

The trim between the cantilever array and the deposition surface is estimated by using the two piezoresistive cantilevers of the side of the array. The precise measurement of the distances d1 and d2 (between the tip of the two cantilevers and the surface, as shown in Figure 2.21) is achieved by following the method described above. With these distances, the trim angle is simply deduced from the following relation:

$$\theta = \arcsin\left(\frac{|d2 - d1|}{d}\right) \qquad (2.14)$$

where d = 3700 µm is the distance separating the two tilt control cantilevers.

5.4.3. Closed-loop operation for automatic tilt monitoring

The closed-loop operation consists in using the output signal of the electronics to control the position stage. In the case of the tilt monitoring, the calculated angle difference is used in the command instruction of the gonio-stage so that the alignment of the cantilever array with respect to the surface is carried out automatically.

The block-diagram, shown in Figure 2.27, describes the closed-loop operation of the tilt control. Supposing that the initial error angle is not zero, the bioplume device is moved toward the surface until bending of both tilt control cantilevers occurs. The two distances d1 and d2 are estimated and the angle is calculated. The desired angle value, i.e. zero for array alignment, is fed in the loop and compared to the measured angle. The resulting difference is the angle error, ε_θ, which is used to appropriately rotate the gonio-stage. Due to possible calibration or measurement errors, this process is repeated until the measured angle equals the input value. Pictures illustrating the closed-loop process from a user point of view are shown in Figure 2.28. From the GUI (graphic user interface), the operator launches the process by clicking the tilt control button, after entering the desired value. Typically, when the starting misalignment angle is 0.1°, the horizontality of the array is achieved after 3 to 4 loops with an accuracy of 1/1000°.

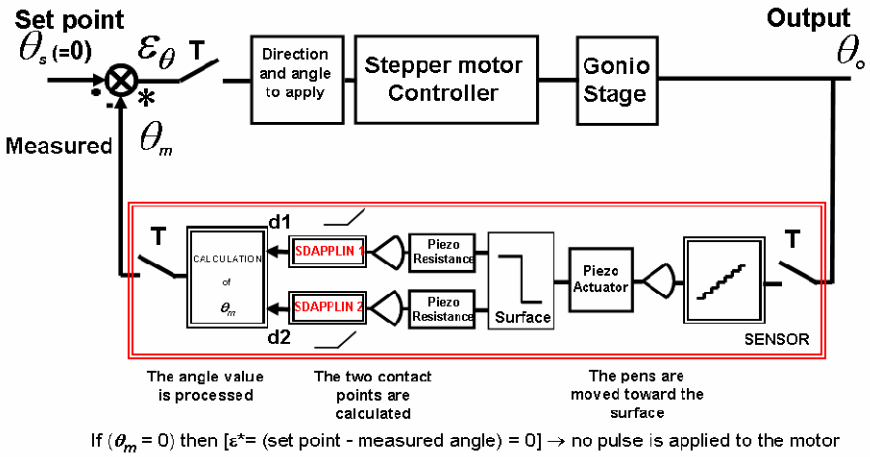

Figure 2.27: *Block diagram of the closed-loop process for automatic tilt monitoring.*

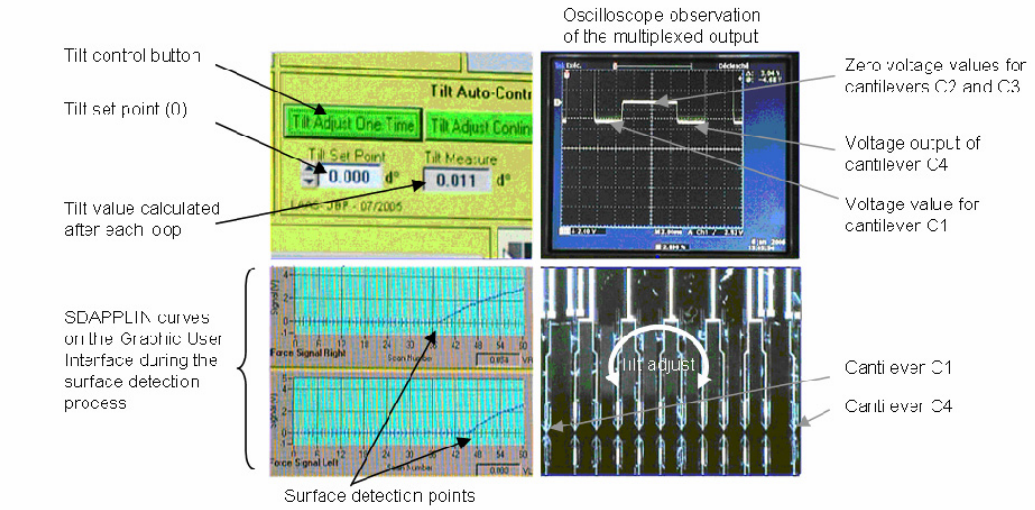

Figure 2.28: *Simultaneous operations during the tilt monitoring and control.*

In a similar manner, a closed-loop is implemented and used to control the contact time and force during the deposition process. The response of the piezoresistors of the depositing cantilevers is used for this aim. One can imagine that such a closed-loop configuration could also be used as a safety net to prevent breaking the cantilevers because of man-made errors: an unexpected significant change in the resistor value of the cantilevers occurring during the displacement of the chip could stop the chip motion.

5.5. Spotting procedure

Experimentally, the bioplume closed-loop configuration is used to detect the loading and deposition surfaces and to measure and correct the trim error before spotting. The angle error is estimated by comparing the two signals of the side cantilevers while approaching the deposition surface. Trim correction is carried out by adjusting the tilt until the signals are equal. The tilt adjustment is not carried out continuously but only when necessary, i.e. usually before the deposition process. The inside sensing cantilevers are then used to detect the loading and the deposition points, ensuring proper liquid transfers between the depositing cantilevers and the surfaces. Once these values are stored in the PC, matrices of spots are automatically printed at chosen locations with specific angles. Loading is previously achieved by dipping the cantilevers in a drop of the liquid to be spotted or in the reservoirs of a dedicated loading chip during a few seconds. During the deposition process the two depositing cantilevers bearing the piezoresistors are used to measure and control the contact time and force. The displacement of the chip can be adjusted; a speed of 10 mm/s ensures a fast and secure operation. The time response of the overall system is estimated to be less than 1 ms, thus deposition times longer than 10 ms are usually used to ensure an accurate contact time.

6. Influence of deposition parameters on the uniformity and the size of the printed features

6.1. Materials and methods

The bioplume spotting system was used to investigate the effect of the trim error on the uniformity of the printed drop matrices. The influence of the contact time and force on the size of the deposited droplets was also studied for different surface wettablities.

For this purpose, liquid drops were deposited onto surfaces exhibiting different wettabilities: gold, silicon and silicon dioxide. Experiments were performed with a water-glycerol mixture (75%-25% in volume) to avoid evaporation. 5 mM of fluorescein was added to the solution for proper observation with a fluorescence microscope. The cleaning of gold and silicon dioxide surfaces was achieved by dipping the samples in a H_2SO_4-H_2O_2 bath for 2 minutes, followed by a water rinse. The resulting equilibrium contact angle of the water-glycerol solution was measured to be around 45° and 8° after the cleaning step for gold and silicon dioxide, respectively. The silicon samples were further dipped into a buffered hydrofluoridric acid (BHF) solution for 30 seconds and rinsed, leading to a 65° contact angle. Previous to any deposit, the trim of the array was automatically adjusted using the closed-loop system and the

surface of the sample was detected using the two depositing cantilevers bearing the piezoresistors.

6.2. Experiments

6.2.1. Tilt of the array

Deposition of matrices of drops was firstly carried out for different trim error angles during a single programmed run. To make sure liquid deposition occurs, the surface was raised by 15 µm from the detected contact point and the contact time was set to 300 ms. The angle between the array and the surface was incremented from one row to another by 0.1° starting from a perfect alignment. Figure 2.29 shows the photograph of the resulting matrices spotted on a gold surface, consisting of 5 rows of 10 parallel 6 × 4 water-glycerol droplets. As expected, the number of depositing cantilevers touching the surface lowers as the trim error increases. Therefore, droplets are missing and the printed matrix is non-uniform, thus demonstrating the importance of the tilt control.

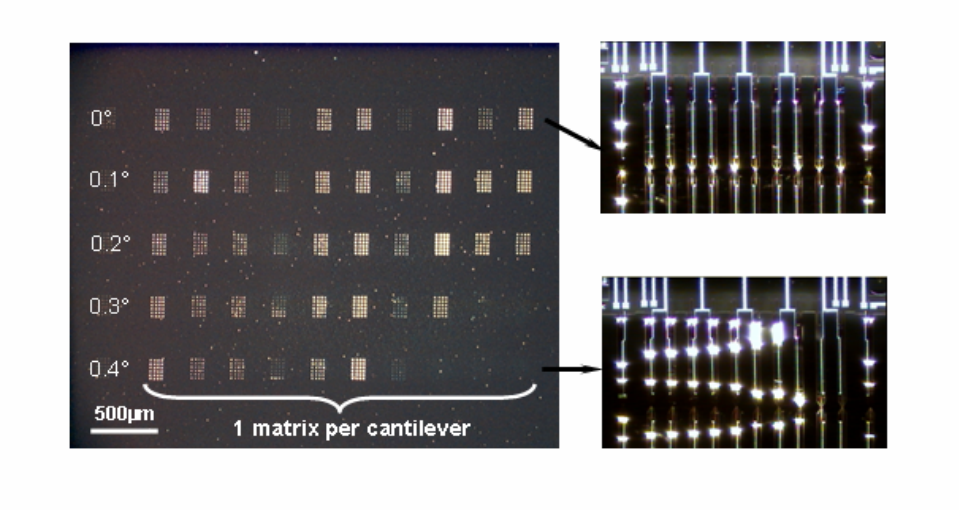

Figure 2.29: *Left: Photograph of water-glycerol droplet matrices realized by increasing the misalignment of the array. Right: Optical photographs of the array while depositing for 2 different tilt angles (Top: 0°; Bottom: 0.4°).*

6.2.2. Contact force

In order to investigate the influence of the contact force used during deposition on the size of the printed spots, rows of droplets were realized by incrementing the displacement of the piezoactuator from 2 µm to 20 µm after the cantilevers touch the surface. As the piezoactuator moves the cantilever array down, the force exerted by the cantilevers onto the surface increases. The deposition time was set to 300 ms. Following the spotting step, the matrices of droplets were observed with a fluorescence microscope. Figure 2.30 shows an optical photograph of droplet rows printed on the different surfaces. Each row corresponds to droplets printed by one cantilever of the array.

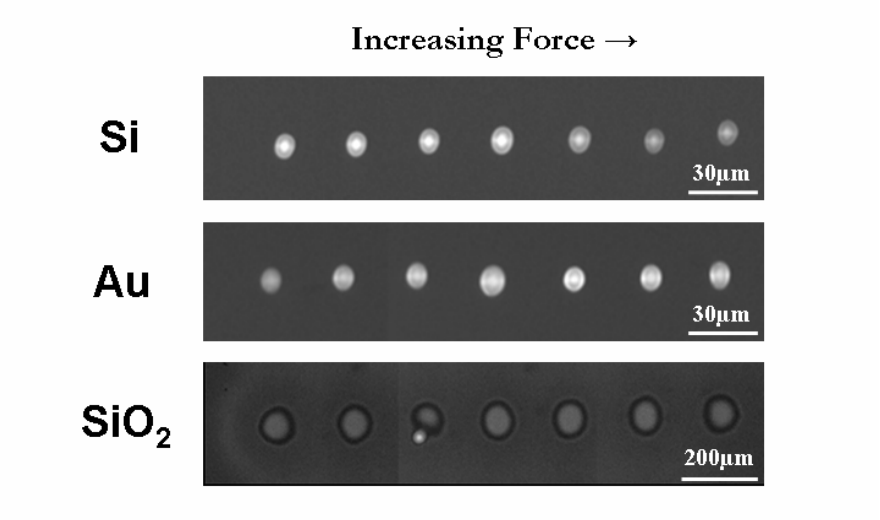

Figure 2.30: *Photographs of printed droplets obtained by increasing the contact force. The cantilever vertical displacement after contacting the surface was incremented from 2 µm to 20 µm (with a 3 µm increment between each drop). Top: Si substrate. Middle: Au surface. Bottom: SiO_2 surface.*

6.2.3. Contact time

An analogous experimental procedure was followed to study the influence of the time during which the cantilevers are in contact with the surface (thus allowing liquid transfer) on the size of the droplets. Rows of drops were deposited with contact times ranging from 20 ms to 20 s. Because of the actuation speed limitation of the spotter, shorter contact times were not included in this experiment. To ensure a proper deposition, the cantilevers were moved 5 µm down the detected surface contact point. Following the deposition, the matrices of droplets were observed with a fluorescence microscope. Droplets printed on the different surfaces with increasing contact times are shown in Figure 2.31.

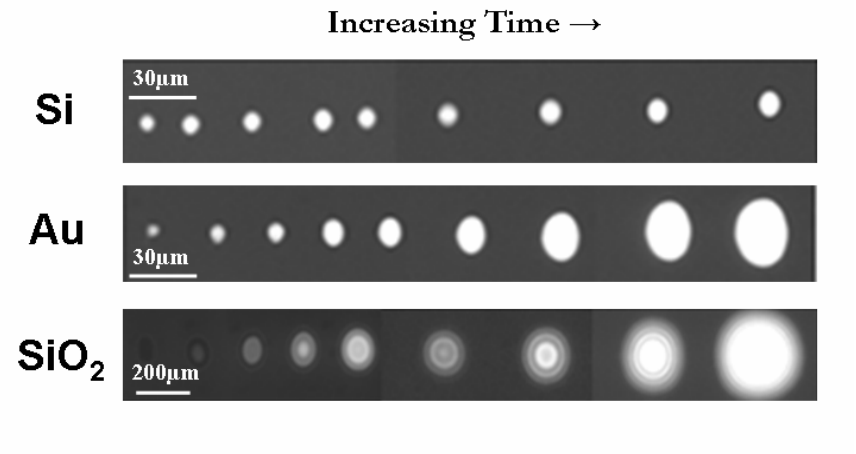

Figure 2.31: *Fluorescent pictures of printed droplets obtained by increasing the contact time. From left to right: 20 ms, 50 ms, 100 ms, 200 ms, 500 ms, 1 s, 2 s, 10 s, and 20 s. Top: Si substrate. Middle: Au surface. Bottom: SiO_2 surface.*

6.3. Results and discussion

The evolutions of the printed spot diameter as a function of contact force and contact time are plotted in Figure 2.32 and Figure 2.33, respectively. Diameter measurements were carried out on the fluorescent pictures shown in Figure 2.30 and Figure 2.31 using an image processing software.

The evolution of the droplet diameters, shown in Figure 2.32, seems linear for the three types of surfaces studied within the range of induced cantilever displacements. From this observation, we conclude that the size of the deposited droplets does not depend on the applied force (it is interesting to recall here that, according to the simulation results, the applied force does not vary linearly with the chip displacement). However, major differences in sizes exist between the droplets printed onto the silicon dioxide surface, and the gold and silicon surfaces. As expected, the more hydrophilic the surface is, the larger the droplets are.

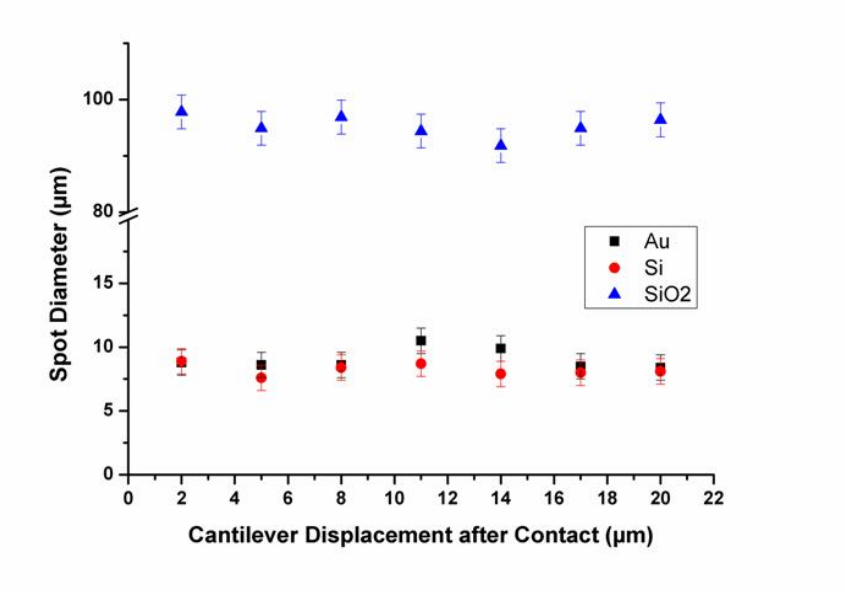

Figure 2.32: *Spot diameter as a function of the force exerted by the cantilever contacting the deposition surface.*

According to Figure 2.33, the contact time seems to influence the size of the printed droplets to a bigger extent. The same behavior is observed in the case of the three surfaces: the diameters increase rapidly within the first second. A plateau is then reached for the most hydrophobic substrate (silicon); the droplets exhibiting approximately a 10 µm diameter even with increasing contact time. We believe that this steady state occurs when the equilibrium between the Laplace pressure of the deposited drop and the pressure of the liquid contained in the cantilever fluidic channel is obtained. For gold and silicon dioxide, the diameter still augments with time. However, this change is more pronounced for the more hydrophilic substrate (silicon dioxide). Thus it seems that the more hydrophilic the surface is, the more important the influence of time on the drop size is.

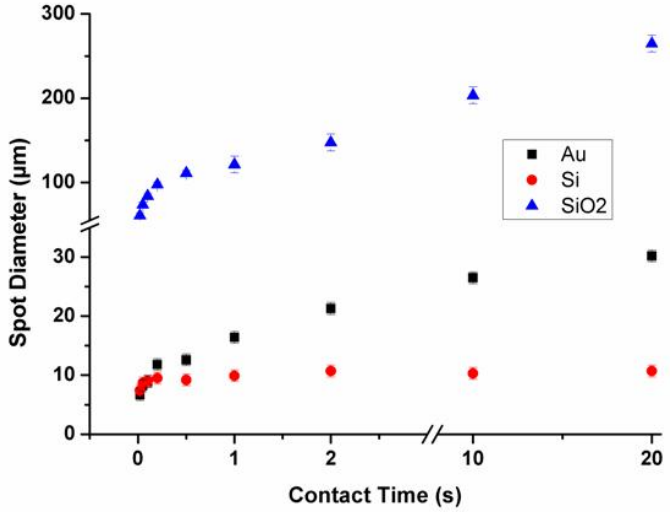

Figure 2.33: *Spot diameter as a function of the contact time during deposition.*

More experiments need to be conducted in order to confirm these behaviors. But we foresee the matrix inhomogeneity to depend on the surface wettability, because the misalignment of the array impacts the time during which each cantilever contacts the surface. Thus, in order to obtain uniform and reproducible matrices, there is a need to control the trim of the array and the contact time during deposition. Once the array is perfectly parallel to the deposition surface, the diameter of the printed drops can be monitored by controlling the contact time between the cantilevers and the substrate.

7. Loading and deposition tests for biological applications

A patterning system dedicated to biochip fabrication and biosensor functionalization at the micrometer scale must be able to locally spot the biomolecules that are to be used as probes or targets. Moreover, the capability to deposit several types of molecules in a single deposition run is essential when considering screening applications that require numerous types of probes. Finally, because most biological solutions are very expensive and available in small quantities, means to reduce wasting materials are highly recommended.

To prove that the bioplume system is suited for biological applications, loading and deposition experiments were conducted with biomolecules. In this section, we firstly demonstrate that various molecules can be addressed at the same location using bioplume without losing their biochemical properties. For this purpose, superposed spots of two complementary oligonucleotides were successively printed on a glass slide and their spot-in-spot hybridization was detected by fluorescent labeling. Secondly, the parallelization of printed molecules was achieved by using a dedicated external loading chip. Finally, preliminary experimentations concerning the active loading of the cantilevers were conducted.

7.1. Deposition of functional biomolecules

In collaboration with the Biochips platform of the Toulouse Genopole (at INSA), we studied the hybridization of two short synthetic oligonucleotides immobilized on a glass slide with the bioplume spotter. We firstly showed that several solutions could be deposited successively with the same cantilevers without cross-contamination thanks to a simple cleaning procedure. Then, the biofunctionality of the deposited oligonucleotide was demonstrated by testing the affinity to the secondary oligonucleotide with a classical procedure. Finally, hybridization of complimentary DNA strands successively deposited with bioplume was achieved, showing that our method permits reducing the volume of reagents used for revelation. Indeed, instead of entirely covering the slide surface with the complementary solution (classical procedure used for microarrays), only tiny droplets of the fluorescent complementary oligonucleotide were spotted on top of the immobilized spots. The hybridization of these two nucleotides deposited as two superposed spots was called "spot-in-spot hybridization".

7.1.1. Materials and methods

The solid supports used in the experiments were proprietary aldehyde-dendrimer-coated-glass slides [21]. Three oligonucleotides were used: an amino-modified oligonucleotide 35-mer NH2 (5'-NH2-GTG ATC GTT GTA TCG AGG AAT ACT CCG ATA CCA TT-3') for the covalent linkage with the aldehyde-surface and its complementary sequence 15-mer Cy5 (5'-Cy5-AA TGG TAT CGG AGT A-3') labeled with a red Cy5 fluorophore. Another oligonucleotide 15-mer Cy3 (5'-Cy3-CAT ATT CGA CGG CAT C-3') functionalized with green Cy3 was used for the study of cross-contamination and for the superposition experiments. The synthetic oligonucleotides were all purchased from Operon (Germany). The molecules were suspended in Na_2HPO_4 buffer (0.1 M, pH 9) and glycerol (25% of the final volume) was added to lower the evaporation rate of the solution.

After deposition, DNA was allowed to covalently immobilize on the surface by leaving the droplet on the slide for 30 min at room temperature. Dendrislides were then treated with 3.5 mg/mL $NaBH_4$ to block unreacted aldehyde functions (during 30 min). Subsequently, $NaBH_4$ was eliminated with a water rinse. Hybridization was carried out with a 3X SSC 0.3% SDS buffer, chosen according to classical microarray protocols. Hybridization times were set to 30 min. After hybridization, slides were immersed in washing solutions to remove non-hybridized oligonucleotides: 5 min in 3X SSC 0.3% SDS, 2 min in 0.1% SDS, 2 min in 1X SSC, and 1 min in 0.1X SSC. All washing and treatment steps were performed with caution directly on the printed slides.

Fluorescence signals were captured with the laser scanner Genepix 4100A (Axon Instruments, CA) and analyzed with the Genepix 6.0 software. Because of the low resolution of the scanner (5 µm) and the size of deposited droplets (20 µm in diameter) the image of each spot contained 4 pixels only.

7.1.2. Validation of the cleaning procedure

The washing procedure was carried out by simply dipping the microcantilevers into water and gently agitating them. To evaluate the efficiency of this method, the following experiments were conducted using several cleaning times: fluorescent oligonucleotides were firstly deposited with bioplume, then a washing step was performed and finally the subsequent deposition of clean buffer was done. We evaluated the immersion time necessary to remove any contaminants by measuring the residual fluorescence of the buffer spots and comparing it to the fluorescence of the firstly deposited oligonucleotide spots. Figure 2.34 shows that a 15 minutes rinse was sufficient to eliminate 96% of the solution previously deposited. After a 60 minutes wash, the fluorescent signal was below detection. Unfortunately, these rinsing times are very long compared to the cleaning procedures used for commercial pins. This time should be lowered to a minute or less in order to be efficient and competitive. This cleaning procedure must be optimized and could be improved by using other chemical reagents for instance.

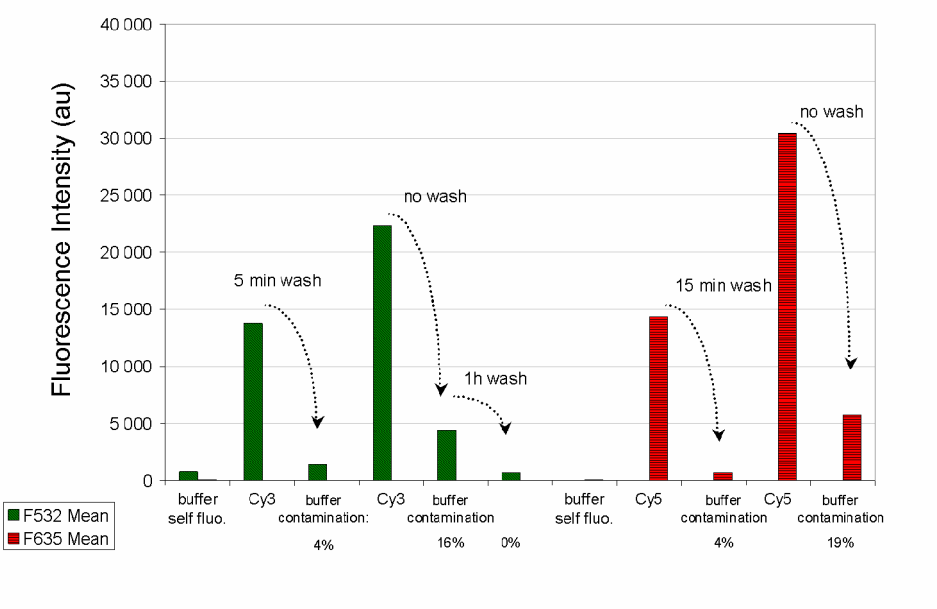

Figure 2.34: *Successive deposition of buffer and Cy3/Cy5 labeled oligonucleotides on a dendrislide, with and without washing the cantilevers between the deposition runs.*

7.1.3. Preservation of the biofunctionality

The biofunctionality of the oligonucleotides deposited with bioplume was checked by following a classic protocol used for microarrays and adapted to the size of the printed spots (20 µm diameter instead of the 200 µm achieved with commercial spotters).

Firstly, bioplume was used to create arrays of 35-mer NH_2 oligonucleotide spots on a dendrislide. Then, buffer alone was spotted as a negative control. After completing the steps enabling DNA immobilization and covalent coupling, the spotted area was

entirely covered with a solution containing the Cy5-labeled complementary oligonucleotides. After waiting for 30 min to allow hybridization reactions, the slide was washed to remove non-hybridized oligonucleotides.

On the laser scanner image, fluorescent signal appeared where 35-mer NH_2 was spotted, but no fluorescence was detected at the location of the buffer spots or on the bare surface. This proves that hybridization occurred and was detected despite the scale reduction and the presence of 25% glycerol.

7.1.4. Spot-in-spot interactions of subsequently deposited oligonucleotides

7.1.4.1. Superposition of deposited biological spots

Spot-in-spot experiments were then conducted in order to demonstrate the successful hybridization between an oligonucleotide and its complementary, both locally deposited with bioplume. The ability to successively deposit droplets containing different molecules at the same location was firstly verified. Means to check the appropriate mixing of the various reagents in the superposed drops were provided. Experimentally, 2 columns of 10 spots of 15-mer Cy5 oligonucleotides were firstly deposited. The microcantilevers were cleaned using the abovementioned procedure and a similar matrix of drops of Cy3-labeled oligonucleotides was spotted. The second deposition was carried out so that half the spots would be deposited on the bare slide, while the other half would be superposed to the 15-mer Cy5. Figure 2.35 shows the scanner image obtained after completion of the deposition process. According to this picture, we obtain a correct superposition of the droplets as yellow spots are observed where the red and green fluorescent drops overlap, thus demonstrating the mixture of both compounds.

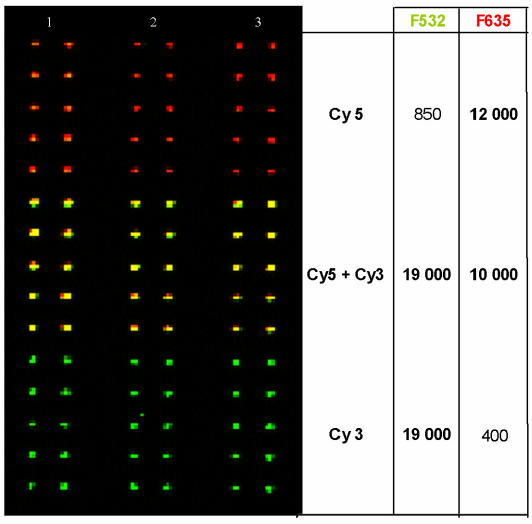

	F532	F635
Cy 5	850	12 000
Cy5 + Cy3	19 000	10 000
Cy 3	19 000	400

Figure 2.35: *Spot-in-spot deposition with micrometer precisions; superposition of Cy3 and Cy5 spots. A 20-spot grid of 15-mer 5'-labeled Cy5 oligonucleotide 10 µM in 25% glycerol is deposited. Cantilevers are washed during 15 min in water. Then, a grid of 15-mer 5'-labeled Cy3 oligonucleotide 1 µM in 25% glycerol is deposited so that 10 spots are superposed.*

7.1.4.2. Spot-in-spot hybridization

A final experiment was conducted to prove that oligonucleotides retain their properties in the superposed droplets. For that purpose, a procedure similar to the one presented above was followed using complementary DNA strands. A grid of 35-mer amino-oligonucleotide was addressed on an aldehyde dendrimer coated glass slide and immobilized via a covalent linkage. Treatment and washing were performed with a pipette on the fixed glass slide. Subsequently, the complementary 15-mer Cy5-labeled oligonucleotide was addressed, so that half of the spots were superposed. After 30 minutes of hybridization, the slide was rinsed. Figure 2.36 shows scanned images obtained before and after this last washing step. As shown in the Figure 2.36, a specific signal is obtained only in the spots where both 35-mer NH_2 and 15-mer Cy5 oligonucleotides were deposited.

This proves that protocols used with commercial apparatuses can be transposed to a smaller scale using bioplume. Compared to protocols usually performed for microarray experiments, volumes of analytes and duration of experiment are considerably reduced. For example, 35-mer NH_2 covalent immobilization on the aldehyde dendrislide was reduced from 15 h to 30 min. The subsequent $NaBH_4$ treatment was also shortened from 3 h to 30 min.

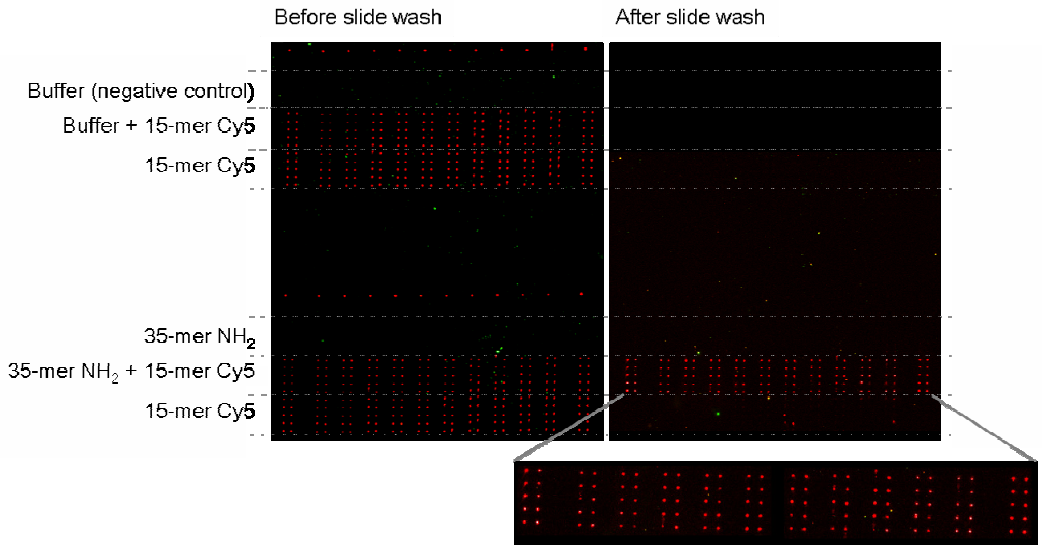

Figure 2.36: *Spot-in-spot hybridization of oligonucleotides on a dendrislide.*

The experiments presented in this section indicate that contact printing with bioplume allows successive superposed deposition of active biomolecules at micrometer-precise locations, possibly allowing the local functionalization of MEMS sensing devices. As deposition of biomolecules at computer-controlled positions is possible, potential use of the device can also be foreseen for molecular assembly. Further experiments should now be conducted to validate spot-in-spot interactions of proteins.

7.2. Deposition of different molecules in a single run

In order to avoid having a complex fluidic system on the bioplume chip (that would raise additional fabrication issues), and to satisfy versatility and ease-of-use criteria, we chose to carry out the loading of the cantilevers by external means, via a loading chip. The deposition of several types of molecules in a parallel manner is possible providing that each cantilever can be loaded with a different solution. For that purpose, we have used an external loading chip specifically fabricated by the CNM-CSIC in Barcelona (partners of the NaPa program) for the bioplume cantilever array.

The microfluidic chip allows feeding the 10 cantilevers with 3 different solutions. The chip includes 3 input reservoirs and 10 dispensing holes, each reservoir being linked to 3 or 4 holes by means of closed microchannels. Liquid is supplied to the input reservoirs by pipetting. Upon capillary forces, the liquid fills up the microchannels and the dispensing holes. Loading of the bioplume chip is then achieved by dipping the cantilevers in the dispensing holes. To avoid the large deflection of the tilt monitoring cantilevers during the bioplume loading, two dispensing holes free from liquid supply are added. The chip dimensions are 20 mm long and 12 mm wide, and each dispensing hole is 200 µm long, 100 µm wide and 200 µm deep. The fabrication process of the fluidic chip relies on CNM technology and includes silicon reactive ion etching and pyrex bonding. Pictures of the fabricated chip are shown in Figure 2.37. Colored liquids were used to demonstrate that liquid could be supplied from the reservoirs to the dispensing holes without mixing.

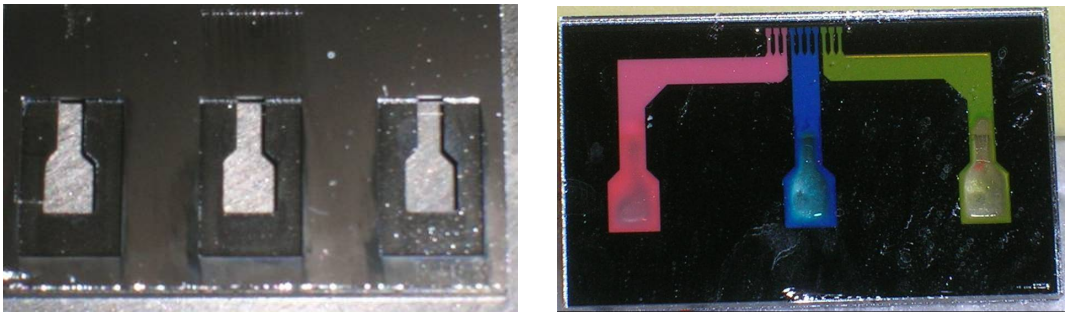

Figure 2.37: *Optical pictures of the CNM fluidic chip. Left: Front side. Right: Back side showing the colored inks filling the channels.*

Loading and printing experiments were then conducted with Cy5 and Cy3 labeled oligonucleotides. Figure 2.38 provides pictures of the loading process. The photograph on the right, showing how loading is achieved from a microdroplet reservoir, illustrates the advantage of using a fluidic chip in terms of reduction of the volume required for loading. The 3 reservoirs were filled with Cy5, Cy3 and Cy3+Cy5 solutions. The bioplume cantilevers were dipped in the dispensing holes, for several seconds to allow proper filling of the cantilever channel, and a matrix of spots was deposited on a glass slide. The spots were then observed with a fluorescence microscope (see Figure 2.39). The green and red fluorescent signals are seen at the location of the Cy3 and Cy5 drops, thus demonstrating the proper operation of the fluidic chip.

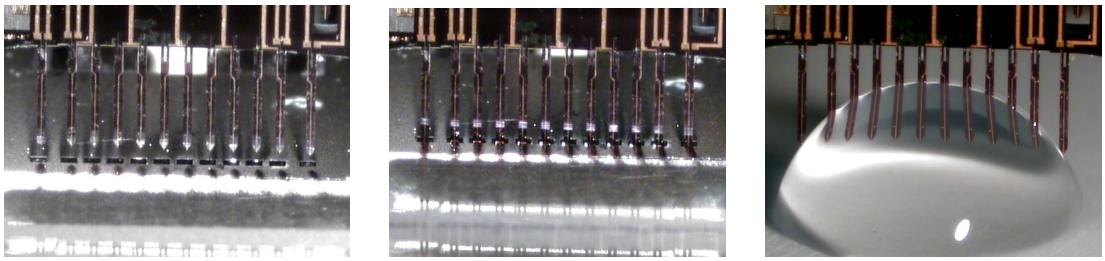

Figure 2.38: *Left and Centre: Photographs of the loading process before and after dipping the cantilevers in the dispensing holes. Right: Picture of the use of a microliter droplet as a loading reservoir.*

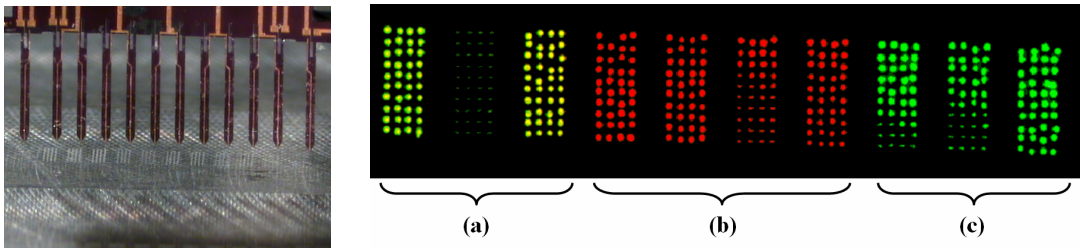

Figure 2.39: *Picture of the bioplume array after deposition showing the printed spot matrix (left). Fluorescence image of the resulting matrix (right): (a) Cy3+Cy5, (b) Cy5, and (c) Cy3.*

7.3. Cantilever loading with electrowetting actuation

In order to reduce the amount of dead volume required for the loading of the cantilevers, we have implemented a liquid actuation scheme based on electrowetting. Electrowetting occurs by applying a voltage between the electrode in the cantilever channel and the liquid to be loaded, resulting in the spreading of the liquid on the electrode. Preliminary experiments were conducted with the fabricated cantilevers to demonstrate the viability of the method. The liquid to be loaded, either pure dimethyl sulfoxide (DMSO) or 50% DI water – 50% glycerol solution was placed in a metallic reservoir. Loading was achieved by dipping the tip of the cantilever in the liquid and applying a voltage between the cantilevers and the metallic reservoir (see Figure 2.40). Dipping of the cantilevers occurred by vertically approaching the liquid surface with an incident angle of 70° between the liquid meniscus and the surface of the cantilevers with a 1° angle accuracy. The small angle deviation from a perpendicular configuration was necessary to avoid any buckling of the cantilevers during the droplets deposition process. To ensure the proper loading of the cantilevers, matrices of spots were obtained by direct contact printing on silicon or gold surfaces. The deposition procedure was carried out at ambient conditions, i.e. temperature of 20 °C and humidity level of about 50%. A CCD camera was used to monitor the loading and the deposition processes. Due to the hygroscopic property of glycerol, the printed droplet matrices could directly be seen under an optical microscope after the deposition process. However, because of the higher evaporation rate of DMSO, fluorescein was added to the solution (resulting in a

final 10 mM fluorescein concentration) to enable the observation of the resulting spots with a fluorescence microscope. The electrowetting phenomenon appeared when applying less than 4 V, resulting in a rise of liquid inside the channel only. The voltage was then slowly increased to keep the liquid moving forward in the channel. The channel and reservoir could be completely filled after setting the voltage to several tens of volts during a couple of seconds. As expected, because the electrodes are not passivated, hydrolysis effects appeared when loading the water-glycerol solution, leading to power consumption and bubble production at the tip of the cantilevers. This effect was less significant when using DMSO, thus enabling a more proper loading (see Fig. 2.41). Deposition of more than 50 droplets per cantilever was then successfully performed onto silicon and gold surfaces. Figure 2.42a shows an array of cantilevers while depositing and the resulting spots can be seen in Figure 2.42b and c.

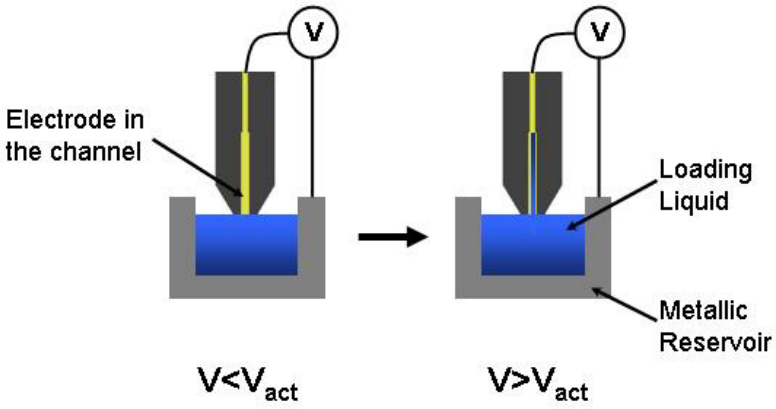

Figure 2.40: *Schematic of the loading experiment. The conductive part of the cantilevers where electrowetting takes place is shown. Left: applied voltage below the actuation voltage; Right: applied voltage above the actuation voltage.*

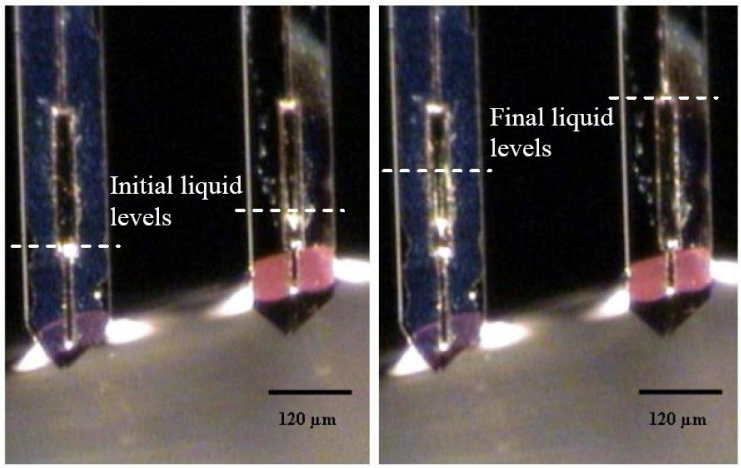

Figure 2.41: *Photographs of the loading of gold covered cantilevers with DMSO. Left: after applying 4 V. Right: after applying almost 30 V.*

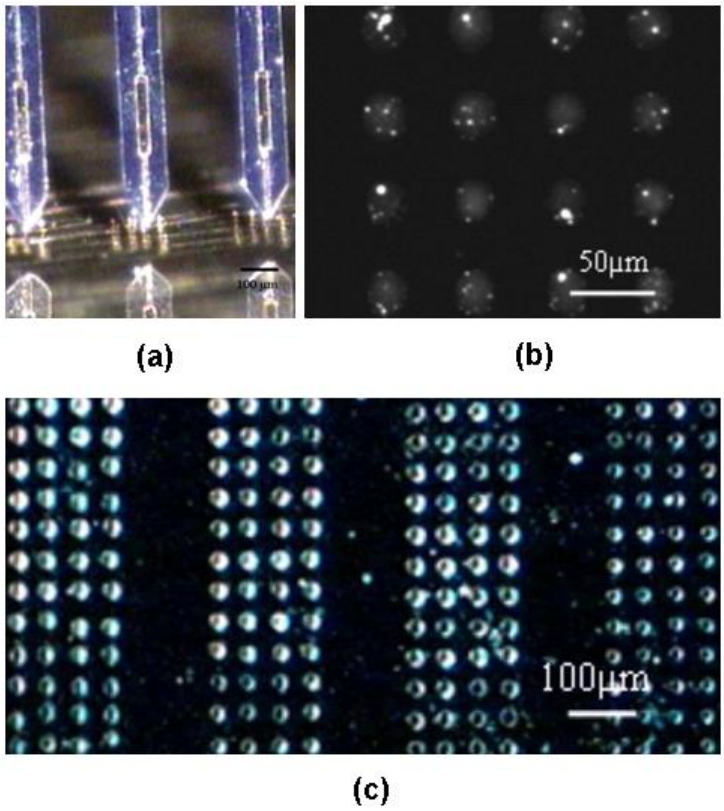

Figure 2.42: *(a) Photograph of gold covered cantilevers while depositing. (b) Fluorescence image of DMSO-fluorescein spots. (c) Picture of printed water-glycerol droplet matrices.*

These results show that electrowetting actuation is a promising solution for cantilever loading. However, the hydrolysis reactions occurring at the tip of the cantilever are to be avoided when using biological samples. Hence, a suitable insulating layer has to be selected to coat the metal electrodes. In this case, the actuation based on electrowetting on dielectric allows using conducting liquids with higher actuation voltages. Finally, a proper surface treatment has to be added to render the cantilevers surface hydrophobic with a low contact angle hysteresis. This is necessary to efficiently implement the electrowetting actuation scheme enabling the reversibility of the phenomenon [22]; and to keep the droplets size comparable to the depositing tip. Because parylene seems to fulfill all these requirements (i.e. it leads to conformal coating, it exhibits a hydrophobic behavior and very good dielectric properties), it has been used as a coating layer onto fabricated cantilevers. Figure 2.43 shows a SEM picture of the tip of the cantilever with the parylene layer conformally coating the channel electrode. Preliminary tests have demonstrated the proper loading of water based solutions without hydrolysis. Systematic loading and deposition experiments are now required to validate the printing ability of the coated device and to estimate the voltage required for complete channel filling.

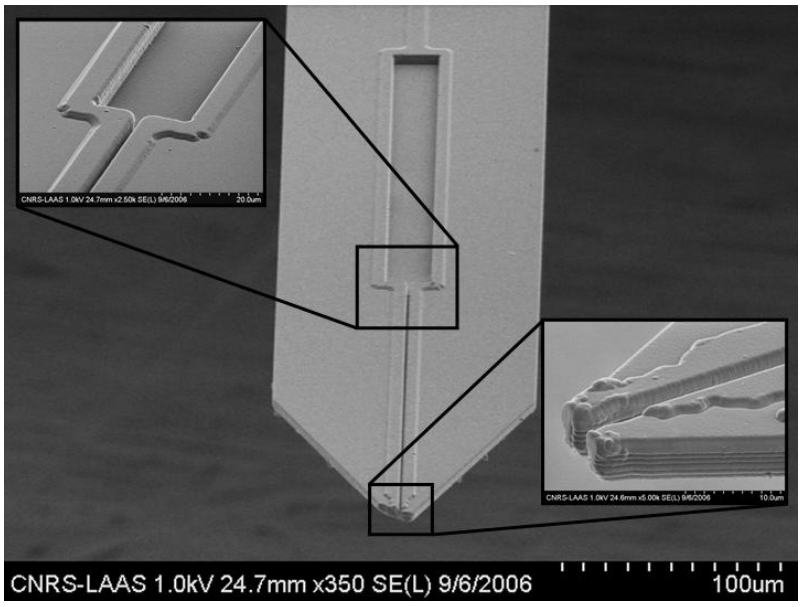

Figure 2.43: *SEM pictures of a cantilever coated with parylene.*

8. Conclusion

In this chapter we have presented a liquid patterning tool, so-called bioplume, based on the use of an array of 12 silicon microcantilevers. Each cantilever enables the deposition of picoliter droplets thanks to a direct contact of the tip and the surface to pattern. The fabrication process of the cantilevers relies on conventional microfabrication techniques and silicon-on-insulator wafers. The cantilevers are 1.5 mm long, 120 µm wide and 5 µm thick. A fluidic channel is incorporated into each cantilever for liquid storage and delivery. The cantilever array is integrated into a closed-loop automated system enabling the control of the droplet homogeneity and the spatial positioning of the microarray. The automated system relies on the use of force sensors, i.e. piezoresistors, integrated into 4 of the 12 cantilevers of the array: 2 force sensing cantilevers placed on the side of the array are used for the adjustment of the trim, whereas 2 depositing cantilevers are used to control the deposition process. A dedicated electronics circuitry, based on a modified Wheatstone bridge, allows measuring the cantilever bending through the piezoresistance variations. The sensitivity of the piezoresistors is approximately 1 V/µm with an estimated noise value of less than 30 mV. These measurements result in a minimum detectable deflection of less than 30 nm. The depositing system comprises of the cantilever array silicon chip fixed on a four-degree-of-freedom automated spotter, the electronic circuit and a PC. The output of the electronics is connected to the PC so that the microsystem is in a closed-loop configuration: the bending of the cantilever occurring when touching a solid surface or a liquid droplet leads to the determination of contact points, which are then used to control the displacement of the array.

Preliminary experiments were conducted with this spotter to study the influence of the contact force and time during deposition on the size of the spots according to different surface wettabilities. We have observed that the drop size is not affected by the deposition force. However, as expected, the drop diameter increases with contact time. The change in drop size with time seems to be more important as the surface is more

hydrophilic. In all cases, the size of the deposited droplets can be controlled by the contact time.

When printing large areas of nonplanar samples, the misalignment and the contact height are expected to vary from one point to another. By using force sensing cantilevers in a closed-loop system, we ensure that the sample topography does not affect the consistency of the printed droplets. Furthermore, surface patterning that consists in a succession of liquid loading and deposition steps can be performed automatically by this system without the need of an external optical setup.

Because it allows the precise control of the deposition parameters, the bioplume system is particularly attractive for biological applications, i.e. biochip fabrication or biosensor functionalization. Indeed, the uniformity of the DNA or protein spots of biochip arrays is of importance to properly compare fluorescence signals from the different spots and thus to validate the results. Moreover, the functionalization of small and fragile MEMS-based sensors requires the precise delivery of droplets with a minimum force exerted on the surface. Experiments have thus been finally conducted to demonstrate the ability of the bioplume spotter to deposit functional biomolecules. These experiments proved that it is possible to address oligonucleotides with the same microcantilevers several times at the same location without contamination. Successful hybridization tests showed that biomolecules do not lose their biological properties after deposition. Furthermore, we successfully used an external fluidic chip in order to load each cantilever with a different solution, thus enabling the deposition of several biomolecules in a single run. Compared to classical microarray protocols, volumes and time of assays were drastically reduced.

In the next chapter, we finally use the bioplume direct liquid patterning system in combination with other deposition means: self-assembly and electro-assisted methods. The mix and match approach enhances the deposition potentials of the system, in terms of variety of deposited materials and 3D control of the printed patterns.

References

[1] P. Belaubre et al., Sensors and Actuators A, 110, p. 130 (2004).
[2] R. Raiteri et al., Sensors and Actuators B, 79, p. 115 (2001).
[3] S. Alexander et al., Journal of Applied Physics, 65 (1), p. 164 (1989).
[4] J. Brugger et al., Sensors and Actuators A, 43, p. 339 (1994).
[5] S. Watanabe, and T. Fujii, Review of Scientific Instruments, 67 (11), p. 3898 (1996).
[6] M. Tortonese et al., Proceedings of the 1991 International Conference on Solid-State Sensors and Actuators (Transducers'91), 24-27 Jun, 1991, San Francisco, USA, p. 448 (1991).
[7] E. Cocheteau et al., Proceedings of the 11th International Conference on Solid-State Sensors and Actuators (Transducers'01), 10-14 Jun, 2001, Munich, Germany, 2, p. 1070 (2001).
[8] D. Banarjee et al., Proceedings of the 7th Conference on Miniaturized Chemical and Biochemical Analysis System (μTAS 2003), 5-9 Oct, 2003, p. 57 (2003).
[9] K. S. Ryu et al., Applied Physics Letters, 85 (1), p. 136 (2004).
[10] C. Quilliet, and B. Berge, Current Opinion in Colloid & Interface Science, 6, p. 34 (2001).
[11] S. K. Cho, H. Moon, and C.-J. Kim, Journal of Microelectromechanical Systems, 12 (1), p. 70 (2003).
[12] W. Satoh, M. Loughran, and H. Suzuki, Journal of Applied Physics, 96 (1), p. 835 (2004).
[13] T. B. Jones, K.-L. Wang, and D.-J. Yao, Langmuir, 20 (7), p. 2813 (2004).
[14] J. R. Hampton, A. A. Dameron, and P. S. Weiss, Journal of the American Chemical Society, 128 (5), p. 1648 (2006).
[15] F. Walsh, "A first course in Electrochemical Engineering", The Electrochemical Consultancy, Romsey (1993).
[16] M. Tortonese, "Force sensors for scanning probe microscopy", Ph.D. thesis, Stanford University (1993).
[17] M. Tortonese, R. C. Barrett, and C. F. Quate, Applied Physics Letters, 62 (8), p. 834 (1993).
[18] C. Bergaud et al., Proceedings of the 15th IEEE International Conference on Micro Electro Mechanical Systems (MEMS'02), 20-24 Jan, 2002, Las Vegas, USA, p. 360 (2002).
[19] D. Saya et al., Sensors and Actuators A, 123-124, p. 23 (2005).
[20] J.-B. Pourciel, L. Jalabert, and T. Masuzawa, Proceedings of the 2002 Japan-USA Symposium on Flexible Automation, July, 2002, Hiroshima, Japan, 1, p. 553 (2002).
[21] E. Trévisiol et al., New Journal of Chemistry, 27, p. 1713 (2003).
[22] H. J. J. Verheijen, and M. W. J. Prins, Langmuir, 15, p. 6616 (1999).

Chapter III

Mix and Match Surface Patterning Methods for Active Control during Deposition

1. Introduction

In this chapter, we propose to demonstrate the compatibility of the bioplume liquid delivery system, presented in the previous chapter, with two other patterning methods: self-assembly and electro-assisted deposition. The interest to combine those techniques is twofold. Firstly, the use of self-assembly and electro-assisted methods provides means to actively control the bioplume deposition process. Secondly, bioplume offers the possibility to localize self-organization and electro-induced reactions in confined and ultra-small volumes, extending the fabrication possibilities inherent to both techniques and allowing their fundamental studies at low scales.

1.1. Liquid delivery and self-assembly

As stated in the first chapter of this thesis, self-assembly is a very powerful way to create patterns onto a surface, but it needs to be associated with other techniques in order to precisely delimit the patterned areas. Bioplume is a tool perfectly suited for this purpose because it enables the local delivery of picoliter droplets. Particles or small entities dissolved in the spotted solution undergo self-organization during the drying of the drop, leaving a pattern within the deposition area. The use of self-assembly is of great interest for our tool. Indeed, it provides means to nanostructure surfaces with micrometer size tips and to create patterns smaller than the minimum printed feature size. Moreover, the precise and reproducible size of the printed drops can be obtained by controlling the number of self-organized entities. In some cases, i.e. for solutions highly concentrated or deposited on hydrophobic surfaces, it is possible to create three-dimensional (3D) patterns. Finally, regarding the numerous entities used in self-assembly processes and their various physico-chemical properties, the capabilities of bioplume are greatly enhanced in terms of the variety of materials and functions that can be deposited. In order to demonstrate the compatibility of bioplume with self-assembly, we have carried out experiments focused solely on the deposition of nanoparticles. This work has been performed in close collaboration with the Institute for Health and Consumer Protection of the Joint Research Center in Ispra, Italy (within the Nano2Life network of excellence), who has provided the different nanospheres and the functionalized surfaces.

1.2. Liquid delivery and electro-assisted methods

As mentioned in the second chapter of this thesis, electro-assisted methods are easily implemented by providing a set of electrode (one in the cantilever channel and the other one onto the deposition surface) and applying a potential difference during the drop deposition. Two phenomena, i.e. electrowetting and electrochemistry, can be induced regarding the passivation state of the substrate electrode and the type of liquid used.

1.2.1. Electrowetting

Electrowetting of conducting and insulating liquids occurs on passivated and bare surfaces, respectively. Electrowetting results in a change of contact angle of the liquid on its contacting surface because of a charge difference at the solid/liquid interface. As a result, the contact angle of the drop can be tuned by adjusting the applied voltage. The primary interest of incorporating the electrowetting scheme to bioplume is the active and precise control of the area of the printed drop during deposition. This feature also facilitates the drop delivery onto superhydrophobic surfaces. We have conducted preliminary experiments with bioplume to demonstrate the benefit of electrowetting for spotting applications.

1.2.2. Electrochemistry

The liquid drop can also be used as an electrochemical cell into which redox reactions are induced by applying a voltage between the bare electrodes of the cantilever and the surface. Electrochemistry is widely used to deposit or etch various materials allowing a precise control of the process by monitoring the number of charges supplied to the cell. Thus, the incorporation of electrochemistry-assisted patterning techniques to the bioplume tool allows the control of material growth during deposition. This is especially interesting for the fabrication of very thick structures. The other advantage inherent to the electrochemical deposition relies on the strength of the bond created between the surface and the material deposited, providing an ideal grafting. It also enables the deposition of various types of materials, e.g. metals and polymers. As a proof-of-concept, we have electrodeposited copper islands and electropolymerized polypyrrole onto gold surfaces for microelectromechanical systems (MEMSs) and biochip applications, respectively. The results presented in this chapter were carried out conjointly with the CREAB group in Grenoble (SPrAM /DRFMC, CEA-G).

2. Local deposition of nanoparticles using bioplume

2.1. Introduction - Motivation for this work

The unique properties of nanostructured materials are the main motivation for the miniaturization of devices in many fields of applications, such as electronics, optical sensors, electrochemistry and biosensors. Among the different nanolithographic techniques, the use of nanosized colloidal particles as building blocks, i.e. colloidal lithography (CL), is an emerging field [1]. CL uses two-dimensional (2D) arrays of

colloidal particles as masks and templates for etching and deposition of nanopatterns. In the CL processing route, the first and more crucial difficulty is the control of the self-assembly process of the particles in a 2D crystalline array onto the surface to be nanostructured. The formation of the particle array takes place during the evaporation of the solvent due to the capillary forces between the particles. Several techniques have been used to induce the ordered arrangement of the particles, such as dip coating [2,3], air- and oil-water interfaces [4], Langmuir-Blodgett processes [5], spin-coating [6], and template assisted techniques [7,8]: the objective of these techniques is to create mesoscopic areas homogenously covered by the arranged particles. In particular, the template assisted deposition allows the creation of geometrically well-defined micropatterns of ordered nanobeads. However, the fabrication process of the microtemplate necessitates the use of classical photolithography steps, which are complex, time-consuming and expensive.

Printing-based techniques are more straightforward in the sense that nanoparticles are directly deposited on the substrate with submicrometer resolution using dedicated tools or stamps [9]. Among those techniques, soft lithography has been optimized for ordering polystyrene beads using elastomeric stamps under pressure while maintaining the temperature above the particle glass transition temperature [10]. Ordered 2D and 3D microstructures have been achieved using this technique. The main drawback of this approach is that the ordering is imposed by the design of the patterned stamp and only one type of particles can be deposited on the whole surface at the same time.

Nanodispensing techniques or dip-pen nanolithography [11,12], based on the use of microcantilevers, are more promising for that purpose since they combine several advantages. The first one is that they permit a direct patterning of the surface with different kinds of nanoparticles without any need for prefabricated patterns. Alignment of the cantilevers with respect to specific regions on the surface is straightforward since the cantilevers themselves can be used as displacement sensors. Moreover the use of cantilever arrays improves the throughput of the direct patterning, allowing the creation of macroscopic patterned areas in a few minutes. The second one is that they make use of a very low amount of nanobead solution and allow minimizing the waste of raw materials.

The bioplume tool, developed in this thesis work, combines all the aforementioned advantages. It is thus perfectly suited to create nanostructured microspots from the direct deposition of nanoparticles in solution. In this section, we aim to validate the use of bioplume for colloidal patterning.

2.2. Nanostructuring surfaces with conjugated silica colloids

In order to prove the feasibility of colloid deposition with the bioplume tool, we have conducted preliminary experiments with the first generation of cantilevers. For this purpose, picoliter droplets containing 300 nm diameter polyethylene glycol and 150 nm diameter amino conjugated silica nanospheres were spotted onto silicon, allylamine and acrylic acid surfaces. Functionalized silica nanobeads were chosen for their interest in biosensors application, as they can be conjugated either with the receptor or the target molecules in order to increase the sensitivity of affinity-based biosensors. We have studied the assembly and the stability of the deposited spherical nanoparticles onto the various substrates.

2.2.1. Materials and methods

2.2.1.1. Sphere synthesis

PEG-600 and amino surface ended amorphous silica nanospheres were synthesized by modifying the standard method of precipitation of alkoxides described by Stöber [13]. Silica nanospheres with polyethylene glycol (PEG) saturated surfaces were obtained by taking advantage of the self-adsorption of the organic PEG to the hydrolyzed alkoxide at basic pH. Amino functionalized nanoparticles were obtained by co-precipitation with an aminosilane. The PEG-600 batch was synthesized by adding into the reaction beaker an aqueous solution of NH_3, PEG-600 (Sigma-Aldrich, Steinheim, Germany), absolute ethanol and tetraethoxysilane (TEOS) respecting the mentioned addition order (all from Fluka, Buchs, Switzerland if not otherwise mentioned). The final concentrations of the precursors were as follows: NH_3 0.2 M, PEG-600 0.02 M and TEOS 0.2 M. In the case of amino functionalized beads, we added 0.01 M aminopropyltriethoxysilane (APTS) replacing PEG-600. The reaction was carried out at 25 °C without stirring until precipitation and left in the reaction medium for 24 h. In order to change to the ethanol storing medium, the nanospheres were centrifuged in 15 ml vials at 5000 rpm and 20 °C. The remaining unreacted liquid was eliminated. Finally, the nanospheres were re-suspended after refilling with ethanol up to the original synthesis concentration of 1.5×10^{13} cm^{-3}.

2.2.1.2. Colloid characterization

The nanoparticle geometry was studied by scanning electron microscopy (SEM), while surface characterization was done by X-ray photoelectron spectroscopy. X-ray photoelectron spectroscopy (XPS) was performed using an Ultra XPS from Kratos Analytical equipped with a monochromatic Al Kα source (150 W). Survey (0-1150 eV Binding Energy (BE) pass energy of 80 eV) and high resolution spectra (20 eV pass energy) were obtained at 90° take off angle (operating pressure 2×10^{-9} Torr). The surface charge was compensated by a flood gun referring all peak energies to the BE of the hydrocarbon peak at 285.0 eV. High resolution C 1s and O 1s spectra were peak fitted after a linear background subtraction, with a G/L function by using the equipment software. Quantitative analysis was performed using element peak areas measured on survey spectra and software referenced relative sensitivity factors (RSF).

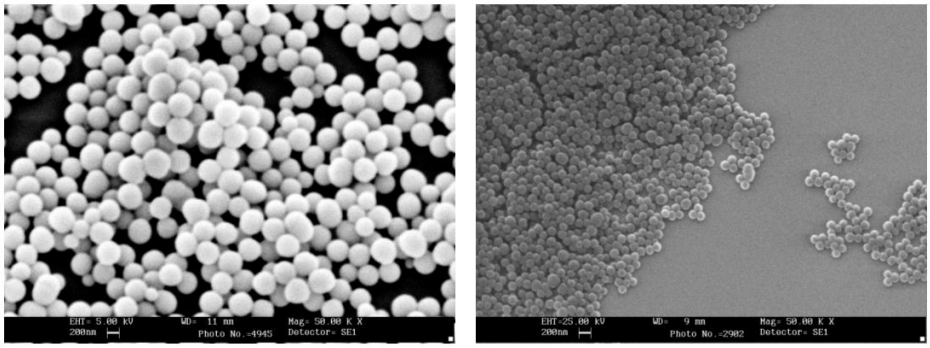

Figure 3.1: *SEM detailed view of PEG-600 (left), and APTS (right) conjugated SiO_2 nanoparticles.*

Sample \ at.conc. (%)	C	O	Si	N
PEG-600	10	53	37	0
APTS	19	50	27	4

Table 3.1: *Surface composition of the PEG-600 and APTS conjugated SiO_2 nanoparticles as derived from XPS analysis.*

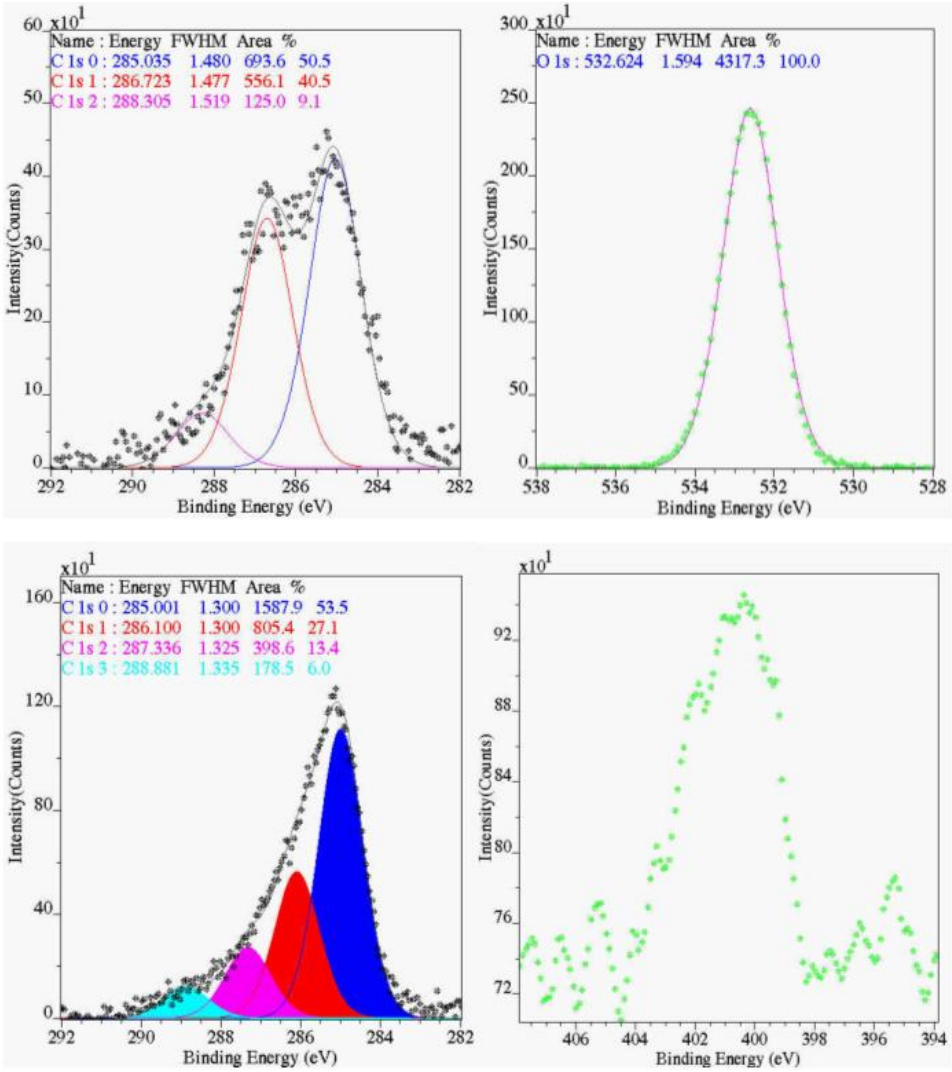

Figure 3.2: *XPS spectra corresponding to PEG-600 nanoparticles (top, C 1s left, O 1s right) and APTS nanoparticles (bottom, C 1s left, N 1s right).*

The synthesized nanoparticles were observed by SEM prior to their use in the microspotter in order to identify the mean particle size and geometry. Figure 3.1 presents the images corresponding to PEG-600 (left) and APTS (right) nanoparticles. Both showed well-defined spherical shapes with mean sizes of 300 nm and 150 nm for PEG-600 and APTS, respectively.

In order to illustrate the surface properties of the nanoparticles, thus the surface properties of the printed spots, a surface characterization was performed using X-ray

photoelectron spectroscopy. An element analysis was extracted from widescan spectra. The results confirmed that the PEG-600 contained a higher oxygen surface content while the presence of nitrogen was confirmed onto the APTS nanoparticles (Table 3.1). The chemical structure of the nanoparticle surface was further investigated by performing high resolution spectra. The C 1s spectrum corresponding to the surfaces of PEG-600 beads is presented on the top of Figure 3.2. The spectrum was satisfactory reproduced by using three components that stand for C-C-C (285.0 eV), C-C-O (286.7 eV) and O-C-O (288.3 eV) bonds, respectively. The relatively high intensity of the second component stands for the surface presence of PEG-600 fragments at almost the same intensity corresponding to the ethoxy radicals remaining on the surface from the TEOS precursor. The monocomponent shape of the O 1s spectrum (532.7 eV) further confirms that oxygen is almost only present in a single bonded organic structure O-C. In the case of the APTS surfaces, the C 1s spectrum is deconvoluted with four contributions (Figure 3.2, bottom). The assignment of the contribution at 286.1 eV to C-N bonds is confirmed by the N 1s spectrum presented on the right hand side.

2.2.1.3. Substrate preparation

Three different kinds of substrates were used for the deposition of nanoparticle droplets. Silicon substrates ((100), n-type, 1-3 Ω.cm) were cleaned by subsequent ultrasonic baths of trichloroethylene, acetone and ethanol. In order to diversify the wettability and the chemical functionalities of the substrates, two wafers were covered with plasma polymerized allylamine (PAL) and acrylic acid (PAA), respectively. The deposition of both polymers was carried out in a capacitively coupled reactor as previously described in [14]. Basically, optimized films were obtained at 35 mTorr, with a 20 W discharge (RF 13.56 MHz) of the precursor (AL or AA, Sigma-Aldrich) assisted by 6 sccm Ar flow.

2.2.1.4. Deposition tool and procedure

Arrays of four silicon cantilevers, previously developed and fabricated in our research group, were used for this deposition test. The experimental protocol started with the cantilever loading. The cantilever tip was dipped into a reservoir containing the nanoparticle suspension during a few seconds. The cantilever array was then moved on top of the deposition surface using an XYZ motion control system. Liquid droplet formation was achieved by putting the cantilever tip in contact with the substrate surface. Matrices of up to a hundred spots were obtained by combining the deposition step with the substrate translation, without the need for a refill. A CCD camera was used to observe droplet formation during the printing of the colloidal suspension on the different surfaces. The deposition procedures were carried out under ambient conditions, i.e. temperature of 21 °C and humidity level of about 50%. As expected, because of evaporation, droplet formation did not occur when the medium solvent consisted of only ethanol or water. To prevent evaporation, two agents were examined: dimethyl sulfoxide (DMSO) and glycerol. DMSO was not compatible with the colloidal solution because the suspension flocculated after DMSO was added. This was probably due to a hydrolytic process induced on the silica beads by DMSO. However, the addition of at least 25% of glycerol led to a successful liquid deposition.

2.2.2. Results and discussion

SEM observations were then carried out to characterize the droplets, check the presence of nanoparticles and study their spatial uniformity. The observations demonstrate that PEG-600 functionalized silica nanoparticles are present on the three types of substrates (as shown for a silicon substrate in Figure 3.3). By varying the contact time during deposition, droplets of various diameters, ranging from about 10 µm (Figure 3.4) to more than 100 µm (Figure 3.5), are obtained. The SEM picture in Figure 3.6, showing the tip of a depositing cantilever, proves that the absorption of colloidal nanoparticles onto the cantilever surface does not block the channel and its aperture. As seen in Figure 3.7, the samples typically exhibit poor uniformity, the density of nanoparticles being higher on the edge of the droplet than in its center. This result is due to the solvent capillary flow that carries particles at the rim of the droplet during its drying [15]. Finally, the deposition of amino functionalized beads is not as successful because the nanoparticles tend to aggregate, thus lowering the spot uniformity. The aggregation of these kinds of nanoparticles is of relevance even in previous steps as observed during the re-suspension of centrifuged products.

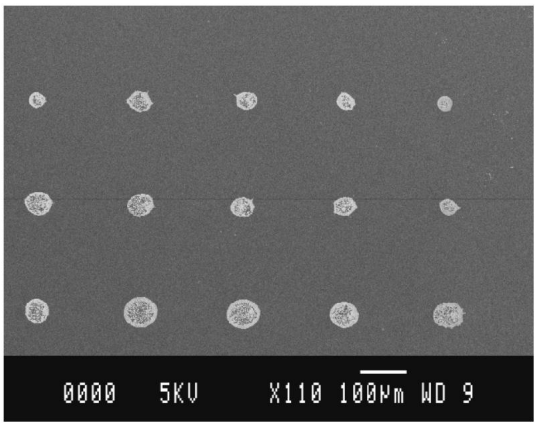

Figure 3.3: *SEM image of a matrix of PEG-600 nanoparticle spots on a silicon substrate.*

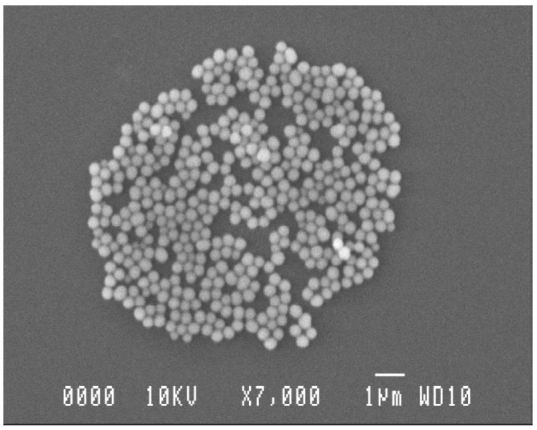

Figure 3.4: *SEM picture of a spot of PEG-600 nanoparticles on a PAL substrate.*

Even if the aggregation of colloids is inhibited in the case of PEG radicals (due to the self-repulsion of these chains in water), the self-organization through capillary forces does not lead to well-defined areas of nanoparticle monolayers. In order to obtain homogeneous monolayer particle spots, a control of the colloid density, colloid surface properties and rate of evaporation is needed. The first parameter is critical as it dictates the importance of the capillary forces acting on the colloid arrangement after deposition. Concentrations too high initiate capillary forces before an initial settlement, while concentrations too low lead to a lack of surface coverage. The surface properties of the colloids determine the effectiveness of the capillary forces in the particle transport. In general, the rate of evaporation can be used to correct some trends. For instance, the organization of a highly concentrated solution can be improved by a reduced evaporation rate, allowing the particle settlement to occur before capillary forces become dominant.

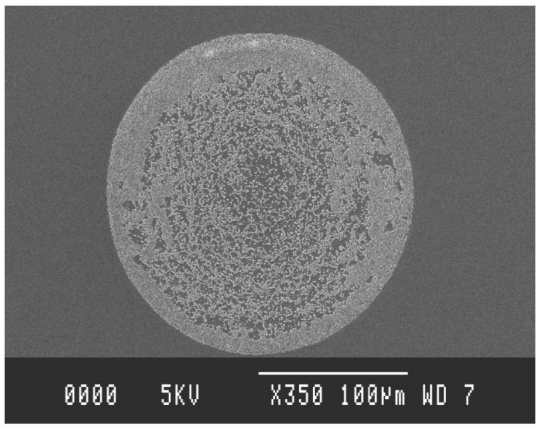

Figure 3.5: *SEM picture of a spot of PEG-600 nanoparticles on a silicon substrate.*

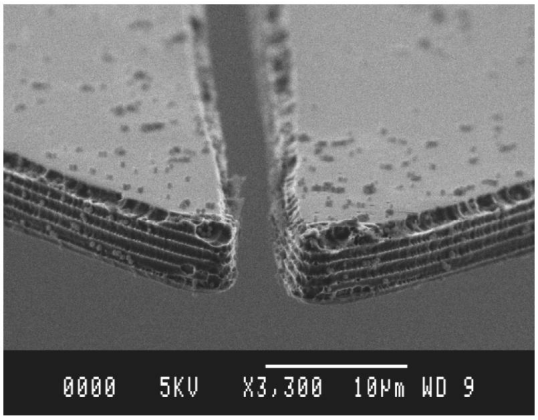

Figure 3.6: *SEM view of the tip of a depositing cantilever after the spotting process.*

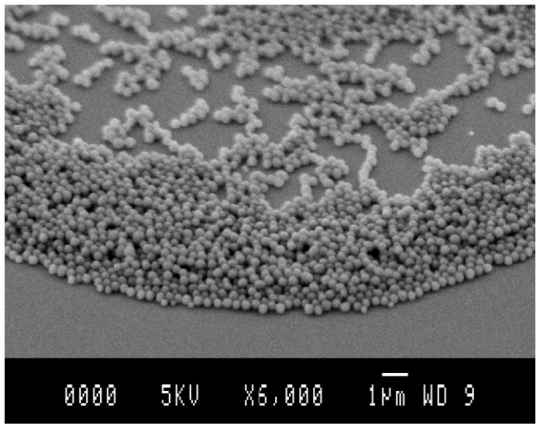

Figure 3.7: *SEM close-up view of a spot of PEG-600 nanoparticles on silicon.*

Regarding the spot stability in aqueous media, the formed colloidal structures are observed to be selectively stable. In fact, dipping samples into distilled water for 5 min does not induce changes in any of the surfaces, even when comparing 100 nm details. A comparison before and after rinsing with the PEG-600 nanoparticles is presented in Figure 3.8. On the other hand, the excitation in ultrasounds completely removes the colloidal pattern. This selectivity in stability is of essential interest for applications in which the nanoparticles are used as masks for creating patterns on substrates. The same kind of selective behavior is observed in the case of the smaller APTS nanoparticles, as observed in Figure 3.9.

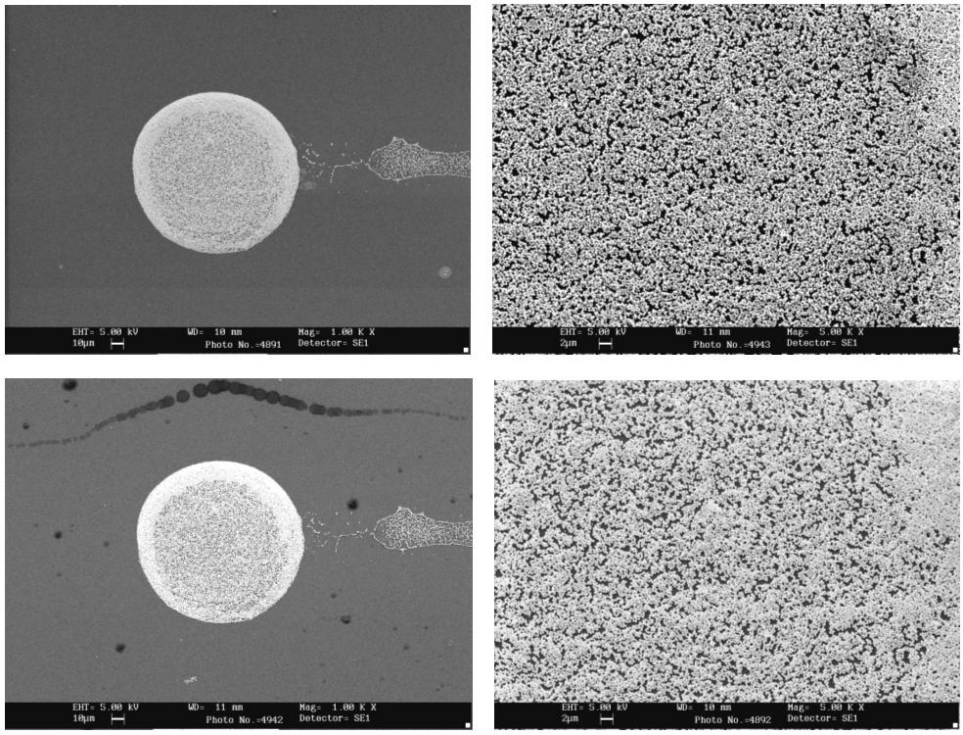

Figure 3.8: *SEM images corresponding to PEG-600 nanoparticles onto PAL substrate before (top) and after rinsing (bottom).*

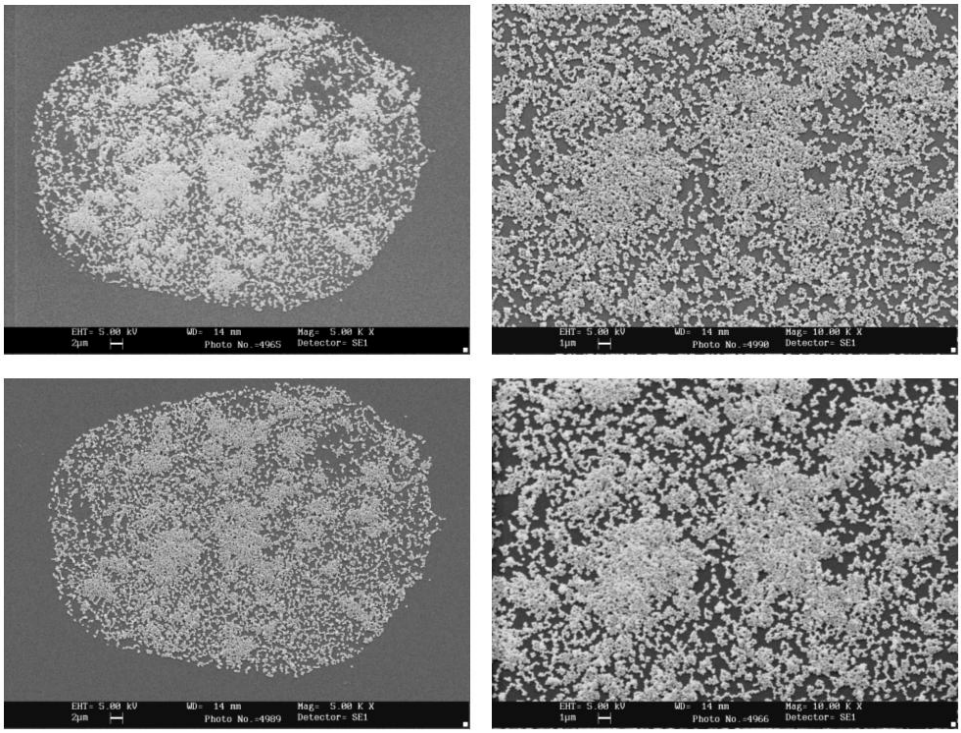

Figure 3.9: *SEM images corresponding to APTS nanoparticles onto PAL substrate before (top) and after rinsing (bottom).*

Finally, the physical and chemical stability of the particles was tested by a silicon dry etch. The PEG-600 SiO_2 nanoparticles were used as masks during a selective reactive ion etching (RIE) of the silicon substrate. The etching operation was carried out using C_4F_8, SF_6, and O_2 gas sources. As shown in Figure 3.10, silicon pillars have been obtained, onto which the masking silica nanospheres can still be seen.

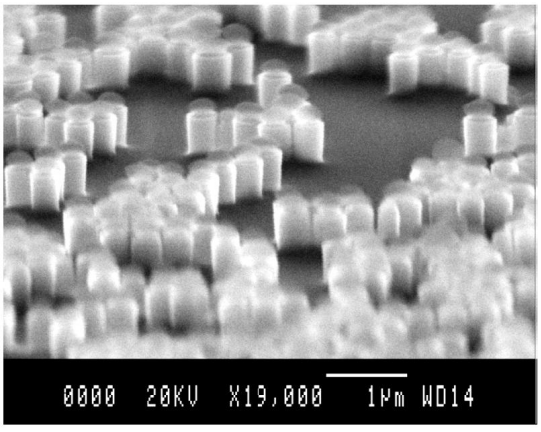

Figure 3.10: *SEM picture of the silicon pillars obtained after a dry etch of a silicon substrate patterned with silica nanoparticles.*

2.3. Formation of crystals of polystyrene nanobeads

Once the ability to pattern nanoparticles with silicon microcantilevers was demonstrated, we conducted a new set of experiments with bioplume in order to achieve the direct deposition of well-ordered crystalline microspots. For this purpose, polystyrene (PS) nanobeads in solution were spotted onto surfaces exhibiting different wettabilities. We studied the influence of the surface wettability and the contact time during deposition on the shape and the size of the spotted colloidal area.

2.3.1. Materials and methods

2.3.1.1. Colloidal solution

Polystyrene (PS) colloidal particles monodispersed (Aldrich, average diameter: 500 ± 50 nm, concentration: 2% of solid content) were dissolved in a solution of dimethyl sulfoxide (DMSO) in order to reach a final concentration of particles, $n_0 = 3 \times 10^{11}$ cm^{-3}.

2.3.1.2. Surface fabrication and characterization

Polyacrylic acid (PAA), polyallylamine (PAL) and fluorocarbon (CF_x) films were deposited by plasma enhanced chemical vapor deposition (PECVD) in three different dedicated capacitively coupled plasma reactors, previously described in [16-18]. Mercaptohexadodecanoic acid self-assembled monolayers (MHD-SAMs) (16-mercaptohexadodecanoic acid, from Sigma-Aldrich) were deposited on a freshly cleaned gold surface following the method described in [19]. The surface static contact angle was measured by a goniometer (Digidrop, France). The surfaces were previously characterized by measuring their contact angle (CA) with water and their roughness, illustrated by the root mean square (RMS) value obtained by atomic force microscopy (AFM). Scanning probe experiments were performed in air with an AFM (SMENA head, Solver electronics, NT-MDT, Russia). A standard silicon cantilever (NT-MDT) was used in resonating mode (ν_{res} = 170 KHz). The results are reported in Table 3.2.

These surfaces have different degrees of wettability, ranging from the hydrophilic PAA surface (CA = 50°) to the hydrophobic CF_x (CA = 105°) and very low values for the RMS roughness (lower than 3 nm for all the surfaces). Moreover, Zeta-potential measurements (not shown) demonstrate that the surfaces exhibit a negative surface charge at neutral pH inducing an electrostatic repulsion of the negatively charged PS nanobeads in water.

	Contact Angle with Water (degrees)	RMS roughness (nm)
Polyacrylic acid (PAA)	50 ± 4	1.8
Mercaptohexadodecanoic acid (MHD)	60 ± 2	2.9
Polyallylamine (PAL)	70 ± 2	2
Fluorocarbon (CF_x)	105 ± 1	2

Table 3.2: *Wettability and roughness of the different surfaces used in the nanobead deposition experiments.*

2.3.1.3. Spotting experiments

PS nanobeads were spotted on surfaces exhibiting four different chemical properties: plasma deposited polyacrylic acid (PAA), polyallylamine (PAL) and fluorcarbon (CF_x) as well as mercaptohexadodecanoic acid (MHD). The deposition of picoliter droplets containing the PS nanoparticles was carried out with the bioplume microspotting system described in the previous chapter of this thesis. The deposition of the nanobeads containing drops occurred as follows: firstly, the cantilevers were loaded via capillary forces, by dipping them into the colloidal solution. Because the volume of the channel is 4×10^{-9} cm^3, corresponding to 4 pL, the estimated number of beads loaded on each cantilever was a few thousand. Proper filling was verified by observing the channel with an optical microscope. Then, the picoliter droplets were deposited by gently touching the sample surface with the cantilever tips, during a contact time varying from 0.1 s to 5 s.

To allow a proper deposition process, a high-boiling-point solvent was added to the PS colloidal suspension. DMSO was selected over glycerol because of its compatibility with the PS bead solution. The addition of DMSO obviously resulted in a decrease of mixture evaporation rate, leading to longer evaporation times of the deposited picoliter droplets. This decrease of evaporation rate, along with surface and particle properties, played a major role in the self-assembly process of the particles within the deposited drops [20].

2.3.2. Results and discussion

After the deposition process and the drying of the drops, we studied the effect of the contact angle of the deposition surface on the size and geometry of the spots by performing SEM analysis. SEM characterizations were done with a low-vacuum scanning electron microscope (LEO 435 VP).

Examples of microspots of nanobeads deposited on the different surfaces at the minimum (0.1 s) and the maximum (5 s) contact times are shown in Figure 3.11. Depending on the surface wettability, the colloidal nanobeads are organized differently.

On highly hydrophilic PAA and MHD surfaces, spots of well-ordered monolayers of particles are obtained. These microspots do not have a definite and consistent geometrical shape. The covered area is on the order of a few hundred of μm^2 in the case of PAA and a few tens of μm^2 in the case of MHD covered surface. The number of particles deposited on the PAA surface for the longest spotting time, i.e. several hundred, is consistent with the number of particles calculated from the solution concentration and the volume of a deposited drop (taking into account the area of the pattern and the contact angle of the surface). This number is also in accordance with the number of particles initially charged on the microcantilevers, allowing several depositions without the need to refill the cantilever.

On the intermediate hydrophilic surface (PAL) having a contact angle between the values for PAA and CF_x, the particle spots cover areas of a few μm^2 and they are in some case organized in perfect hexagonal shapes.

On CF_x (hydrophobic) surface, the organization of the particles evolves in function of the contact time. For short contact time, i.e. $t = 0.1$ s, only few particles are deposited onto the surface, while for longer times, i.e. $t > 0.1$ s, they create organized 3D structures. The spot area is in the range of a few μm^2 and it does not change considerably for $t > 1$ s.

The evolution of the spotted area as a function of the contact angle and the different deposition times is shown in Figure 3.12. These results are in accordance with the conclusions of the study presented in the previous chapter (concerning the influence of the contact time on the drop size).

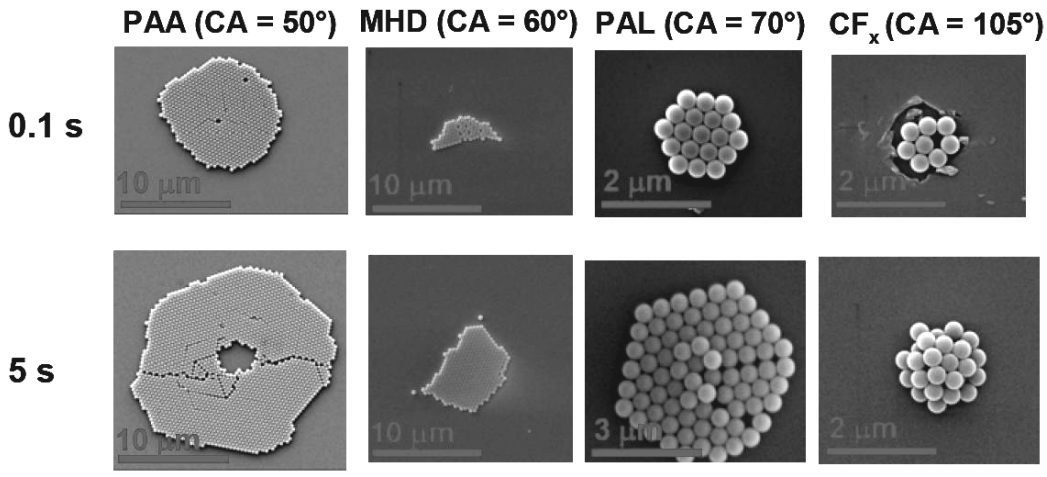

Figure 3.11: *SEM pictures of the microspots of PS nanoparticles on the different substrates for the minimum (0.1 s) and the maximum (5 s) contact time.*

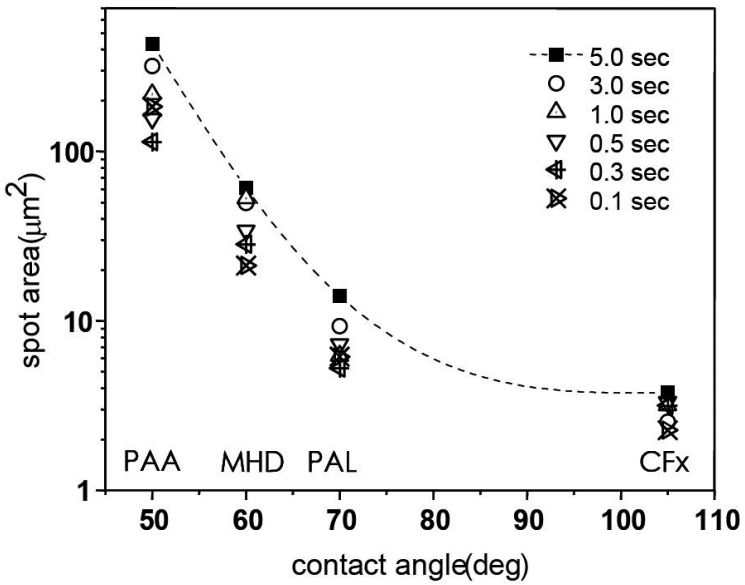

Figure 3.12: *Evolution of the spotted area as a function of the contact angle and the different deposition times.*

The spot size and shape onto the different surfaces is controlled by the size and surface properties of the particles, the number of colloids in the deposited droplet, the wettability of the surface, and the properties of the solvent. It has been well documented how the contact angle with water (CA) together with the evaporation rate of the liquid

influence the organization of nanobeads during the drying process of ultra-small droplets [21]. On the hydrophilic surfaces (PAA, MHD and PAL with CA < 90°), the presence of a high-boiling-point liquid (DMSO) in low concentration helps the formation of a hexagonally packed crystalline monolayer of particles. The homogeneity of the monolayered spot depends on the number of particles remaining in the droplet (N). In our system, with a time-constant concentration of nanobeads, N is proportional to the volume of the drop released from the microchannel (V_{rel}). V_{rel} is a complex function of the surface contact angle, θ, and the contact time between the cantilever and the surface (τ). This volume increases with time until the pressure equilibrium is reached between the drop in the channel and the one on the surface.

$$N \propto V_{rel} = V_{rel}\left(\mathrm{CA}(\tau), \tau\right) \tag{3.1}$$

For low CA, as in the case of PAA, and for high τ (e.g. 5 s), the droplet spreads on the surface. During the drying process of such a hydrophilic surface, the solvent reflows toward the edge of the drop because of the contact line pinning. As a result, the particles tend to aggregate at the rim of the drop, leading to the well-known "coffee-ring" shape. Because of the small drop volume, N is not sufficient to form a homogeneous monolayer covering the entire drop area. Thus, monolayers are seen at the rim of the drop, whereas there is a low concentration of particles in the centre. For lower contact times, homogeneous monolayered crystalline spots are formed because the number of deposited particles is in accordance with the number of particles necessary to cover the drop surface. An accurate control of the contact time, τ, leads to the deposition of the desired number of particles for a given drop surface. In specific cases, the formation of perfect hexagonal microspots is possible, i.e. when the number of particles is equal to:

$$N^{hex}(p) = 1 + \sum_{k=1}^{p-1} 6k \tag{3.2}$$

where p is the number of particles on the side of the hexagon. The other prerequisite to obtain a hexagon is that the diameter of the drop must be comparable to several times the diameter of the deposited particles (e.g. in the case of the spots created on the PAL surface). We observed the formation of several perfect hexagons constituted by 19 particles as shown in Figure 3.13b. Figure 3.13a (N = 15) shows the typical geometry of the particles when their number in the droplet is lower than 19 but higher than 7. Some of the particles are organized in a perfect circle which contains the remaining particles. This configuration is probably energetically favored with respect to the formation of a hexagon with a large number of vacancies. The formation of perfect crystals depends on the homogeneity of the size of the nanobeads. As shown in Figure 3.13a, the higher the number of particles is, the lower the probability to form a perfect crystal is, since the probability to create defects increases due to the presence of particles with different sizes. On the hydrophobic surface (CF_x with CA > 90°), the formation of 3D structures is due to the concentration of the particles at the centre of the droplets during the drying process [22]. Because the drying of the droplet occurs at constant contact angle, the entrapped particles settle down on a small area. Giving the fact that the volume deposited provides more particles than is required to cover the drop surface, the particles form several layers. For very short τ (0.1 s), very few particles (N < 10) are deposited and the smallest spot size is achieved.

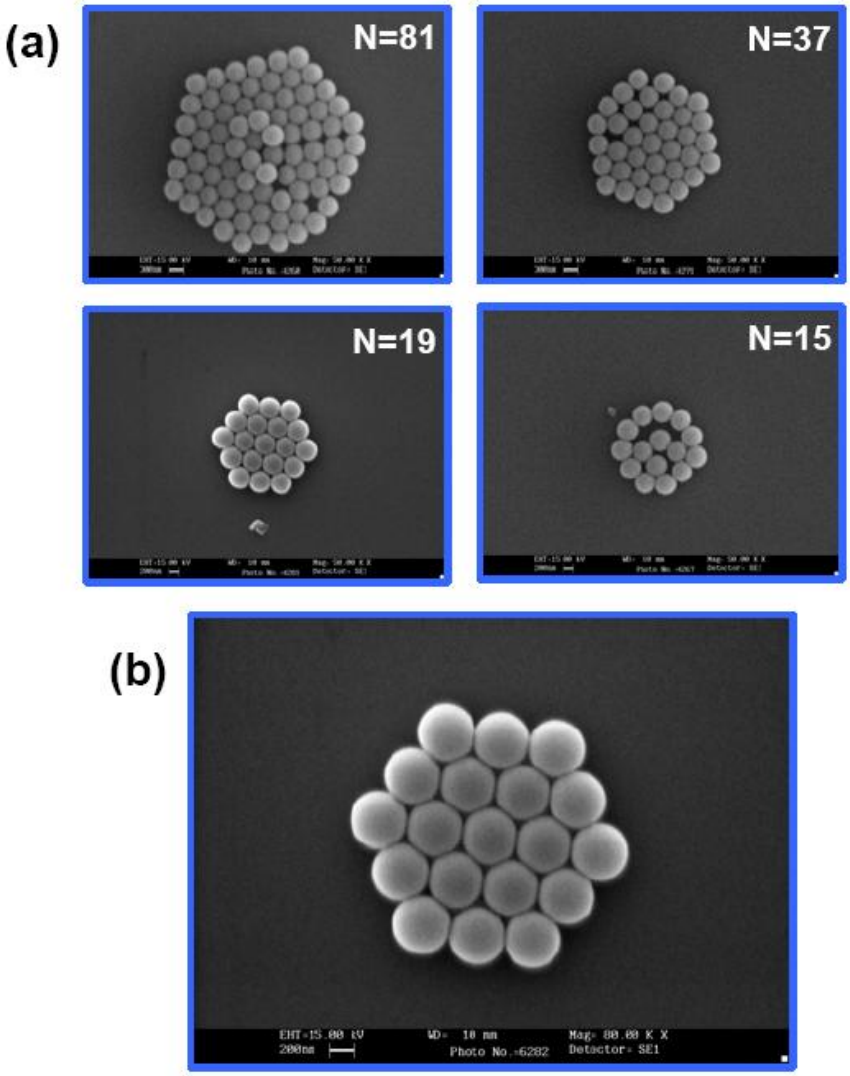

Figure 3.13: *(a) Spot shape for different numbers of particles (N). (b) Zoom for N = 19.*

2.4. Conclusion

Bioplume was successfully used to directly create areas of well-organized nanoparticles. In the first attempt to demonstrate the compatibility of our liquid-based patterning system with the self-assembly process, picoliter droplets containing functionalized silica beads were deposited with microcantilevers. Beads of different functionalities (polyethylene glycol and amino surface ended) and various substrates (silicon, allylamine and acrylic acid surfaces) were used for this purpose. Varying the contact time during deposition resulted in spots with different diameters, ranging from 10 µm to 100 µm. Up to a hundred spots could be patterned without a need to reload the cantilevers. After drying the sample, nanobeads were observed on the surface, within the drop area, proving the successful particle deposition. However, the deposited spots exhibited a higher density of nanoparticles along the triple contact line. In a second

attempt, a solution of polystyrene particles was used with bioplume. The size and uniformity of the particles, the bead concentration and the solvent composition were chosen to favor the formation of well-ordered crystals. The wettability of the substrates and the duration of the contact between the cantilevers and the substrate were used to control the printed area and thus the number of deposited particles. Crystals with typical dimensions ranging from a few μm^2 to a few hundred of μm^2 were successfully created. Particularly, by an accurate control of the contact time on polyallylamine surfaces, a very precise number of spotted beads were deposited, allowing the self-assembly of perfect hexagonal features.

3. Electrochemistry and electrowetting in picoliter droplets

3.1. Control of the droplet size using electrowetting actuation

3.1.1. Introduction

Because the electrowetting phenomenon results in a change of liquid contact angle, it can be used to tune the size of a patterned area. Indeed, upon the application of a voltage between a drop and the contacting surface, the contact angle decreases, i.e. the surface becomes more wettable. As a result, in the case of a drop of constant volume, the drop spreads on the surface and its contact area increases. In the particular example shown in Figure 3.14, the surface of the drop is multiplied by a factor of 2. To prove the interest of electrowetting for the control of the size of the drops deposited with bioplume, we have conducted a simple prospective experiment detailed below.

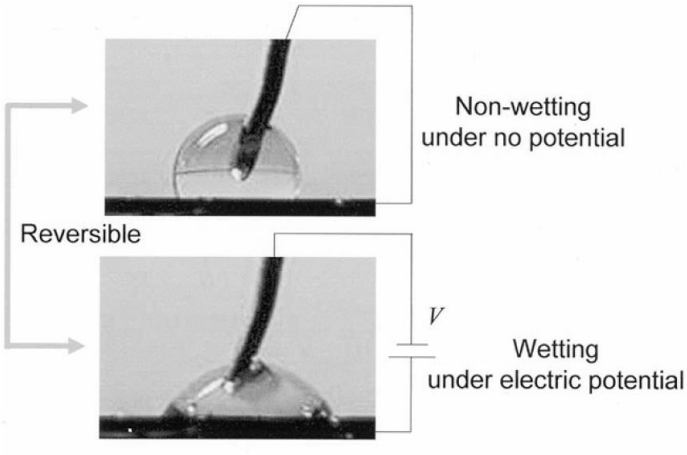

Figure 3.14: *Picture of basic electrowetting on dielectric experiment [23].*

3.1.2. Experimental set up

Experiments were carried out with the bioplume spotter, a 33120A function generator from Hewlett-Packard, and a voltage amplifier A800 from FLC Electronics (amplification gain of 70). The liquid deposited was a mixture of water-glycerol (50%). 1 mM fluorescein was added to the solution to facilitate the observation of the contact area left by the spreading of the droplets.

Substrates were specifically fabricated for the purpose of this study because the surface onto which electrowetting can be implemented must exhibit specific properties. The conducting surface has to be insulated to allow the use of conducting liquids. This electrowetting condition is usually referred as electrowetting on dielectric (EWOD). Moreover, the surface must be hydrophobic and exhibit a low contact angle hysteresis for efficient actuation. Specific coatings were thus selected to satisfy these requirements. A silicon wafer heavily doped with phosphorus was used as a starting substrate. Then, a 1 µm thick thermal silicon dioxide was grown in a dedicated furnace. The oxide was patterned and contact with the conducting silicon was realized by depositing and curing an AlSi layer. Finally, a 1 µm thick teflon layer was spun onto the oxide surface to obtain a hydrophobic coating. The resulting coating exhibited a 105° equilibrium contact angle with water. A 1 kHz sinusoidal voltage signal was delivered by the function generator and fed into the amplifier. The output of the amplifier was connected to the substrate and the electrode of the cantilever channel.

Rows of droplets were spotted on the fabricated samples with various voltages, following the experimental procedure shown in Figure 3.15. For each deposition, the contact time was set to 500 ms. The voltage applied between the cantilever and the surface was turned on and set to the desired value before spotting. Upon contact of the cantilever with the surface, drops were formed with contact angle θ_e depending on the applied voltage, as expressed by the Lippmann-Young equation:

$$\cos(\theta_e) = \cos(\theta_i) + \frac{1}{2}\frac{c}{\gamma}V^2 \tag{3.3}$$

with c, the surface capacitance, V, applied voltage, γ, the surface tension of the fluid and θ_i, the initial equilibrium contact angle of the sessile droplet.

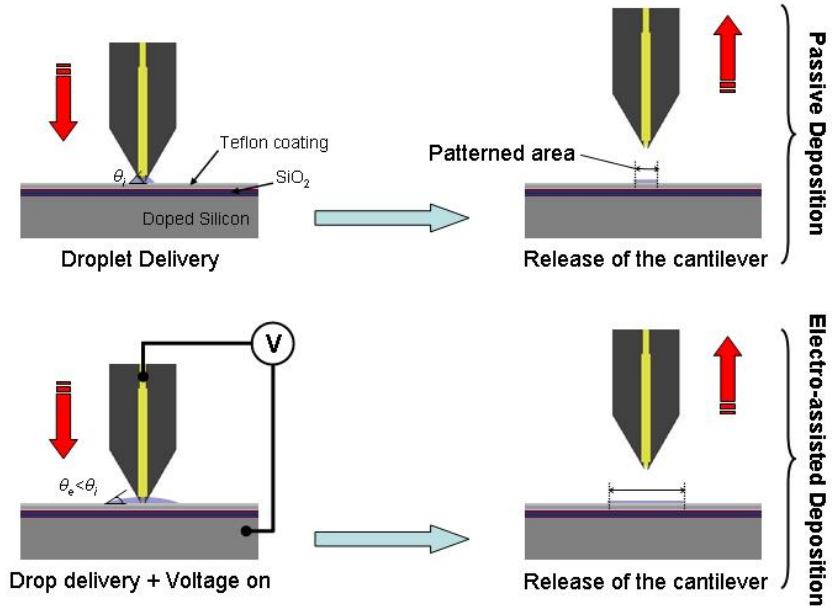

Figure 3.15: *Principle of operation of the electrowetting-assisted deposition for the control of the drop size.*

3.1.3. Results and conclusion

Rows of 5 drops were spotted with root-mean-square (RMS) voltages ranging from 0 V to 140 V, with a 35 V increment. Following the deposition process, the samples were observed with a fluorescence microscope. Figure 3.16 shows a picture of the resulting spots.

As expected the area of the spots increases gradually with the applied voltage. Indeed, during the deposition process, the spreading of the drop causes fluorescent molecules to cover a larger surface. However, uncertainties prevail concerning the volume of the deposited liquid. Indeed, during the release of the cantilever from the surface, the liquid meniscus breaks and leaves a drop having an unknown contact angle. It is difficult to predict if the drop retrieves its initial contact angle upon voltage removal or if it keeps its wetting properties because of residual charges in the liquid or the substrate. The answer might lie between these hypotheses and can only be found by investigating means to estimate the volume of the deposited drop. Nevertheless, the preliminary results presented in this thesis are very promising.

We have demonstrated that the size of the patterned area can be tuned with the use of electrowetting actuation during deposition. This is a relevant improvement compared to the passive method that consists in controlling the drop size by monitoring the contact time. Indeed, the deposition time is kept very short and the achieved range of patterned areas is more significant for surfaces with similar wetting properties (compared to the results presented in the previous chapter concerning the influence of the contact time on the drop size). Finally, this deposition scheme helps the formation of drops onto hydrophobic surfaces, thus enhancing the reproducibility of the printing process on these surfaces.

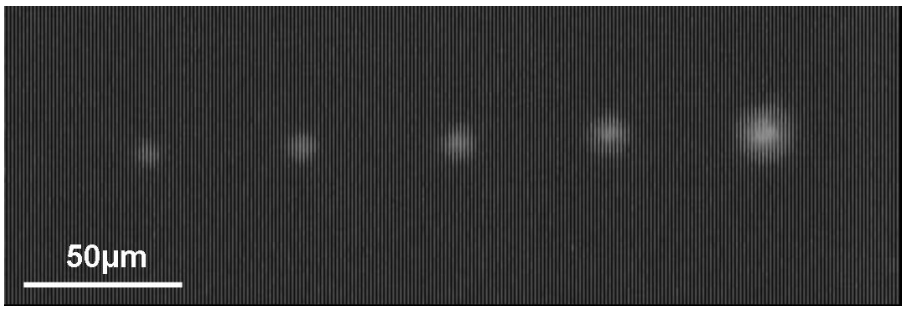

Figure 3.16: *Fluorescent picture of a series of droplets printed using electrowetting actuation. RMS voltage applied during the spotting process, from left to right: 0 V, 35 V, 70 V, 105 V, and 140 V.*

3.2. Copper electrodeposition localized in picoliter droplets using microcantilever arrays

The demonstration of electrochemistry as an active means to control the deposition process with bioplume was firstly carried out by electroplating metal onto conductive substrates.

3.2.1. Introduction - Motivation for this work

Electroplating is a technique now widely used in the fabrication of MEMSs as it offers the potential to rapidly create high aspect ratio structures at ambient temperature. Structures are usually electrodeposited into polymer molds patterned thanks to a photolithographic step, thus requiring expensive optical masks and aligners [24]. More recently, a simple maskless fabrication tool using sharp-tipped electrodes dipped into a plating solution for local electrodeposition has been developed [25,26]. The local electrochemical deposition technique allows the fabrication of complex 3D structures for rapid prototyping and post processing steps at wafer and single packaged chip levels [27]. A similar improved technique relies on the use of microjet print heads to better control the local electrochemical growth via the electrolyte flow rate in the nozzle [28,29]. However, for both techniques, the sample is partially immersed in the plating solution and undesired chemical reactions can possibly damage surrounding unprotected structures already fabricated on the sample. Bioplume allows solving these issues by locally depositing the electrolyte and confining the electrochemical reactions in the deposited droplets. Thus, it combines the advantage of direct patterning via electrochemical means with the precise localization of the redox reactions.

3.2.2. Principle of operation and experimental set up

Electrochemical reactions are created inside the printed droplets of electrolyte thanks to the gold electrode patterned in the channel of each bioplume cantilever. Applying a voltage between the cantilever electrode and the conducting surface leads to the electrodeposition of species contained in the electrolyte onto the surface covered by the droplet. The amount of deposited material is monitored by the duration of the voltage pulse, i.e. the chosen electrodeposition time.

To assess the electrochemical-assisted deposition capability of bioplume, rows of copper microbumps were electroplated on gold surfaces. The electrochemical deposition experiments were conducted using our microspotter, samples consisting of 100 nm Ti / 700 nm Au layers evaporated onto a silicon wafer, a mixture of commercial solutions purchased from Enthone and a PG580 potentiostat from Princeton Applied Research. The electrodes were connected to the potentiostat so that the cantilever electrode was anodically polarized and used as the counter electrode, while the sample surface was cathodically polarized, thus used as the working electrode. Rather than adding a third electrode in the cell, which would be very challenging because of the small volume of the droplet, the reference electrode was shunted to the counter electrode [30]. Copper bumps were formed by bringing the cantilever tip in contact with the surface to create microdroplets containing the cupric sulfate based solution and applying a voltage pulse between the cantilever electrode and the conducting surface. The optimized potential value of 1.9 V was used in these experiments to provide enough

energy to the electrochemical cells for the reduction of copper ions onto the sample surface. The deposition of copper occurred via the following electrochemical reaction:

$$Cu^{2+} + 2\ e^{-} \rightarrow Cu \qquad (3.4)$$

A schematic of the experimental setup showing a single cantilever depositing copper dots is seen in Figure 3.17. Because bioplume consists of an array of ten microcantilevers, each spotting step produces the deposition of ten droplets in parallel, leading to the creation of ten electrochemical cells.

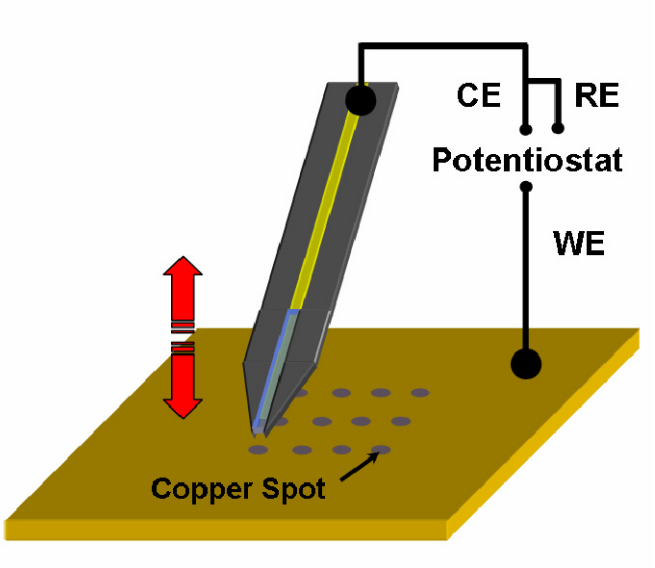

Figure 3.17: *Schematic of the experimental setup.*

3.2.3. Results and discussion

Several rows of spots were printed by applying the voltage during various time periods, ranging from 30 s to 300 s. The current flowing through the ten parallel cells was recorded as a function of time by the potentiostat. The resulting amperogram plot obtained for a 60 s deposition time experiment and the total charge supplied to the cells are shown in Figure 3.18 (using the American current polarity convention). The plots are in accordance with what is usually observed in classical electrochemical experiments [30]. The positive current peak seen at the beginning of the amperogram is due to the charge of the electrical double layer. The fast consumption of charges required to create the double layer is then followed by an exponential decay of the current, corresponding to the rapid depletion of reactive ions at the interface, until the current reaches a steady state value during the deposition process. This stationary current is limited by the diffusion of copper ions from the bulk solution to the reducing interface and leads to a constant increase of the amount of charges consumed by the cell. Once the deposition time is elapsed, the potential is set back to 0 V, resulting in the discharge of the double layer and the occurrence of a negative current peak at the end of the amperogram.

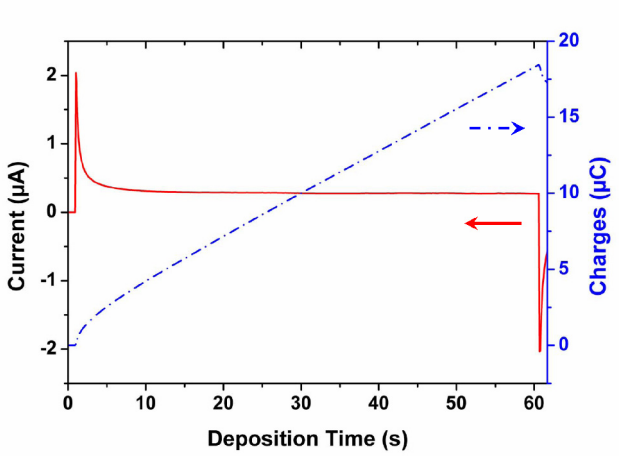

Figure 3.18: *Time evolution of the current across the ten electrochemical cells (left) and the total number of charges supplied to the cells (right) for a 60 s deposition time experiment.*

After the deposition process, the samples were rinsed with de-ionized (DI) water, dried with a nitrogen flow and observed with an optical microscope and a SEM. The optical photograph of the resulting matrix of copper dots and their SEM observation (see Figure 3.19) demonstrate the electrodeposition of copper using the spotter in the pseudo-chronoamperometry configuration. As expected, the diameter of the copper dots (typically 20 µm) corresponds to the area of the printed droplets. Figure 3.20 provides SEM pictures of single copper bumps for various deposition times, illustrating how copper grows within the drop area. The pictures clearly show that the growth starts from nucleation sites localized around the cantilever electrode. The coverage of the entire surface of the dot is then only obtained after a given period of electrodeposition, standing between 60 s and 90 s. However, the thickness of plated material and the size of copper grains are not uniform over the spot area (see Figure 3.21). These discrepancies might be due to the uneven current density lines inside the droplet created by the two electrodes of dissimilar geometries [31].

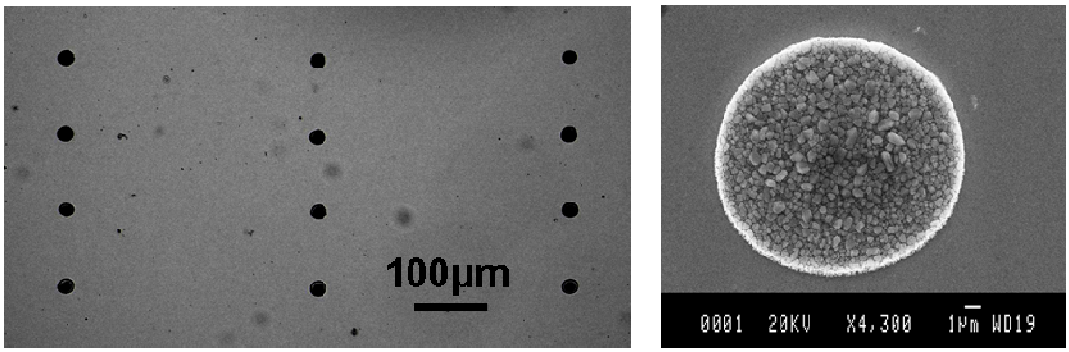

Figure 3.19: *Optical photograph of a matrix of copper dots (right), and SEM picture of a copper bump obtained by electroplating during 300 s (left).*

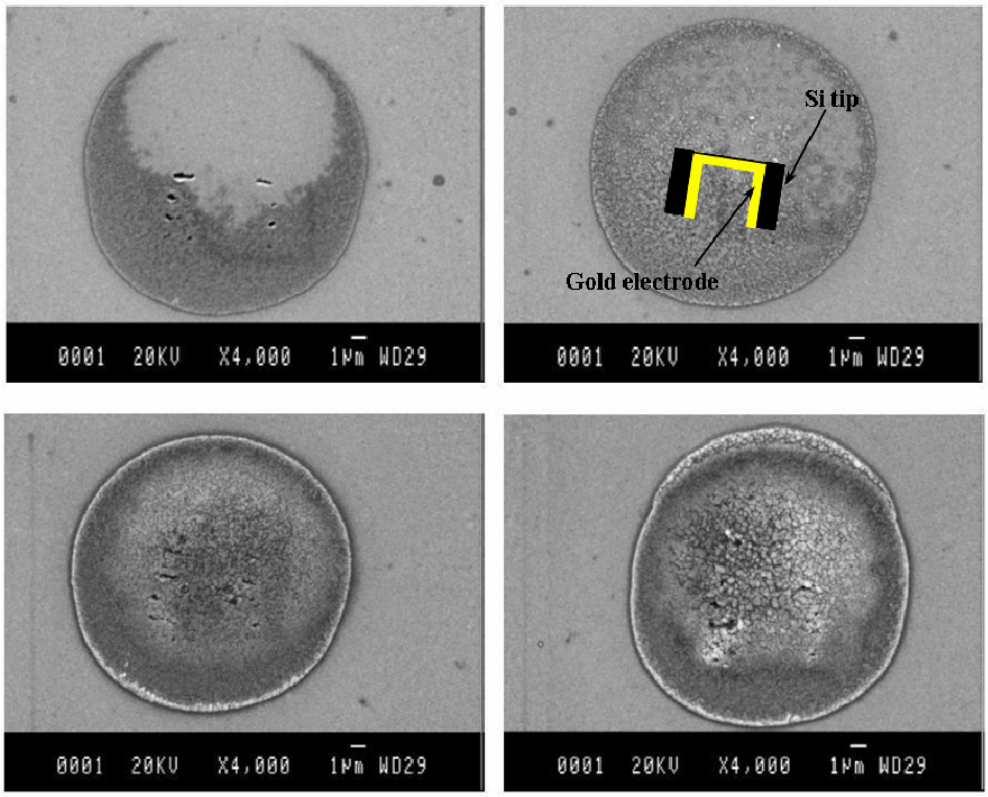

Figure 3.20: *SEM pictures of copper bumps. Top left: 30 s deposition time; Top right: 60 s deposition time; Bottom left: 90 s deposition time; Bottom right: 120 s deposition time. The section of the cantilever tip is schematized on the 60 s copper spot to show the position of the cantilever during deposition.*

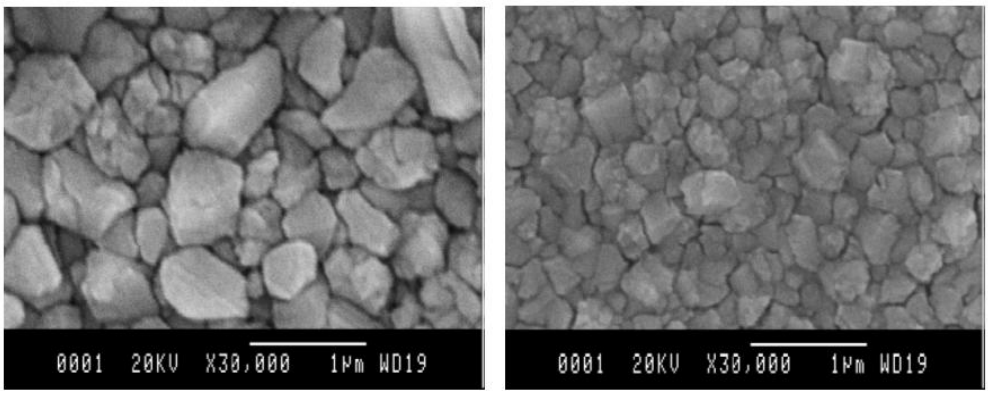

Figure 3.21: *SEM close-up views of the center (left) and the edge (right) of a copper spot, showing large and small copper grains.*

Finally, a rough estimation of the mean thickness of the resulting copper spots was achieved by using an AFM in tapping mode (Nanoscope 4 from Digital Instruments). Figure 3.22, on the left, shows a typical 3D view of a scanned dot.

Sections of imaged spots were used to obtain the mean spot height (Figure 3.22, on the right). Two perpendicular sections passing through the center of each dot were realized and the estimated mean thickness was taken as the average of the highest and the lowest points of those sections. The variation of the spot height as a function of the total number of consumed charges (related to the deposition time) is plotted in Figure 3.23 for three of the ten spots created during each deposition experiment. Hypothesizing that the printed spots exhibit similar surface areas, the volume and thus the mass of the deposited copper is directly related to the spot height. Hence the observed linear relationship between the spot height, thus the deposited mass, and the total number of charges is consistent with Faraday's law, given hereafter:

$$m = \frac{A}{aF} Q \tag{3.5}$$

where A and a are the atomic mass and the electrovalence of copper, respectively, Q is the number of charges, and F the Faraday's constant.

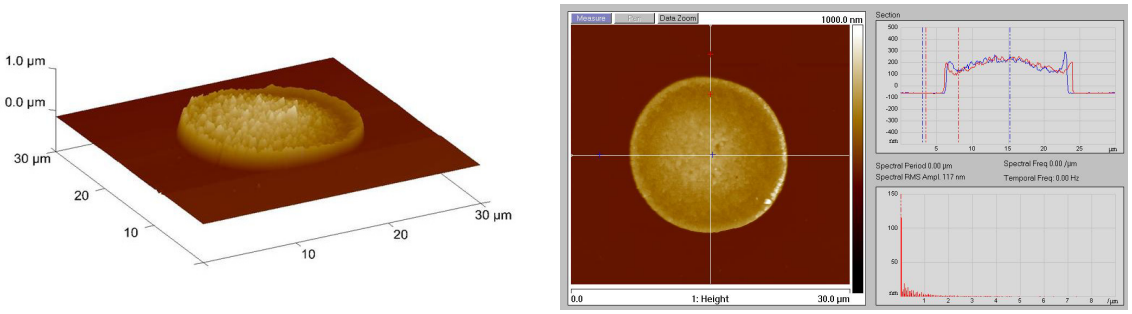

Figure 3.22: *3D AFM image of a copper spot (left), and example of the measurement of the thickness of electroplated copper carried out on an imaged dot (right).*

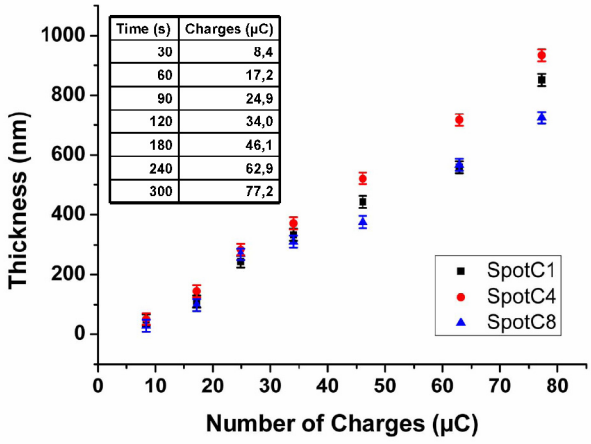

Figure 3.23: *Variation of the estimated copper bump thickness as a function of the total number of charges consumed during each experiment (the number of charges corresponding to each deposition time is given in the table).*

3.2.4. Conclusion

The electrospotting capability of the bioplume system was demonstrated by the successful electrodeposition of matrices of copper spots using a commercial plating solution. This deposition method offers the advantage to precisely control the amount of deposited material by monitoring the duration of the applied voltage pulse. Therefore, the bioplume tool enables the fabrication of electroplated microstructures at precise locations with controlled thicknesses. Numerous materials, such as metals and alloys, organic and inorganic chemicals, and conductive polymers, can be printed with this technique by simply changing the electrolyte loaded on the cantilever and applying the potential of the corresponding desired redox couple. The aim of the following section is to prove that local electopolymerization of functionalized polymers can be carried out with bioplume and that the fabrication of biochips can greatly benefit from our electrospotting system.

3.3. Fabrication of oligonucleotide chips using parallel cantilever-based electrochemical deposition in picoliter volumes

3.3.1. Introduction - Motivation for this work

For fabricating biochips, the accurate registry of small amounts of molecules or particles in well-defined areas along with their specific properties is of great significance for screening phenomena with unprecedented sensitivity [32].

To that end, advanced photolithography processes, template-assisted patterning and printing-based techniques have been developed to pattern surfaces with submicrometer features. Although photolithography and template-assisted techniques are promising routes for that purpose, they both have a main limitation in terms of versatility since they rely on the use of appropriate surface chemistries and pre-patterned surfaces on which molecule arrangement will take place afterwards [33]. Printing-based techniques are more straightforward in the sense that molecules or particles are directly deposited on the substrate with submicrometer resolution using dedicated tools or stamps. Among those techniques, microcontact printing has been optimized for patterning biologically active proteins. The main drawback of this approach is that the arrangement of the biomolecules is imposed by the design of the patterned stamp and only one type of molecules can be deposited on the whole surface at the same time. Moreover, the alignment of the stamp with respect to prepatterned features is hardly achievable in a reproducible manner. These drawbacks constitute a major limitation when facing the problem of patterning specific areas on the surface of biosensors for multiple detection analysis.

Dispensing techniques, based on the use of microcantilevers or nanopipettes, are more promising for that purpose since they combine several advantages. The first one is that they permit a direct patterning of the surface with different kinds of materials without any need for prefabricated patterns. In addition, self-assembly occurring within a small amount of liquid between the tip and the surface can help to optimize a precise arrangement of functional groups on a confined area. Secondly, alignment of the cantilevers with respect to specific regions on the surface can be provided by using the cantilevers as positioning sensors. Moreover, to overcome the serial nature of cantilever-based techniques, parallel approaches can be developed to meet specific requirements in terms of throughput and fabrication costs. For the fabrication of

biochips, when compared to dip-pen nanolithography (DPN) or related techniques, miniaturized silicon quills bring two main salient features. The first one is that the presence of channels and reservoirs ensuring a continuous liquid transfer is a key factor to keep biomolecules biologically active during the fabrication process. This is hardly achievable with DPN where indirect-patterning methods are preferred, based on the use of inorganic self-assembled monolayers in a relative humid environment to tune the reactivity of the surfaces for subsequent biological interactions. Another important point is that the fabrication process is favored in terms of deposition time because it is not a diffusion-limited process as it is the case with DPN.

In addition to these advantages, bioplume enables electrochemical reactions to occur within small volumes of liquids. This feature is of great interest since Livache and co-workers have demonstrated that the use of conductive polymers in conjunction with electrochemistry is extremely relevant for efficient DNA probe immobilization [34]. The electrochemical deposition permits the active grafting of biomolecules on metallic surfaces with a real-time control. This ensures proper orientation and packing of chemical or biological functional groups on the surface. With regard to the fabrication of biochips, controlling the surface arrangement is mandatory since the sensitivity of affinity-based biosensors is dictated either by the amount of receptor molecules immobilized on the sensor surface or by the amount of target molecules reaching the sensor surface during the measurement process. Following this concept, the CREAB group proposed an electrospotting method based on polypyrrole technology to design biochips [35]. Their electrospotting tool consists of a pipetman tip, which contains a platinum wire used as a counter electrode, or a custom stainless-steel pin. In addition to the fact that the spot size is fixed to a large extent by the tip diameter (e.g. 800 or 350 μm), the aforementioned technology exhibits some inherent limitations that need to be addressed for the design of highly parallelized biochips. In fact, the immobilization of one oligonucleotide probe requires successive steps, including electrolytic solution uptake, electrodeposition process and washing, which are time consuming. Moreover, electrodeposition volumes are somewhat high and electrodeposited spots present typical sizes which are not adapted to high parallelization. The use of bioplume that allows electrochemical reactions in picoliter droplets, a significant reduction of the tip size compared to what is available, and the parallelization of deposited solutions, has the potential to greatly improve the electrospotting method for biochip fabrication. Thus, we propose in this section to conduct dedicated electrochemical experiments using bioplume and polypyrrole technology aiming at controlling the assembly and the packing of oligonucleotides on the surface in a confined area.

3.3.2. Experimental procedures

A typical experiment is depicted in Figure 3.24: the depositing cantilevers are simultaneously filled up with the same solution (approximately 28 pL of electrolyte per cantilever) by dipping them in an electrolytic drop containing pyrrole monomers before they are moved to a precise location at a gold-substrate surface (Figure 3.24a). Then, they are gently brought into contact with the surface, the mechanical deflection of the two positioning cantilevers giving a qualitative feedback on the tilt of the array and the applied contact force with respect to the surface (Figure 3.24b). Concomitantly to cantilever mechanical contact, due to substrate wettability, a drop of electrolyte is deposited onto the surface. The drop size, which is controlled by both cantilever array orientation and contact time through surface wettability, reaches diameters from 5 to 25

µm (corresponding to electrolyte volumes ranging from 33 fL to 4 pL, hypothesizing an hemispherical drop). An electrochemical pulse of 2 V is then applied between the anodically polarized gold substrate and the cantilever used as a counter electrode (Figure 3.24c) for electropolymerization times ranging from 25 to 500 ms before setting back the cantilevers from the gold surface (Figure 3.24d). All the experiments were performed in atmospheric conditions at 23 °C and a relative humidity of about 30%.

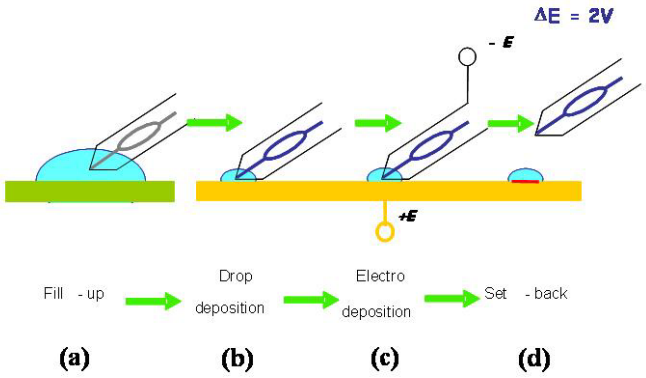

Figure 3.24: *Principle of electrospotting with cantilevers.*

3.3.2.1. Reagents

Oligonucleotide probes bearing pyrrole units (pyrrole-ODN) monomers were synthesized following a procedure already described elsewhere [36]. The pyrrole-ODN CP and M5 used in this work present the respective sequences: 5'-Py-(T)10-GCC TTG ACG ATA CAG C-3' and 5'-Py-(T)11-GGA GCT GCT GGC G-3'. Stock solutions of pyrrole (1 M) were prepared from pyrrole dissolved in HPLC grade acetonitrile and were kept at -20 °C. All chemicals were of the highest purity available and were used without further purification.

3.3.2.2. Hybridization procedure and revelation

Polypyrrole-ODN films were characterized in terms of bioavailability through hybridization with biotinylated complementary targets at 45 °C for 15 min. Following a quick wash with phosphate buffer saline solution at room temperature, the DNA chip was then incubated for 10 min in the dark with a solution of 10% streptavidin-R-phycoerythrin diluted in the washing buffer, rinsed and mounted between slides. Finally, the fluorescence was recorded with an epifluorescence microscope equipped with a CCD camera and an image analysis software (Imagepro plus). Biochip regeneration was accomplished by dipping in 0.2 M NaOH for 1 minute.

3.3.3. Demonstration of polypyrrole electropolymerization

Following the procedure described above, the electrodeposition of functionalized polypyrrole spots was carried out with bioplume. Figure 3.25 displays a SEM picture of a typical polypyrrole-ODN spot array obtained for a 200 ms electrodeposition time.

These spots, which exhibit a smooth surface and a circular shape, are reproducible in terms of size, i.e. 22 µm under the considered experimental conditions. This morphology is identical to those already obtained using electrospotting [37] but is completely different from those already observed for polypyrrole films that exhibit cauliflower-like structures. Indeed, the latter morphology is always obtained for important deposition times (e.g. electrodeposition charge densities higher than 20 $mC.cm^{-2}$) whereas the herein described arrangements are obtained for very short deposition times, from 50 to 200 ms, giving rise to charge densities lower than 1.2 $mC.cm^{-2}$. Another important feature, indicated by the arrow in the inset of Figure 3.25, is the presence of small dots within the polypyrrole layer that can be attributed to the mechanical indent of the depositing cantilever on the gold layer due to the contact force. The same type of mechanical indents was also observed in the deposited copper spots previously presented. Those indents, observed for each spot, prove that the imaged films were fabricated with the cantilever array. This preliminary experiment demonstrates the feasibility of polypyrrole electrodeposition at the femtoliter level using the cantilever-based deposition system.

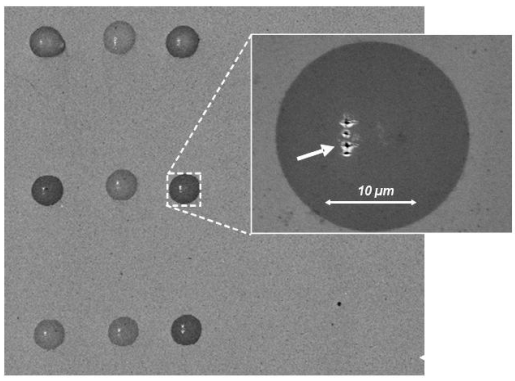

Figure 3.25: *SEM picture of polypyrrole-ODN spots obtained for a 200 ms electrospotting duration.*

3.3.4. Demonstration of the functionality of electropolymerized polypyrrole-ODN films

The next step was devoted to the extension of the described technology for the fabrication of DNA chips using a specific polypyrrole technology. For that purpose, pyrrole-ODN were electrocopolymerized with unsubstituted pyrrole monomers at the gold surface leading to the localized deposition of biologically active and mechanically stable polymer films. The electrodeposition process was done using an electrolytic aqueous solution containing sodium phosphate buffer saline (0.05 M phosphate buffer, 0.05 M NaCl, 10% in volume of glycerol at pH = 6.8) as supporting electrolyte, pyrrole and pyrrole-ODN at concentrations of 20 mM and 1 µM, respectively. As depicted in Figure 3.26, corresponding fluorescence images were obtained after hybridization with complementary biotinylated oligonucleotides and subsequent recognition using streptavidin-phycoerythryn as a fluorescent label.

Figure 3.27 displays chronoamperograms along with the corresponding fluorescence images obtained with poly(pyrrole/pyrrole-ODN) copolymer electrodeposition obtained under different experimental conditions for the same electrodeposition time. The aim was to study the impact of monomer (pyrrole and pyrrole-ODN) concentration ratios with two different electrolytes on the electropolymerization process and ODN probe bioavailability in terms of fluorescence response (intensity and/or homogeneity). First of all, the obtained chronoamperograms exhibit a classical shape, that may be associated to diffusion controlled behavior of the monomer units, whatever the monomer concentration and the type of electrolyte. This demonstrates the reliability of our approach and its versatility in terms of the variety of electrochemical conditions that can be used. As aforementioned, the electrodeposition charge reached a typical charge density of 1.2 $mC.cm^{-2}$ which corresponds to 10 nC for 10 cantilevers used in parallel. This is coherent with the typical charges obtained using classical electrodeposition cavities. This charge density is sensitively higher than the value obtained without pyrrole (an average value of 2.5 nC for 10 cantilevers is typically obtained) in the electrolytic solution, thus proving the effectiveness of the electrodeposition process in a confined volume.

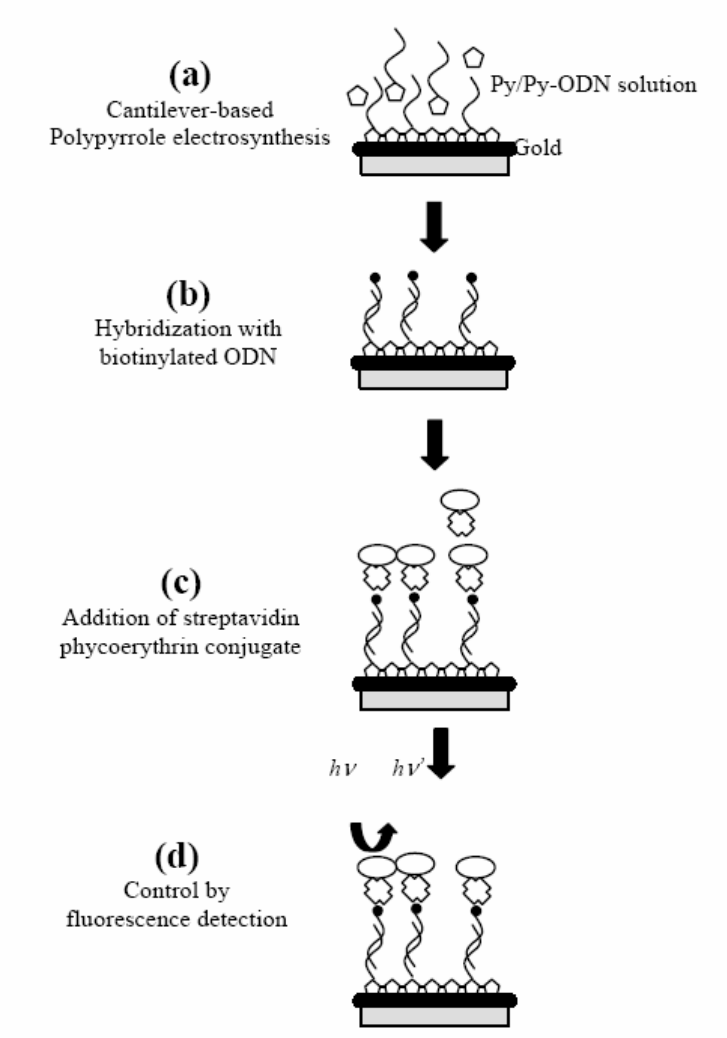

Figure 3.26: *Schematic representation of the procedure used to obtain fluorescence images with electropolymerized oligonucleotides.*

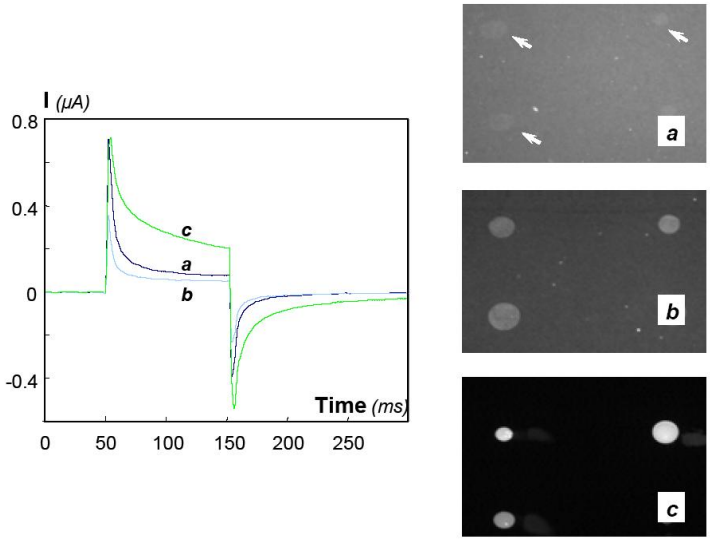

Figure 3.27: *Chronoamperograms and corresponding fluorescence pictures of electropolymerization experiments. (a) Electrolyte A with 20 mM of Py and 1 µM of Py-ODN. (b) Electrolyte A with 200 mM of Py and 10 µM Py-ODN. (c) Electrolyte B with 200 mM of Py and 10 µM of Py-ODN.*

3.3.4.1. Optimization of electrolyte composition

As illustrated in Figure 3.27a, the recorded fluorescence signal of the spots obtained under non-optimized conditions is rather weak (average background signal of 40 against average spot fluorescence intensity of 60 in a 256 grey level scale) since the recorded contrast (calculated as the ratio (signal-background)/background) does not exceed 0.5. Indeed, the electrodeposition process of polypyrrole-ODN coatings was first developed and optimized for the modification of gold microelectrodes immersed in large tank of electrosynthesis solution. This configuration is markedly different for the herein described electrochemical nanocells in terms of mass transfer, interfacial availability of monomer units, electrosynthesis volume and also physico-chemical behavior including electrolyte evaporation and substrate wettability.

To adapt the experimental protocol to this constrained configuration, these intrinsic parameters were modulated through the adjustment of monomer concentrations and modification of the electrolyte nature. More precisely, the influence of the monomer concentration was studied by increasing 10 times the monomer concentrations (pyrrole and pyrrole-ODN) using the electrolytic aqueous solution containing sodium phosphate buffer saline (0.05 M phosphate buffer, 0.05 M NaCl, 10% in volume of glycerol at pH = 6.8) referred to as electrolyte A in Figure 3.27. The corresponding fluorescence intensity was increased three times (see Figure 3.27 case (a) versus case (b)) with a good homogeneity whereas the corresponding electrodeposition charge was divided by a factor of 2. This decrease may be associated to the increased incorporation of biological probes within the film that limits film growing through steric hindrance.

As previously mentioned, the electrolyte nature may impact film formation [38] and fluorescence signal. We investigated such an impact by using a complex formulation made of a mixture of water (49% VV), DMSO (20%), acetonitrile (30%) and glycerol (1%) as solvent and lithium perchlorate (150 mM) referred to as electrolyte

B in Figure 3.27. As can be seen for case (c), the recorded fluorescence signal, as well as the electrodeposition charge, is drastically enhanced compared with the previously used water-based solution. The increase in electrodeposition charge may be associated to a higher electropolymerization rate linked to an enhanced wetting of the gold substrate due to the impact of acetonitrile on polypyrrole electrodeposition [39].

3.3.4.2. Successive electropolymerization steps

An important feature of bioplume lies in the possibility to perform successive electrodeposition steps with a single liquid loading in order to fabricate several biochips in a same batch. This is possible since the complete available electrolyte volume represents about 30 pL for a few pL required for each spot. In addition, the use of DMSO and glycerol limits electrolyte evaporation during the whole deposition process. Nonetheless, the remaining critical aspect concerns the possible variation of the pyrrole concentration over time after multiple deposition steps. This can drastically impact the number of available molecules grafted on the surface, thereby changing the recognition properties of biochips fabricated in a batch process.

To address this problem, a multiple electrodeposition process with a single loading has been performed. After liquid loading, the cantilever array was used 15 times and the resulting spots were characterized in terms of fluorescence intensity with the protocol previously used for hybridization and fluorescent labeling. Figure 3.28 depicts the evolution of the contrast average obtained under optimized conditions (measured for the ten cantilevers) along 15 successive electrodeposition steps. Despite the slight decrease of the contrast average with electrodeposition iteration from 20 for the first deposition to 15 for the last one, the fluorescence contrast remains within a range compatible with a proper use of polypyrrole based biochips. Moreover, the standard deviations obtained for the ten parallelized spots are relatively identical, taking values in the range of 1 to 2. Finally, these experiments highlight the reproducibility of the electrodeposition process and demonstrate the possibility to carry out successive biochip manufacturing without reloading the cantilevers.

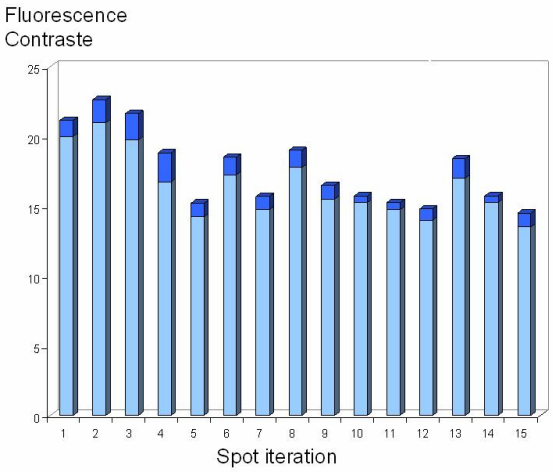

Figure 3.28: *Evolution of the average contrast (clear blue) and of the contrast standard deviation (dark blue) calculated for the 10 concomitantly synthesized spots according to the number of deposited spot row (up to 15).*

3.3.5. Proof-of-concept: 2-ODN probe biochip

The last aspect to be considered in order to demonstrate the effectiveness of our approach for making DNA chips concerns the specificity of the coatings toward their DNA targets. For that propose, using the previously described protocol, we have designed a biochip with two rows of spots made of two different ODN probes, hereafter denoted M5 and CP (see experimental section for corresponding ODN sequences), as can be seen in the schematic representation in Figure 3.29(a). To avoid any cross-contamination with residual oligonucleotides during the successive electrocopolymerization, each polypyrrole synthesis was followed by a washing step of the cantilever array consisting in dipping the array in ethanol and afterwards in water before drying. Figures 3.29(b) and 3.29(c) demonstrate the specificity of the electrodeposition step through successive probe hybridization with M5 and CP complementary targets. One can notice that no fluorescence signal is observed on the non-specific spots, thus demonstrating the good specificity of the different electropolymerized coatings obtained with the cantilever array.

Figure 3.29: *(a) Schematic of a fabricated polypyrrole-ODN matrix composed of one row of CP and one row of M5 ODN. (b) Fluorescence picture after hybridization with M5 complementary strand at 0.1 µM. (c) Fluorescence picture after hybridization with CP complementary strand at 0.1 µM.*

3.3.6. Conclusion

We have demonstrated that the deposition system developed during this thesis work can be used as an electrospotting tool that enables the fabrication of oligonucleotide chips featuring micrometer spots of different sequences with high reproducibility and specificity. The generic method proposed here, based on the use of polypyrrole electrochemistry in picoliter volumes, has been optimized for oligonucleotide probes but can be extended to a wide range of biological probes providing some optimization (in terms of concentration and buffer solutions) is made to adapt previous protocols dedicated to more conventional electrochemical depositions [40]. The work presented here can therefore help to address some of the recent issues in surface patterning for generating biochips at reduced scales. It can be further improved both in terms of resolution and diversity of deposited biomolecules to meet specific requirements for screening purposes with enhanced sensitivity.

4. Conclusion

In this chapter, we have investigated extended printing capabilities of the bioplume system. The spotter has been used in combination with the self-assembly and the electro-assisted deposition methods to enhance the versatility and the control of the patterning process.

Picoliter droplets of colloidal solution were deposited with bioplume and studies of the particle self-assembly within the drops were carried out to provide methods for fabricating nanostructured well-defined spots with specific chemical functionalities. In a first attempt to demonstrate the possibility to print colloid spots, functionalized amorphous silica nanospheres were deposited on coated silicon surfaces. The selection of SiO_2 beads was based on the possibility to saturate their surfaces with functional amino groups or antifouling polyethylene glycol derivatives. These aspects further support the idea of the use of nanoparticles as active parts of biomedical devices, such as biosensors and tissue engineering supports. Matrices of colloid spots ranging from 10 µm to 100 µm in diameter were successfully patterned. SEM characterizations of the nanoparticle geometry and spatial distribution within the spots revealed the colloid aggregation at the droplet rim and the selective stability of the printed patterns. The polyethylene glycol SiO_2 nanoparticle-conjugates were used as masks during a selective reactive ion etching of the silicon substrate and silicon nanopillars were obtained. Another set of experiments was then carried out to achieve the ordering, at a single particle level, of polystyrene nanobeads in hexagonal packing. The surface wettability and the duration of the contact between the cantilevers and the substrate were used to control the printed area and thus the number of deposited particles. Well-defined nanobead microcrystals were successfully fabricated thanks to the adequate composition of the colloidal solution and the accurate control of the deposition parameters. Particularly, the self-assembly of perfect hexagonal features was obtained on polyallylamine surfaces. These structures can be of high interest in the field of photonics, since they are perfectly ordered structures with finite and tunable size. In general, this novel method of directly patterning particle during deposition opens a wide series of possible applications in the field of surface micro- and nanopatterning: printed nanobead crystals can be exploited as a mask for colloidal lithography processes with the possibility to create microarrays of nanostructured materials.

Control of the deposition process using electro-assisted methods was also investigated by using the gold electrodes fabricated within the channel of each bioplume cantilever. Electrowetting effects and electrochemical reactions can both take place inside the deposited microdroplets upon the application of a voltage difference between the cantilever electrode and the substrate. Electrowetting allows changing the drop contact angle with the surface, while electrochemistry provides means to control the deposition process via induced specific chemical reactions.

Drop size monitoring was achieved by using electrowetting during deposition. Water-glycerol picoliter droplets were printed onto passivated substrates exhibiting hydrophobic surfaces. The voltage was turned on during deposition, causing the drop to spread onto the surface. Spotted matrices of drops showed that the patterned area increases with the applied voltage, thus demonstrating the principle of electrowetting-assisted deposition. The preliminary results presented in this thesis are of interest for the improvement of direct liquid-based patterning tools. Indeed, the implementation of the electrowetting actuation scheme is straightforward and simple; still, it allows controlling the size of the patterns, accessing a wide range of areas with a tip of fixed dimensions, reducing the deposition time, and ensuring a proper printing on hydrophobic surfaces.

Bioplume was finally successfully used as an electrospotting tool, combining spotting technology and electrical addressing via the physical localization of the electrodeposition process in a mobile electrochemical cell. To demonstrate the capability of the system, arrays of 20 µm diameter copper islands were firstly electrodeposited onto gold surfaces. As expected, the copper bumps exhibited increasing heights as a result of longer deposition times. The electrochemistry implementation is thus an interesting added feature since it enables the fabrication of electroplated microstructures with controlled thicknesses. As a wide range of metals may be electrodeposited or etched using this technique (leading to metal bumps or holes, respectively) possible applications include the repair of microelectronic circuits, the fabrication of MEMSs, or the chemical and physical micropatterning of surfaces. The electrospotting principle was further used to structure surfaces with micrometer size ODN spots through electro-copolymerization of pyrrole and ODN bearing pyrrole monomers. This method leads to the localized deposition of biologically active and mechanically stable polymer films and is very promising for the development of robust and uniform biochips. Fluorescence was observed after hybridizing fabricated spots with biotinylated complementary ODN, followed by a streptavidin-phycoerythrin revelation, thus proving the biological functionality of the polymer spots. Furthermore, in order to demonstrate the specificity of the coatings toward their DNA targets, we have designed a simple biochip with two different ODN probes. Specificity was demonstrated as no fluorescence signal was observed on the non specific spots. Finally, statistical operations were carried out on successively deposited droplets without any cantilever refill. The good reproducibility of the fluorescence signal provided by each spot highlights the reproducibility of the process and exemplifies the possibility to successively fabricate biochips without refilling the cantilevers. It is foreseen that electrospotting with bioplume enables the rapid fabrication of biochips with a controlled probe density and ODN spots which conserve their specificity.

References

[1] S.-M. Yang et al., Small, 2, p. 458 (2006).
[2] A. S. Dimitrov, and K. Nagayama, Langmuir, 12, p. 1303 (1996).
[3] B. G. Prevo, and O. D. Velev, Langmuir, 20, p. 2099 (2004).
[4] R. Aveyard et al., Langmuir, 16, p. 1969 (2000).
[5] B. V. Duffel et al., Journal of Materials Chemistry, 11, p. 3333 (2001).
[6] C. Hulteen, and R. P. V. Duyne, Journal of Vacuum Science and Technology A, 13, p. 1553 (1995).
[7] D. Qin et al., Advanced Materials, 11, p. 1433 (1999).
[8] F. Juillerat et al., Nanotechnology, 16, p. 1311 (2005).
[9] Y. Lu, Y. Yin, and Y. Xia, Advanced Materials, 13, p. 34 (2001).
[10] K. Y. Suh et al., Applied Physics Letter, 85, p. 2643 (2004).
[11] K. B. Lee et al., Science, 295, p. 1702 (2002).
[12] J.-M. Nam, C. S. Thaxton, and C. A. Mirkin, Science, 301, p. 1884 (2003).
[13] W. Stober, A. Fink, and E. Bohn, Journal of Colloid and Interface Science, 26, p. 62 (1968).
[14] M. Manso Silvan et al., Applied Nanoscience, 1, p. 47 (2004).
[15] R. D. Deegan et al., Nature, 389, p. 827 (1997).
[16] A. Valsesia et al., Plasma Processes and Polymers, 2, p. 334 (2005).
[17] M. Manso Silvan et al., Surface and Interface Analysis, 36, p. 733 (2004).
[18] L. M. Lacroix et al., Surface Science, 592, p. 182 (2005).
[19] M. Akram, M. C. Stuart, and D. K. Y. Wong, Analytica Chimica Acta, 504, p. 243 (2004).
[20] J. Park, and J. Moon, Langmuir, 22, p. 3506 (2006).
[21] M. Schnall-Levin, E. Lauga, and M. P. Brenner, Langmuir, 22, p. 4547 (2006).
[22] Y. Masuda, T. Itoh, and K. Koumoto, Advanced Materials, 17, p. 841 (2005).
[23] S. K. Cho, H. Moon, and C.-J. Kim, Journal of Microelectromechanical Systems, 12, p. 70 (2003).
[24] A. B. Frazier, and M. G. Allen, Journal of Microelectromechanical Systems, 2, p. 87 (1993).
[25] J. D. Madden, and I. W. Hunter, Journal of Microelectromechanical Systems, 5, p. 24 (1996).
[26] J. C. Lin et al., Journal of Micromechanics and Microengineering, 15, p. 2405 (2005).
[27] R. A. Said, Nanotechnology, 15, p. S649 (2004).
[28] J. D. Whitaker, J. B. Nelson, and D. T. Schwartz, Journal of Micromechanics and Microengineering, 15, p. 1498 (2005).
[29] J. B. Nelson, and D. T. Schwartz, Journal of Micromechanics and Microengineering, 15, p. 2479 (2005).
[30] A. J. Bard, and L. R. Faulkner, "Electrochemical Methods: Fundamentals and Applications", 2nd ed. Wiley, New York (2001).
[31] A. B. Frazier, and M. G. Allen, Journal of Microelectromechanical Systems, 6, p. 91 (1997).
[32] N. L. Rosi, and C. A. Mirkin, Chemical Reviews, 105, p. 1547 (2005).
[33] T. Kraus et al., Advanced Materials, 17, p. 2438 (2005).
[34] T. Livache et al., Biosensors and Bioelectronics, 13, p. 629 (1998).
[35] T. Livache et al., Synthetic Metals, 121, p. 1443 (2001).
[36] T. Livache, et al., Nucleic Acids Research, 22, p. 2915 (1994).
[37] T. Livache, H. Bazin and G. Mathis, Clinica Chimica Acta, 278, p. 171 (1998).

[38] S. Sadki et al., Chemical Society Reviews, 29, p. 283 (2000).
[39] B. J. Hwang, R. Santhanam, and Y. L. Lin, Electrochimica Acta, 46, p. 2843 (2001).
[40] L. Grosjean et al., Analytical Biochemistry, 347, p. 193 (2005).

Conclusion

The interest in patterning surfaces with micro- and nanometer resolutions has been growing fast in recent years, illustrating the tremendous potential of patterning techniques for both fundamental investigations and technological applications in photonics, molecular electronics, and biosensors. Numerous techniques have been developed allowing patterning a wide range of materials with various feature characteristics (resolution, minimum size, uniformity, etc.). These methods exhibit differences in term of complexity, cost and time required for the fabrication of patterns. Consequently, the varieties of tool characteristics and application requirements result in the need to select the most appropriate technique for a given application. Among the various patterning methods, liquid dispensing techniques relying on the use of microcantilevers are very promising for several reasons. The first one is that they permit a direct patterning of the surface with different kinds of materials without any need for prefabricated patterns. Secondly, alignment of the cantilevers with respect to specific regions on the surface is straightforward since the cantilevers themselves can be used as displacement sensors. Moreover, parallel approaches can be developed to meet specific requirements in terms of throughput and fabrication costs.

In this thesis, we have presented a direct patterning tool relying on the use of an array of silicon microcantilevers. Significant improvements were carried out to guarantee a high degree of control over location and geometry of the fabricated patterns: the integration of force sensors and the use of self-assembly and electro-assisted methods. Proof-of-concept experiments were conducted to demonstrate the versatility of our deposition system in terms of deposited materials and spot sizes.

The principle of the bioplume system is to use an array of silicon cantilevers enabling the local deposition of picoliter droplets thanks to a direct contact of the tip and the surface to pattern. In this work, we designed cantilevers with an integrated fluidic channel and proposed a fabrication process based on conventional microfabrication techniques and silicon-on-insulator wafers. The fabricated cantilever array was integrated into a closed-loop automated system allowing the control of the droplet homogeneity and the spatial positioning of the microarray. The automated system relied on the use of force sensors, i.e. piezoresistors, integrated into the cantilevers to adjust the trim and to control the deposition parameters, i.e. contact force and time. A dedicated electronics circuitry, based on a modified Wheatstone bridge, was used to allow the measurement of the cantilever bending with a final sensitivity of approximately 1 V/µm and a minimum detectable tip displacement of less than 100 nm. The bioplume patterning system was finally built using the cantilever array, a four-degree-of-freedom automated spotter, the electronic circuit and a PC.

Because the most obvious application of bioplume is the fabrication of biochips and the local functionalization of biosensors, experiments were conducted to demonstrate the ability of the spotter to directly deposit functional biomolecules. These experiments proved that it was possible to address oligonucleotides with the same microcantilevers several times at the same location without contamination. Successful hybridization tests showed that the biomolecules did not lose their biological properties after deposition. The use of an external dedicated fluidic chip demonstrated the possibility to load each cantilever with different molecules and thus that several molecules could be printed in a parallel manner. Finally, means to fill the channels with liquids by using electric field actuation were proposed to reduce the volumes required for the loading process.

To further enhance the deposition potentials of the bioplume system, in terms of the variety of deposited materials and 3D control of the printed patterns, mix and match approaches were then tested. We used the bioplume direct liquid patterning system in combination with other deposition means: self-assembly and electro-assisted methods.

The spotting system was employed to simply and directly create microspots of nanobeads without the need of a prepatterned surface. Picoliter droplets of colloidal solutions (functionalized silica and polystyrene nanobeads) were deposited onto surfaces exhibiting different wettabilities. The direct patterning of perfectly crystalline spots was achieved with polystyrene particles. By controlling the wettability of the surface to pattern and the contact time during deposition it was possible to tune the shape and the size of the spotted colloidal area. In a particular case it was possible to create microspots shaped like perfect hexagons.

Control of the deposition process using electro-assisted methods was also investigated by using the gold electrodes fabricated within the channel of each bioplume cantilever. Drop size monitoring was achieved by using electrowetting during deposition. We demonstrated that droplets with a wide range of contact areas could be patterned onto highly hydrophobic surfaces by simply applying a voltage between the cantilever and the surface.

Finally, the bioplume spotter was successfully used as an electrospotting tool, enabling electrochemical reactions to occur within the picoliter droplets. To prove the capability of the system, arrays of 20 µm diameter copper islands were firstly electrodeposited onto gold surfaces. As expected, the copper bumps exhibited increasing heights as a result of longer deposition times. The electrospotting principle was further used to structure surfaces with micrometer size ODN spots through electro-copolymerization of pyrrole and ODN bearing pyrrole monomers. The biological functionality of the polymer spots and the specificity of the films toward their DNA targets were successfully demonstrated.

In conclusion, the bioplume patterning tool, developed within the framework of the integrated European project NaPa, has reached an interesting maturity state in terms of versatility of printed materials and control over the deposition process. This patterning tool is foreseen to be of interest for fundamental research and applications in various technological fields because of its simplicity, ease-of-use and cost. The overall characteristics, provided in Table C.1, can be used as comparison means regarding the techniques previously described in this thesis and aiming at patterning surfaces with micrometer scale features.

Bioplume is specifically adapted for biological applications as, compared to classical microarray protocols, volumes and time of manipulation are drastically reduced. Moreover, because the typical spot sizes are in the range of 10 to 20 µm, bioplume fulfill all the prerequisites to overcome the challenge of miniaturization of

biological assays. The added electrospotting feature is very promising for the development of robust and uniform biochips. Because the printed liquid droplet size and polymer film thickness are controlled by the contact time during deposition and the electropolymerization charge, reproducible spots can be created with this technique. The interest of our approach for the development of biosensors is also envisioned because it allows the precise and local deposition of nanoparticle-based conjugates on transducers surfaces. In general the direct method of colloidal particle deposition opens a wide series of possible applications in the field of surface micro- and nanopatterning: printed nanobead crystals can be exploited as masks for colloidal lithography processes, with the possibility to create microarrays of nanostructured materials. Furthermore, these structures can be of high interest in the field of photonics, since they are perfectly ordered structures with finite and tunable size. Finally, the electrochemistry implementation is an interesting method to fabricate electroplated microstructures with controlled thicknesses. As a wide range of metals may be electrodeposited or etched using this technique (leading to metal bumps or holes, respectively) possible applications include the repair of microelectronic circuits or the fabrication of MEMSs. It is foreseen that several entities can be printed quickly on the same sample by simply changing the electrolyte charged on the cantilevers and applying the potential of the corresponding desired redox couple.

From a prospective point of view, the bioplume system is well suited for a size reduction of the droplets down to the femtoliter range and below because it is only limited by the shrinkage of the cantilever dimensions. The last section of this thesis describes the preliminary work that has been carried out on the next generation of bioplume cantilevers aiming at reducing the size of the printed spots.

Tool	Ink-jet	**Bioplume**	Dip-pen
Type	Non-contact	*Contact*	Contact
Environment	Atmospheric conditions	*Atmospheric conditions*	High humidity
Resolution - Range Volume	>20 µm → >100 µm 10 pL	*<10 µm → 100 µm* *<1 pL*	15 nm → 100 nm X
Deposited Area	Very large (>10 cm²)	*Large* *(>1 cm²)*	Very small (≈ mm^2)
Deposition rate	<1000 drops/s	*>10 drops/s*	Very low
Volume available	Very large (> 1 µL)	*30 pL on each cantilever* *≈ µL via the loading chip*	X
Materials	Biological solutions Polymers Particles Cells	*Biological solutions* *Polymers* *Metals* *Particles*	SAMs Biological entities Particles
Substrates	No restriction	*Flat surface*	Very flat surface
Controls	Volume ejected	*Force*	Force
In-situ characterization	X	*X*	AFM
Pros	- Mature technology - Available on the market - Parallel - Inexpensive - Simple	- *Parallel* - *Inexpensive* - *Simple* - *Disposable* - *Electrochemistry* - *Electrowetting*	- Mature technology - Available on the market - Parallel - Electrochemistry
Cons	- Accuracy - Difficult alignment - Limited viscosities	- *High-boiling point solvent required*	- Very slow

Table C.1: *Table providing the characteristics of the bioplume system developed in this thesis work. The characteristics of the two mature technologies available on the market (ink-jet and dip-pen) and designed to pattern surfaces at different scales are given, as a comparison means.*

Prospective Outlook

The bioplume deposition system presented in this thesis can help to address some of the recent issues in surface patterning at a micrometer scale. It can be further improved in terms of resolution to reach the submicrometer scale, thus filling the gap between the silicon pins and the scanning probe lithography (SPL) tools. To that end, a specific fabrication process has been developed to obtain in-plane sharp cantilever tips, the use of which being compatible with the deposition system framework developed so far. Preliminary experiments were performed, showing the potential of our approach.

1. Further reduction of the spot size - Nanobioplume

Variation of the spot size can be achieved by controlling the contact time of the cantilever with the surface during deposition. The minimum spot size is thus obtained for a minimum contact time, assuming that deposition occurs. The wettability of the surface and the tip can also be adjusted in order to decrease the size of printed features. However, the only way to downsize the droplets deposited by direct contact tools, regardless of the deposition parameters, is to shrink the tip dimensions.

2. Proposed solution

The bioplume cantilevers presented in this thesis enable the deposition of droplets with diameters in the range of tens of micrometers. Reduction of drop size can not be achieved because it is limited by the size of the channel. However, this goal can be reached by adding an ultrasharp nanotip at the extremity of the channel. Thus, we propose to create such a tip by simply adding a few steps to the current cantilever fabrication.

Fabrication techniques of nanometric structures include electron beam lithography, FIB milling and so forth. However, most of these techniques are time-consuming, not really adapted for mass fabrication and not always compatible with standard micromachining. Ried and co-workers have developed incisive tips fabricated by anisotropic etching of silicon by tetramethyl ammonium hydroxide (TMAH) with vertical walls of SiO_2 as masking layers [1]. The supplementary fabrication steps we propose rely on anisotropic etching of silicon by TMAH with Si_3N_4 film and local oxidation of silicon (LOCOS) as masking layers [2-4]. By this collective method, symmetrical sharp in-plane nanotips with curvature radius of less than 100 nm are

obtained with high uniformity without depending on the precision of photolithography and alignment techniques.

3. Fabrication process

The fabrication process of the in-plane silicon nanotip is shown in Figure P.1. The starting substrate is the same type of SOI wafers used for the fabrication of bioplume, i.e. the top silicon layer is 5 µm thick and the intermediate SiO_2 layer is 1 µm thick. A Si_3N_4 film with a thickness of 20 nm is firstly formed by low pressure chemical vapor deposition (LPCVD) (Figure P.1a). Then, the Si_3N_4 film is patterned in a rectangular shape aligned along the <110> direction to allow the formation of a V-shaped microchannel during the subsequent humid etch step (Figure P.1b): silicon is etched by TMAH (22%, 85 °C) (Figure P.1c). The initial rectangle is narrow enough (5 µm wide) so that the bottom of the microchannel does not reach the intermediate SiO_2 layer. Then, a 300 nm silicon dioxide layer is thermally grown in the channel (Figure P.1d). Because the silicon covered by the Si_3N_4 film can not be oxidized, oxide grows only in the microchannel. This process is generally called local oxidation of silicon (LOCOS). The Si_3N_4 film is patterned for a second anisotropic etching of silicon by TMAH (Figure P.1e). In this case also, the opened pattern has a rectangular shape and overlaps the first 25 µm of the top part of the microchannel. This overlapping length determines the final length of the in-plane nanotip. The Si_3N_4 film is etched by reactive ion etching (RIE) and the second anisotropic etching of silicon is performed (Figure P.1f). The Si_3N_4 and SiO_2 films serve as etching masks. The symmetrical in-plane nanotip (12 µm long) with a high aspect ratio is formed within the microchannel. The second anisotropic etch is stopped as soon as the SiO_2 intermediated layer appears. Finally, the Si_3N_4 and SiO_2 films are removed by RIE and buffered hydrofluoric acid (BHF) etch (Figure P.1g). After obtaining the in-plane nanotip, the fabrication of the cantilever can be carried out using the fabrication process introduced in Chapter II.

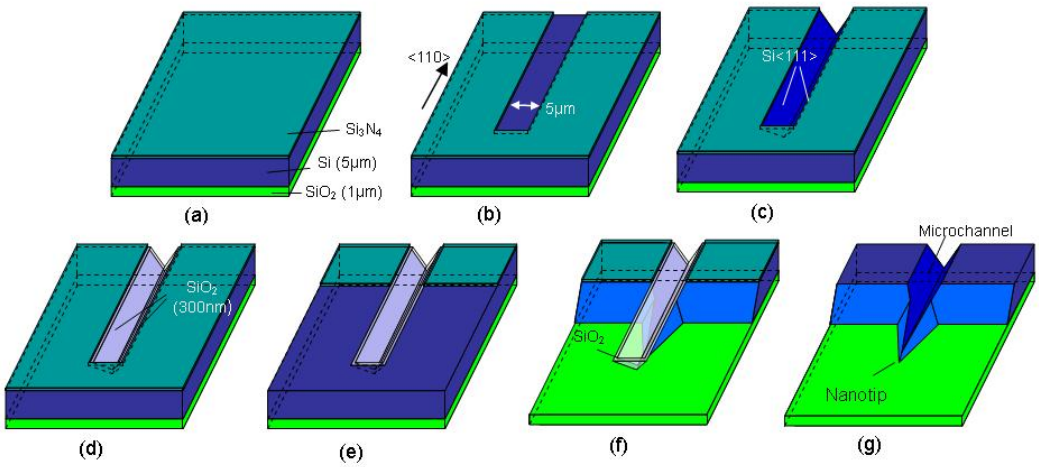

Figure P.1: *Fabrication process of the in-plane silicon nanotip. (a) Deposition of Si_3N_4. (b) Patterning of Si_3N_4. (c) Silicon anisotropic etching by TMAH. (d) Thermal oxidation (LOCOS). (e) Patterning of the Si_3N_4 layer. (f) Anisotropic etching by TMAH. (g) Removal of the Si_3N_4 and the SiO_2 layers.*

As a proof-of-concept, simple silicon cantilevers (i.e. without the piezoresistances and the channel electrode) were fabricated using the above-mentioned technique. Scanning electron microscope (SEM) pictures of the fabricated nanotips are seen in Figure P.2. Deposition experiments, described below, were done with these cantilevers in order to prove their reliability.

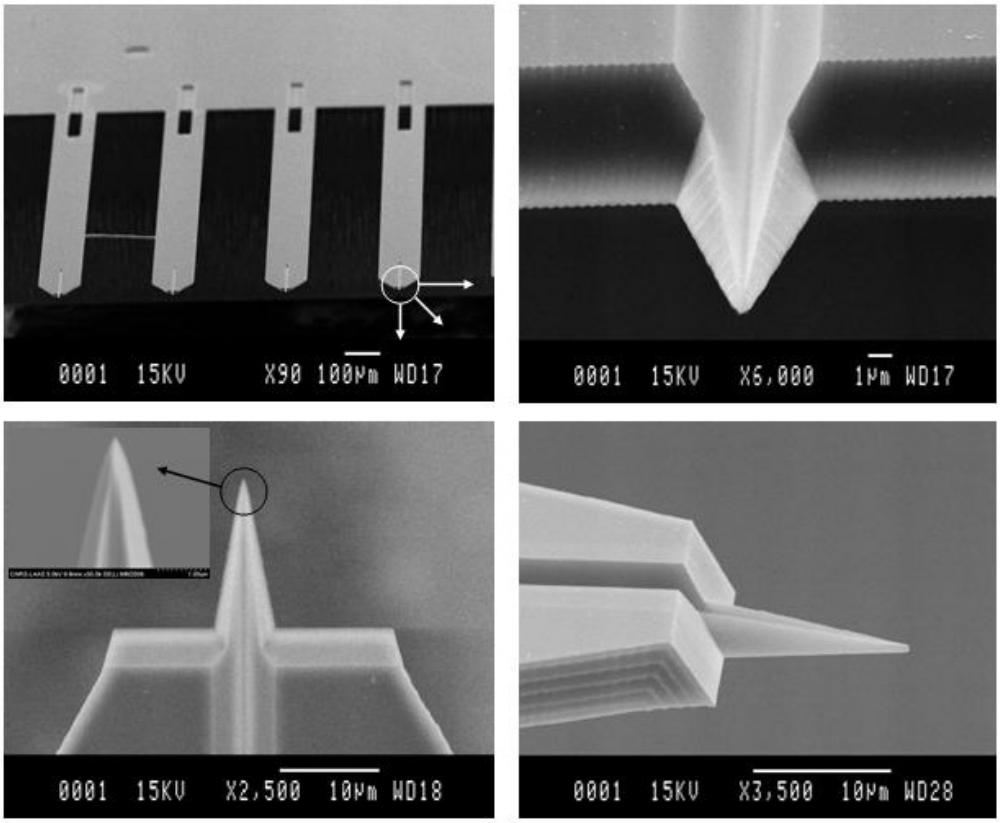

Figure P.2: *SEM images of the cantilever array and close-up views of the nanotips.*

4. Preliminary deposition tests with nanobioplume

The bioplume positioning system was used to conduct the experiments. A water-glycerol mixture (30%-70%) was used as the deposition solution. After loading the cantilevers by dipping them in a reservoir drop, matrices of droplets were automatically deposited. The deposition test was conducted at ambient conditions, i.e. temperature of 20 °C and humidity of 50%. In order to observe the effect of the surface wettability of the nanotip and the substrate upon the droplet size, silicon cantilevers with both hydrophilic and hydrophobic nanotips were used. Silicon and silicon dioxide surfaces were used as hydrophobic and hydrophilic substrates, respectively. Prior to any deposition, surfaces and tips were cleaned with appropriate procedures.

5. Results

Using hydrophobic nanotips, hardly any depositions were observed on the hydrophobic substrates, probably because of the fast evaporation of the small droplets. However, when printing on hydrophilic substrates, matrices of 2 µm diameter droplets with high uniformity were obtained for a contact time of 50 ms, as shown in Figure P.3c. It was demonstrated that in this case, the droplet diameter decreases subsequently to the reduction of contact time.

With hydrophilic nanotips, droplets with diameters of about 3 µm to 4 µm were obtained on hydrophobic Si substrates. In this case varying the contact time did not lead to any major differences in drop size. In the case of hydrophilic silicon nanotips printing on hydrophilic substrates, the deposited droplets were significantly larger, with a diameter of more 10 µm. In this case also, the droplet diameter depended on the contact time. The diameter was reduced to about 5 µm for a 50 ms contact time.

The results concerning the effect of the surface wettability agree well with the work done by Meister and co-workers [5], in which simulations of shapes of liquid meniscus created between an AFM tip and a substrate were carried out for different surface wettabilities. This is also consistent with the results presented in Chapter II of this thesis.

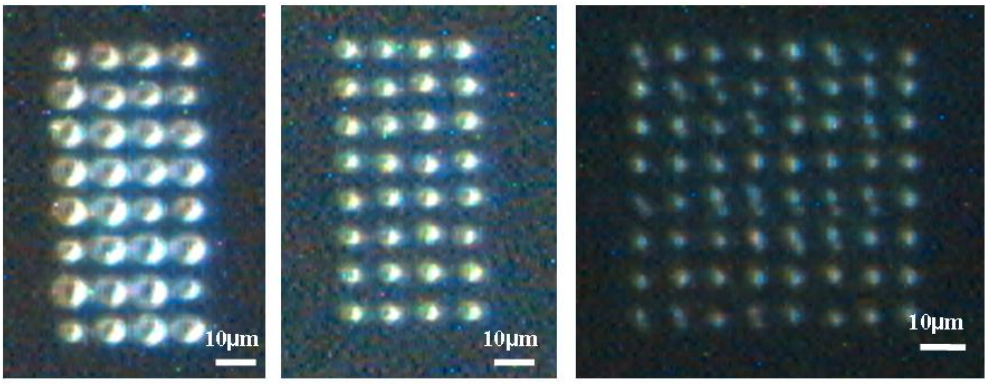

Figure P.3: *Optical microscope images of water-glycerol droplet matrices deposited by hydrophobic nanotips on a hydrophilic SiO2 surface. Contact time: (a) 300ms, (b) 100ms, and (c) 50ms.*

6. Conclusion

Cantilever arrays with in-plane nanotips were fabricated with high uniformity using a conventional micromachining process based on TMAH anisotropic etching. By using this cantilever array with nanotips, depositions of matrices of water-glycerol droplets with diameters of about 2 µm were carried out with a 10 µm interspot distance. The density of printed patterns was increased by a factor of at least 5^2 compared to what was accomplished with bioplume. Further reduction of the drop diameter printed with nanobioplume could be achieved by considering treatment methods of the nanotip and the substrate and by adjusting the contact time in order to reach submicrometer capabilities.

References

[1] R. P. Ried et al., Journal of Microelectromechal Systems, 6, p. 294 (1997).
[2] K. Kakushima et al., Proceedings of the 14th International Conference on Micro Electro Mechanical Systems (MEMS'01), 21-25 Jan, 2001, Interlaken, Switzerland, p. 294 (2001).
[3] G. Hashiguchi et al., Analytical Chemistry, 75, p. 4347 (2003).
[4] M. Saito et al., Sensors and Actuators A, 130-131, p. 616 (2006).
[5] A. Meister et al., Applied Physics Letters, 85, p. 6260 (2004).

List of Publications

Part of the work presented in this thesis has contributed to the following publications:

Journal papers

- **T. Leïchlé**, M. Manso Silvan, P. Belaubre, A. Valsesia, G. Ceccone, F. Rossi, D. Saya, J.-B. Pourciel, L. Nicu, and C. Bergaud, "Nanostructuring surfaces with conjugated silica colloids deposited using silicon-based microcantilevers", *Nanotechnology*, 16 (4), p. 525 (2005).

- **T. Leïchlé**, L. Nicu, E. Descamps, B. Corso, P. Mailley, T. Livache, and C. Bergaud, "Copper electrodeposition localized in picoliter droplets using microcantilever arrays", *Applied Physics Letters*, 88, 254108 (2006).

- **T. Leïchlé**, D. Saya, J.-B. Pourciel, F. Mathieu, L. Nicu, and C. Bergaud, "Liquid loading of silicon-based cantilevers using electrowetting actuation for microspotting applications", *Sensors and Actuators A*, 132 (2), p. 590 (2006).

- **T. Leïchlé**, D. Saya, J.-B. Pourciel, F. Mathieu, C. Bergaud, and L. Nicu, "A closed-loop MEMS-based spotter integrating position sensors with nanometric precision for the control of droplet uniformity", *IEEE NTC Review on Advances in Micro, Nano, and Molecular Systems*, vol. 1, p. 337 (2006).

- A. Valsesia, **T. Leïchlé**, L.-M. Lacroix, L. Nicu, F. Bretagnol, P. Colpo, F. Rossi, and C. Bergaud, "Deposition of nanobead hexagonal crystals using silicon microcantilevers", *Small*, 2 (12), p. 1444 (2006).

- D. Saya, **T. Leïchlé**, J.-B. Pourciel, C. Bergaud, and L. Nicu, "Collective fabrication of in-plane silicon nanotip for parallel femtoliter droplet deposition", *Journal of Micromechanics and Microengineering*, In Press (2007).

- L. Tanguy, **T. Leïchlé**, and L. Nicu, "Dynamic spreading of a liquid finger driven by electrowetting: theory and experimental validation", *Journal of Applied Physics*, In Press (2007).

- E. Descamps, **T. Leïchlé**, B. Corso, S. Laurent, P. Mailley, L. Nicu, T. Livache, and C. Bergaud, "Fabrication of oligonucleotide chips using parallel cantilever-based electrochemical deposition in picoliter volumes", *Advanced Materials*, Accepted for publication (2007).

Conference papers

- **T. Leïchlé**, D. Saya, P. Belaubre, J.-B. Pourciel, F. Mathieu, J.-P. Laur, L. Nicu, and C. Bergaud, "Liquid loading of silicon-based cantilevers using electrowetting actuation for microspotting applications", Proceedings of the *13th International Conference on Solid-State Sensors, Actuators and Microsystems (Transducers'05), 5-9 June, 2005, Seoul, Korea*, vol. 1, p. 135.

- P. Belaubre, J.-B. Pourciel, D. Saya, **T. Leïchlé**, F. Mathieu, L. Nicu, and C. Bergaud, "First step towards a fully automated trim control for liquid deposition device at the microscale using piezoresistive cantilevers row", Proceedings of the *13th International Conference on Solid-State Sensors, Actuators and Microsystems (Transducers'05), 5-9 June, 2005, Seoul, Korea*, vol. 1, p. 648.

- **T. Leïchlé**, D. Saya, J.-B. Pourciel, F. Mathieu, C. Bergaud, and L. Nicu, "A closed-loop MEMS-based spotter integrating position sensors with nanometric precision for the control of droplet uniformity", Proceedings of the *1st IEEE International Conference on Nano/Micro Engineering and Molecular Systems (IEEE-NEMS), 18-21 January, 2006, Zhuhai, China*, p. 732.

- V. Bardinal, E. Daran, C. Vergnenègre, **T. Leïchlé**, Y. Segui, T. Camps, J.-B. Pourciel, V. Conedera, L. Gavin-Djidina, and M. Guirardel, "Design and fabrication of polymer microlenses arrays for VCSELs using a cantilever-based microsystem", Proceedings of *SPIE, Photonic Europe, 3-6 April, 2006, Strasbourg, France*, vol. 6185, 618510.

- L. Tanguy, **T. Leïchlé**, and L. Nicu, "Theoretical considerations for continuous electrowetting in U-shaped channels", *5th International Meeting on Electrowetting, 31 May - 2 June, 2006, Rochester, USA*.

- D. Saya, **T. Leïchlé**, J.-B. Pourciel, C. Bergaud, and L. Nicu, "Collective fabrication of in-plane silicon nanotip for parallel femtoliter droplet deposition", Proceedings of the *32nd International Conference on Micro- and Nano- Engineering (MNE'06), 17-20 September, 2006, Barcelona, Spain*, p. 47.

- **T. Leïchlé**, E. Descamps, B. Corso, S. Laurent, P. Mailley, T. Livache, J.-B. Pourciel, C. Bergaud, and L. Nicu, "MEMS-based picoliter electrochemical cell array for the fabrication of oligonucleotide chips", Proceedings of the *10th International conference on Miniaturized Systems for Chemistry and Life Sciences (μTAS), 5-9 November, 2006, Tokyo, Japan*, p. 774.

- N. Berthet, **T. Leïchlé**, E. Trévisiol, J.-B. Pourciel, D. Saya, C. Bergaud, L. Nicu, and J.-M. François, ""Spot-in-spot" hybridization of oligonucleotides deposited on a glass slide by a microcantilever-based device", Proceedings of the *10th International conference on Miniaturized Systems for Chemistry and Life Sciences (μTAS), 5-9 November, 2006, Tokyo, Japan*, p. 1217.

Life is what happens to you
While you're busy making other plans.

John Lennon

Bioplume: A MEMS-based Picoliter Droplet Dispenser with Electrospotting Means for Patterning Surfaces at the Micro- and the Nanometer Scales

Abstract:
The interest in patterning surfaces with micro- and nanometer resolutions has been growing fast in recent years, illustrating the tremendous potential of patterning techniques for both fundamental investigations and technological applications in photonics, molecular electronics, and biosensors. Among the various patterning methods, liquid dispensing techniques relying on the use of microcantilevers are very promising for several reasons. The first one is that they permit a direct patterning of the surface with different kinds of materials without any need for prefabricated patterns. Secondly, alignment of the cantilevers with respect to specific regions on the surface is straightforward since the cantilevers themselves can be used as displacement sensors. Moreover, parallel approaches can be developed to meet specific requirements in terms of throughput and fabrication costs. In this thesis, we present a liquid spotter (so-called bioplume) based on the use of silicon microcantilevers. Droplets are formed on the surface by a direct contact method. The fabricated cantilever array is integrated to a closed-loop automated system allowing the control of the droplet homogeneity and the spatial positioning of the microarray. The system relies on the use of force sensors, i.e. piezoresistors, integrated into the cantilevers to adjust the trim and to control the deposition parameters, i.e. contact force and time. By using a specific external loading chip, different liquids can be loaded onto the cantilevers, enabling the parallel deposition of several entities in a single deposition run. Besides, an electrode is incorporated in the channel to allow using electrowetting and electrochemistry. The former is used to actively load the cantilever and to control the drop size during delivery, while the latter is used to drive electrochemical reactions in the deposited picoliter droplets. This tool has been used to print biological solutions, to electrodeposit copper, to electropolymerize functionalized pyrrole and to directly create crystalline microspots of nanobeads. The control of the printed features (resolution, thickness, and composition), the versatility of the printed materials and the added electro-assisted features demonstrate the tremendous potential of the bioplume tool for research work and industrial applications.

Keywords:
Silicon microcantilevers, Surface patterning, Picoliter droplets, Electrowetting, Electrodeposition, Self-assembly, Piezoresistors

---

Bioplume: Système de Dépôt de Microgouttes Parallélisé pour la Structuration et la Fonctionnalisation Electro-assistées de Surfaces aux Echelles Micro- et Nanométriques

Résumé de la thèse:
Les techniques de structuration et de fonctionnalisation de surfaces aux échelles micro- et nanométriques connaissent un intérêt croissant lié aux possibilités qu'elles offrent pour l'étude des phénomènes fondamentaux à faibles échelles et aux avancées technologiques qu'elles permettent dans les domaines de l'électronique, de la photonique et de la bio-ingénierie. Parmi les nombreuses techniques qui ont été développées durant les dernières décennies, les méthodes reposant sur l'utilisation de microleviers pour le dépôt de faibles volumes de liquide offrent, entre autre, l'avantage d'être directes et parallélisées, et sont particulièrement adaptées aux applications biologiques. Les travaux présentés dans cette thèse portent sur la conception et la réalisation d'un système de dépôt de gouttes micrométriques à l'aide de matrices de leviers en silicium. L'originalité de ce système, nommé bioplume, repose sur l'intégration de capteurs de forces et sur l'utilisation de méthodes de dépôt assistées par champ ou par auto-assemblage pour contrôler in situ la taille, l'uniformité et la composition des motifs réalisés. Le système fonctionne en boucle fermée afin d'automatiser la fabrication de micromatrices de spots tout en garantissant la correction des erreurs d'alignement et le contrôle de la force exercée et du temps de dépôt. Après avoir validé le chargement assisté par électromouillage et le dépôt de solutions biologiques, nous utilisons les phénomènes d'auto-organisation afin de créer directement, à partir de solutions de nanoparticules, des microspots cristallins. Enfin, à l'aide d'électrodes incorporées aux leviers, des réactions électrochimiques sont induites dans les volumes de liquides déposés (de l'ordre du picolitre), permettant l'électrodéposition de cuivre et l'éléctropolymérisation de pyrroles. Les nombreuses fonctionnalités apportées à ce système pendant cette thèse permettent d'étendre ses capacités, faisant de bioplume une solution fiable et complémentaire aux techniques de jet d'encre et de dip-pen en terme de taille de motifs.

Mots-clés:
Microleviers, Structuration de surfaces, Microgouttes, Electromouillage, Electrodéposition, Auto-assemblage, Piézorésistances